

Synthesis, molecular modeling, and biological evaluation of novel imatinib derivatives as anticancer agents

Fulya GÜNAY^{1,2}, Sevcan BALTA¹, Yuk Yin NG², Özlem ULUCAN², Zuhale TURGUT¹, Ömer Tahir GÜNKARA^{1*}

¹Department of Chemistry, Faculty of Arts and Science, Yıldız Technical University, İstanbul, Turkey

²Department of Genetics and Bioengineering, Faculty of Engineering and Natural Sciences, İstanbul Bilgi University, İstanbul, Turkey

Received: 13.07.2021 • Accepted/Published Online: 06.09.2021 • Final Version: 23.02.2022

Abstract: Different derivatives of imatinib were synthesized by a 3-step reaction method. The structures of the new compounds were characterized by spectroscopic methods. For quantitative evaluation of the biological activity of the compounds, MTT assays were performed, where four BCR-ABL negative leukemic cell lines (Jurkat, Reh, Nalm-6 and Molt-4), one BCR-ABL positive cell line (K562), and one non-leukemic cell line (Hek293T) were incubated with various concentrations of the derivatives. Although imatinib was specifically designed for the BCR-ABL protein, our results showed that it was also effective on BCR-ABL negative cell lines except for Reh cell line. Compound 9 showed lowest IC₅₀ values against Nalm-6 cells as 1.639 μ M, also the values of Compound 10 for each cell were very close to imatinib. Molecular docking simulations suggest that except for compound 6, the compounds prefer a DFG-out conformation of the ABL kinase domain. Among them, compound 10 has the highest affinity for ABL kinase domain that is close to the affinity of imatinib. The common rings between compound 10 and imatinib adopt exactly the same conformation and same type of interactions in the ATP binding site with the ABL kinase domain.

Key words: Imatinib derivatives, tyrosine kinase inhibitors, BCR-ABL inhibitors, leukemia, anti-cancer agents, molecular docking.

1. Introduction

Imatinib mesylate (Gleevec®, STI-571), (Figure 1) is the first generation of FDA approved protein-tyrosine kinase inhibitor, especially treatment of CML (Chronic Myelogenous Leukemia) and GIST (Gastrointestinal Stromal Tumors) [1-6]. It contains 2-(phenylamino)pyrimidine heterocycle core that functions for targeting BCR-ABL (the Breakpoint Cluster Region-the Abelson proto-oncogene) activity leading to decrease tyrosine kinase activity; methyl group on this core occupies the selectivity to BCR-ABL; aryl piperazine core increases oral bioavailability and pyrimidine core occupies cellular activity [7]. There are three different general methods for the synthesis of imatinib mesylate [8-14]. There are also some patents [8], [15-19] in which imatinib is obtained by directly reacting the commercially sold aminopyrimidine and the aryl piperazine derivatives. Moreover, there are flow-based [13], [20-22], microwave-assisted [23], copper-catalyzed [24], palladium-catalyzed [25], BrettPhos-catalyzed [26-27] methods for synthesizing imatinib.

Imatinib is specific for the tyrosine kinase domain in ABL and BCR-ABL gene products, it has been reported that treatment with BCR-ABL inhibitors, significantly reduces the application of hematopoietic cell transplantation for treatment of CML [28]. It binds ABL1 kinase in ATP-binding site and stabilizes an inactive conformation of the catalytic domain where the well-known “DFG” triad (Asp-Phe-Gly) is in an out conformation [1].

After prolonged treatment of imatinib, due to mutations at kinase domain site in ATP binding site, the drug activity changes. Over-stimulated BCR-ABL1 fusion protein causes genomic instability in CML stem cells and causes more than 50 hotspot mutations to accumulate in the ABL1 kinase domain. Complexity or having more than one mutation also changes the patient's outcome against the drug. ABL1 point mutations reduce the accessibility of the drug's binding site, limiting the enzyme's flexibility [28-29].

For this reason, PD180970, CGP76030, BMS-354825, AMN 107 or Nilotinib, and, more recently, AP24534 have been developed. There are also novel approaches to imatinib resistance, such as Farnesyltransferase inhibitors (SCH66336) and Proteasome inhibitors (Bortezomib), that have been reported to have growth inhibitory properties on leukemia [30-36].

* Correspondence: gunkara@yildiz.edu.tr

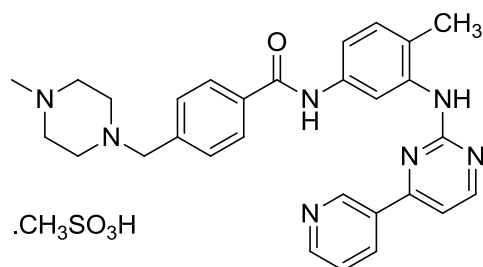


Figure 1. Imatinib mesylate molecular structure.

In this study, it was aimed to synthesize and investigate the biological activity of new imatinib derivatives that potentially inhibit the growth of cancer cells. The designed compounds were synthesized, and their structural formula was confirmed by different spectral data. Anti-cancer activities of all the newly synthesized compounds were examined by MTT (3-(4,5-dimethylthiazol-2-yl)-2,5-diphenyltetrazolium bromide) assay.

Additionally, we performed extensive molecular docking simulations to evaluate the binding preference of newly synthesized compounds to different conformations of wild type ABL and BRAF (v-Raf murine sarcoma viral oncogene homolog B) kinases.

2. Materials and methods

2.1. Chemistry

2.1.1. Chemicals and instruments

All chemicals used were purchased from Merck and Aldrich without further purification. Trimetazidine HCl was obtained from the World Medicine Drug Company (Fisher Scientific), Imatinib was purchased from Sigma Aldrich (SML1027-100MG). Sonication was performed in an Intersonik ultrasound cleaner (model: MIN4) with a frequency of 25 kHz, an US output power of 100 W, a heating 200 W. Heidolph RV Laborata 4000 rotary evaporator was used to evaporate the solvent. A TLC Merck 5554 with silica gel layers with fluorescent indicator and a Camag (254/366 nm) UV lamp were used. The melting points of the pure materials were measured on the Stuart apparatus. FTIR spectra of the starting materials and the obtained products were taken on a "Perkin Elmer Spectrum One" FTIR spectrometer by ATR technique. ^1H and ^{13}C NMR spectra were obtained from a "Bruker 500 MHz" spectrometer in CDCl_3 . Chemical shifts were reported in ppm (parts per million) with respect to internal standard TMS (Tetramethylsilane). LC-MS spectra were obtained by Agilent 6200 series TOF/6500 series TOF/Q-TOF Mass Spectrometer. All crude products were purified with Teledyne Isco CombiFlash Rf 200 system and RediSep Rf Gold Silica Columns.

2.1.2. General procedure for the synthesis of intermediate containing benzamide

1 mmol (186.05 mg) 3-bromo-4-methylaniline (Compound 2) was placed in a two-necked round bottom flask. It was dissolved in dry DCM (dichloromethane) (4 mL) under inert atmosphere at 0°C . 1 mmol (138.205 mg) of overheated K_2CO_3 was added the reaction mixture and stirred at the same temperature. After that, 1 mmol (189.04 mg) 4-chloromethylbenzoylchloride (Compound 1) was dissolved with dry DCM (4 mL) and injected dropwise into the reaction medium. While continuing the addition, yellow crystals formed in the reaction medium. The mixture was stirred at 0°C for 1 h. After completion of the reaction, the yellow crystals were filtered, washed with DCM, and dried [13, 20-21].

2.1.2.1. *N*-(3-Bromo-4-methylphenyl)-4-(chloromethyl)benzamide (Compound 3) [13].

Yellow solid, (This compound was crystallized with DCM, yield: 98%, Rf: 0.54 (1:3 Ethylacetate/n-Hexane), m.p. 157°C); IR (ATR) ν_{max} 3452 (NH), 3284, 2985, 1641 (C=O), 1577, 1499, 1441, 1384, 1299 cm^{-1} ; ^1H NMR (600 MHz, CDCl_3): δ = 2.38 (s, 3H, CH_3), 4.63 (s, 2H, CH_2), 7.21 (d, $J=8.2$ Hz, 1H, Ar-H), 7.47 (d, $J=1.5$ Hz, 1H, Ar-H), 7.51 (d, $J=8.5$ Hz, 2H, Ar-H), 7.84 (brds, 1H, NH), 7.85 (dd, $J=8.5, 1.7$ Hz, 2H, Ar-H) 7.89 (s, 1H, Ar-H) ppm; ^{13}C NMR (150 MHz, CDCl_3): δ = 22.35 (CH_3), 45.29 (CH_2), 119.17 (CAr), 123.95 (CAr), 124.89 (CAr), 127.49 (CAr), 128.99 (2xCAr), 130.91 (2xCAr), 134.21 (CAr), 134.59 (Cq), 136.55 (Cq), 141.42 (Cq), 164.97 (C=O) ppm.

2.1.3. General procedure for the synthesis of intermediates containing aryl piperazine (Compound 4a-4b)

0.3 mmol (101.59 mg) *N*-(3-Bromo-4-methylphenyl)-4-(chloromethyl)benzamide (Compound 3) and 0.39 mmol aryl piperazine [2-(piperazin-1-yl)pyrimidine or 1-(2,3,4-trimethoxybenzyl) piperazine dihydrochloride] were taken into a round bottom flask. The starting materials were dissolved in dry acetone (10 mL) under inert atmosphere. Then, 0.9 mmol (124.38 mg) of overheated K_2CO_3 was added to the reaction mixture. The mixture was heated and stirred at 55°C overnight

under inert atmosphere. After completion of the reaction, the reaction mixture was filtered and the solvent was evaporated under reduced pressure. The crude products 4a and 4b were purified using flash chromatography.

2.1.3.1. *N*-(3-Bromo-4-methylphenyl)-4-((4-(pyrimidin-2-yl)piperazin-1-yl)methyl)benzamide (Compound 4a)

Brownish gummy solid (This compound was purified by flash column chromatography using ethylacetate/*n*-hexane 5:1 as eluent, Rf: 0.45 (5:1 ethylacetate/*n*-hexane), yield : 60%, m.p. 105°C); IR (ATR) ν_{\max} 3283 (br) (NH), 3081 (w), 2991 (w), 2947 (w), 1737 (s) (C=O) 1252 (vs), 1017 (vs) cm^{-1} ; $^1\text{H NMR}$ (500 MHz, CDCl_3): δ 2.37 (s, 3H, CH_3), 2.50 (t, $J=2.4$ Hz, 4H, N-CH_2), 3.60 (s, 2H, CH_2), 3.83 (t, $J=2.4$ Hz, 4H, N-CH_2), 6.48 (t, $J=4.7$ Hz, 1H, Ar-H), 7.19 (d, $J=8.3$ Hz, 1H, Ar-H), 7.46 (d, $J=8.4$ Hz, 2H, Ar-H), 7.48-7.49 (m, 1H, Ar-H), 7.81 (d, $J=8.2$ Hz, 2H, Ar-H), 7.88 (d, $J=2.2$ Hz, 1H, Ar-H), 7.94 (brds, 1H, NH), 8.29 (d, $J=4.7$ Hz, 2H, Ar-H) ppm; $^{13}\text{C NMR}$ (125 MHz, CDCl_3) δ 22.3 (CH_3), 43.7 (2x N-CH_2), 53.0 (2x N-CH_2), 62.6 (CH_2), 109.8 (CAr), 119.2 (CAr), 123.9 (CAr), 124.8 (Cq), 127.1 (2xCAr), 129.4 (2xCAr), 130.8 (CAr), 133.5 (Cq), 133.9 (Cq), 136.8 (Cq), 142.6 (Cq), 157.7 (2xCAr), 165.5 (C=O) ppm; HRMS (ESI⁺) m/z calcd for $[\text{C}_{23}\text{H}_{24}\text{BrN}_5\text{O}] + \text{H}^+$ 467.3786, found 468.1215 ($[\text{C}_{23}\text{H}_{24}\text{BrN}_5\text{O}_4] + \text{H}^+$).

2.1.3.2. *N*-(3-Bromo-4-methylphenyl)-4-((2,3,4-trimethoxybenzyl)piperazin-1-yl)methyl)benzamide (Compound 4b)

Pale yellowish gummy solid (This compound was purified by flash column chromatography using DCM/MeOH 10:1 as eluent, Rf: 0.54 (10:1 DCM/MeOH), yield 46.3%; m.p.135°C); IR (ATR): ν_{\max} 3290 (br) (NH), 2936 (m), 2819 (m), 1651 (s) (C=O), 1235 (m), 1093 (vs) cm^{-1} ; $^1\text{H NMR}$ (500 MHz, CDCl_3): δ = 2.37 (s, 3H, CH_3), 2.48 (brds, 8H, N-CH_2), 3.50 (s, 2H, CH_2), 3.55 (s, 2H, CH_2), 3.85 (s, 3H, O- CH_3), 3.86 (s, 3H, O- CH_3), 3.88 (s, 3H, O- CH_3), 5.30, 6.62 (d, $J=8.20$, 1.5 Hz, 1H, Ar-H), 6.64 (d, $J=8.60$, 1H, Ar-H) 6.98 (d, $J=8.60$ Hz, 1H, Ar-H), 7.19-7.21 (dd, $J=8.2$, 0.5 Hz, 1H, Ar-H), 7.27 7.40-7.42 (dd, $J=1.5$ 0.5Hz, 1H) 7.48-7.50 (ddd, $J=8.5$ 1.4, 0.5 Hz, 2H, Ar-H), 7.78-7.88 (ddd, $J=8.5$, 1.7, 0.5 Hz, 2H, Ar-H) ppm; $^{13}\text{C NMR}$ (125 MHz, CDCl_3): δ = 22.29 (CH_3), 52.84 (CH_2), 53.20 (CH_2), 55.95 (2x CH_2) 56.00 (2x CH_2), 60.68 (O- CH_3), 61.13 (O- CH_3), 62.51 (O- CH_3), 106.96 (CAr), 119.10 (CAr), 123.86 (CAr), 124.78 (CAr), 125.16 (CAr), 126.94 (2xCAr), 129.36 (2xCAr), 130.81 (CAr), 133.32 (Cq), 133.87 (Cq), 136.79 (Cq), 142.89 (Cq), 152.63 (Cq), 152.90 (Cq), 165.46 (C=O) ppm; HRMS (ESI⁺) m/z calcd for $[\text{C}_{29}\text{H}_{34}\text{BrN}_3\text{O}_4] + \text{H}^+$ 569.5099, found 569.5200 ($[\text{C}_{29}\text{H}_{34}\text{BrN}_3\text{O}_4] + \text{H}^+$).

2.1.4. General procedure for the synthesis of intermediates containing morpholine (Compound 4c)

0.3 mmol (116.79 mg) of *N*-(3-Bromo-4-methylphenyl)-4-(chloromethyl)benzamide (Compound 3) was taken into a round bottom flask and 2.6 mmol (226.46 mg) morpholine was added onto it. The reaction mixture was sonicated at 55°C for 30 minutes without solvent. After completion of the reaction, the crude product (4c) was recrystallized with ethyl acetate.

2.1.4.1. *N*-(3-Bromo-4-methylphenyl)-4-(morpholinomethyl)benzamide (Compound 4c)

Cream-white, gummy solid; (This compound was purified by crystallization with EtOAc, Rf: 0.7 (7:1 DCM/MeOH), yield 76.7%; m.p.116°C); IR (ATR) ν_{\max} 3268 (s) (NH), 3023 (w), 2920 (m), 1636 (vs) (C=O), 1260 (w), 1036 (vs) cm^{-1} ; $^1\text{H NMR}$ (500 MHz, CDCl_3): δ = 2.38 (s, 3H, CH_3), 2.52 (brds, 4H, N-CH_2), 3.62 (s, 2H, CH_2), 3.75 (t, $J=2.5$ Hz, 4H, O- CH_2), 7.20 (d, $J=8.4$ Hz, 1H, Ar-H), 7.48 (m, 3H, Ar-H), 7.82 (d, $J=8.2$ Hz, 2H, Ar-H), 7.92 (d, $J=2.1$ Hz, 1H, Ar-H), 7.97 (brds, 1H, NH) ppm; $^{13}\text{C NMR}$ (125 MHz, CDCl_3): δ = 22.3 (CH_3), 43.3 (CH_2), 53.5 (CH_2), 62.7 (CH_2), 63.8 (CH_2), 66.6 (CH_2), 119.2 (CAr), 123.9 (CAr), 124.8 (Cq), 127.2 (2xCAr), 129.7 (2xCAr), 130.8 (CAr), 133.8 (Cq), 134.0 (Cq), 136.7 (Cq), 165.4 (C=O) ppm; HRMS (ESI⁺) m/z calcd for $[\text{C}_{19}\text{H}_{21}\text{BrN}_2\text{O}_2] + \text{H}^+$ 390.2942, found 390.1805 ($[\text{C}_{19}\text{H}_{21}\text{BrN}_2\text{O}_2] + \text{H}^+$).

2.1.5. General Procedure for the Synthesis of Imatinib Derivatives (Compound 5-10)

In a 10 mL oven dried schlenk tube, equipped with a rubber septum, 0.214 mmol compound 4a, 4b or 4c, 0.214 mmol corresponding aromatic amine [2-amino-4-methylpyrimidine, 2-aminopyrazine or 2-amino-4-methylpyridine] 0.297 mmol (33.4 mg) Potassium tert-butoxide, 0.01712 mmol (9.9 mg) Xphos, 0.00856 mmol (7.8 mg) Tris (dibenzylideneacetone) dipalladium(0) were added. Subsequently, 1 mL dry toluene and 1 mL dry tert-butanol were added into the tube, and the resulting mixture was heated and stirred at 160°C for 24 h under inert atmosphere. The reaction completion was monitored by TLC. Upon completion of the reaction, the mixture was filtered through celite, washed with DCM, then the solvent was evaporated under reduced pressure. The residue was purified by flash chromatography.

2.1.5.1. *N*-(4-Methyl-3-((4-methylpyrimidin-2-yl)amino)phenyl)-4-((4-(pyrimidin-2-yl)piperazin-1-yl)methyl)benzamide (Compound 5)

Brownish gummy solid; (This compound was purified by flash column chromatography using DCM/MeOH 10:1 as eluent, 0.54 (10:1 DCM/MeOH), yield 40.0%; m.p.89°C); IR (ATR) ν_{\max} 3280 (br) (NH), 3026 (w), 2850 (w), 1651 (s) (C=O), 1219 (w), 1029 (s) cm^{-1} ; $^1\text{H NMR}$ (500 MHz, CDCl_3): δ = 2.32 (s, 3H, CH_3), 2.43 (s, 3H, CH_3), 2.52 (brds, 4H, N-CH_2), 3.49 (brds, 1H, NH), 3.61 (s, 2H, CH_2), 3.84 (t, $J=2.5$ Hz, 4H, N-CH_2), 6.48 (t, $J=$ Hz, 1H, Ar-H), 6.75 (brds, 1H, NH), 7.16-7.21 (m, 1H, Ar-H), 7.44-7.51 (m, 3H, Ar-H), 7.79-7.88 (m, 3H, Ar-H), 8.28-8.30 (m, 3H, Ar-H), 8.38-8.40 (m, 1H,

Ar-H) ppm; ^{13}C NMR (125 MHz, CDCl_3): $\delta = 19.4$ (CH_3), 22.3 (CH_3), 43.6 (2xN- CH_2), 52.9 (2xN- CH_2), 62.6 (CH_2), 109.8 (CAr), 119.1 (CAr), 123.8 (CAr), 124.7 (Cq), 127.0 (3xCAR), 129.3 (3xCAR), 130.7 (CAr), 133.3 (2xCq), 133.8 (Cq), 136.7 (2xCq), 142.5 (Cq), 157.6 (2xCAR), 161.6 (Cq), 165.5 (C=O) ppm; HRMS (ESI⁺) m/z calcd for $[\text{C}_{28}\text{H}_{30}\text{N}_8\text{O}] + \text{H}^+$ 495.2621, found 495.2607 $[(\text{C}_{28}\text{H}_{30}\text{N}_8\text{O}) + \text{H}]^+$.

2.1.5.2. *N*-(4-Methyl-3-((4-methylpyrimidin-2-yl)amino)phenyl)-4-((4-(2,3,4-trimethoxyphenyl)piperazin-1-yl)methyl)benzamide (Compound 6)

Yellowish gummy solid (This compound was purified by flash column chromatography using DCM/MeOH 7:1 as eluent, 0.50 (7:1 DCM/MeOH), yield 58.1%; dcm.p.320°C); IR (ATR) n_{max} 3293 (br) (NH), 2932 (s), 1651 (s) (C=O), 1200 (m), 1093 (vs) cm^{-1} ; ^1H NMR (500 MHz, CDCl_3): $\delta = 2.28$ (s, 3H, CH_3), 2.41 (s, 3H, CH_3), 2.50 (brds, 8H, N- CH_2), 3.52 (s, 2H, CH_2), 3.54 (s, 2H, CH_2), 3.85 (s, 3H, O- CH_3), 3.86 (s, 3H, O- CH_3), 3.88 (s, 3H, O- CH_3), 6.59 (d, J= 5.0 Hz, 1H, Ar-H), 6.62 (d, J= 8.5 Hz, 1H, Ar-H), 6.92 (brds, 1H, NH), 6.99 (d, J= 8.5 Hz, 1H, Ar-H), 7.16 (d, J= 8.3 Hz, 1H, Ar-H), 7.38 (d, J=8.1 Hz, 1H, Ar-H), 7.44 (d, J= 7.3 Hz, 1H, Ar-H), 7.78 (d, J= 8.1 Hz, 2H, Ar-H), 8.03 (brds, 1H, NH), 8.25 (d, J= 5.0 Hz, 1H, Ar-H), 8.33 (d, J= 1.9 Hz, 1H, Ar-H) ppm; ^{13}C NMR (125 MHz, CDCl_3): $\delta = 17.6$ (CH_3), 24.2 (CH_3), 52.7 (2xN- CH_2), 55.9 (2xN- CH_2), 61.2 (CH_2), 106.1 (CAr), 112.3 (CAr), 115.2 (CAr), 123.9 (Cq), 127.0 (CAr), 129.3 (3xCAR), 134.0 (Cq), 136.5 (Cq), 138.0 (Cq), 142.2 (Cq), 152.7 (2xCAR), 161.1 (C=O) ppm; HRMS (ESI⁺) m/z calcd for $[\text{C}_{33}\text{H}_{38}\text{N}_6\text{O}_4] + \text{H}^+$ 597.7271, found 597.7280 $[(\text{C}_{33}\text{H}_{38}\text{N}_6\text{O}_4) + \text{H}]^+$.

2.1.5.3. *N*-(4-Methyl-3-(pyrazin-2-ylamino)phenyl)-4-((4-(pyrimidin-2-yl)piperazin-1-yl)methyl)benzamide (Compound 7)

Yellowish gummy solid (This compound was purified by flash column chromatography using DCM/MeOH 10:1 as eluent, Rf: 0.60 (10:1 DCM/MeOH), yield 50.8%, m.p.143°C; IR (ATR) n_{max} 3291 (br) (NH), 2919 (m), 2812 (w), 1651 (s) (C=O), 1583 (vs), 1546 (s), 1493 (vs), 1445 (s), 1142 (w), 1005 (m) cm^{-1} ; ^1H NMR (500 MHz, CDCl_3): $\delta = 2.39$ (s, 3H, CH_3), 2.53 (brds, 4H, N- CH_2), 3.52 (s, 2H, CH_2), 3.86 (brds, 4H, N- CH_2), 6.50 (t, J= 4.6 Hz, 1H, Ar-H), 7.21 (d, J=8.2 Hz, 2H, Ar-H), 7.28 (brds, 1H, NH), 7.48 (m, 5H, Ar-H), 7.83 (d, J= 7.7 Hz, 2H, Ar-H), 7.91 (s, 1H, ArH), 7.95 (brds, 1H, NH), 8.31 (d, J= 4.6 Hz, 2H, Ar-H) ppm; ^{13}C NMR (125 MHz, CDCl_3): $\delta = 22.3$ (CH_3), 43.7 (2x CH_2), 53.0 (2x CH_2), 62.6 (CH_2), 109.9 (CAr), 119.2 (2xCAR), 123.9 (2xCAR), 124.8 (Cq), 127.1 (2xCAR), 129.4 (2xCAR), 130.8 (2xCAR), 133.5 (Cq), 133.9 (2xCq), 136.8 (Cq), 142.5 (Cq), 157.7 (2xCAR), 161.6 (Cq), 165.5 (C=O) ppm; HRMS (ESI⁺) m/z calcd for $[\text{C}_{27}\text{H}_{28}\text{N}_8\text{O}] + \text{H}^+$ 481.5722, found 481.3640 $[(\text{C}_{27}\text{H}_{28}\text{N}_8\text{O}) + \text{H}]^+$.

2.1.5.4. *N*-(4-Methyl-3-((4-methylpyrimidin-2-yl)amino)phenyl)-4-(morpholinomethyl)benzamide (Compound 8)

Cream-white gummy solid (This compound was purified by flash column chromatography using DCM/MeOH 10:1 as eluent, Rf: 0.40 (10:1 DCM/MeOH), yield 54.8%, m.p.157°C); IR (ATR): $n = 3286$ (br) (NH), 3084 (w), 2922 (m), 2854 (m), 1711 (s) (C=O), 1261 (m), 1006 (w) cm^{-1} . ^1H NMR (500 MHz, CDCl_3): $\delta = 2.32$ (s, 3H, CH_3), 2.38 (s, 3H, CH_3), 2.52 (brds, 4H, N- CH_2), 3.62 (s, 2H, CH_2), 3.98 (t, J= 2.2 Hz, 4H, O- CH_2), 4.03 (brds, 1H, NH), 6.93 (d, J= 2.8 Hz, 1H, ArH), 7.20 (d, J= 3.2 Hz, 1H, Ar-H), 7.48-7.53 (m, 3H, Ar-H), 7.84 (d, J= 4.2 Hz, 2H, Ar-H), 7.92 (s, 1H, ArH), 7.97 (brds, 1H, NH), 8.36 (d, J= 2.8 Hz, 1H, ArH) ppm; ^{13}C NMR (125 MHz, CDCl_3): $\delta = 22.3$ (CH_3), 25.9 (CH_3), 43.5 (N- CH_2), 53.6 (N- CH_2), 62.4 (O- CH_2), 62.6 (CH_2), 66.6 (O- CH_2), 110.2 (CAr), 119.1 (CAr), 123.86 (CAr), 124.8 (Cq), 127.2 (3xCAR), 129.6 (2xCAR), 130.7 (CAr), 133.5 (Cq), 133.9 (Cq), 136.7 (Cq), 156.3 (Cq), 165.3 (Cq), 165.5 (C=O), 168.4 (Cq) ppm; HRMS (ESI⁺) m/z calcd for $[\text{C}_{24}\text{H}_{27}\text{N}_5\text{O}_2] + \text{H}^+$ 418.2243, found 418.1865 $[\text{C}_{24}\text{H}_{27}\text{N}_5\text{O}_2] + \text{H}^+$.

2.1.5.5. *N*-(4-Methyl-3-((4-methylpyridin-2-yl)amino)phenyl)-4-(morpholinomethyl)benzamide (Compound 9)

Cream-white gummy solid, (This compound was purified by flash column chromatography using DCM/MeOH 7:1 as eluent, Rf: 0.60 (7:1 DCM/MeOH), yield 49.4%, m.p.155-157°C); IR (ATR) n_{max} 3292 (br) (NH), 2919 (m), 2852 (m), 1652 (s) (C=O), 1605 (vs), 1563 (m), 1524 (m), 1417 (w), 1261 (m), 1112 (vs), 1006 (vs), 865 (vs), 801 (vs) cm^{-1} ; ^1H NMR (500 MHz, CDCl_3): $\delta = 2.33$ (s, 3H, CH_3), 2.38 (s, 3H, CH_3), 2.52 (t, J= 2.2 Hz, 4H, N- CH_2), 3.65 (s, 2H, CH_2), 3.98 (t, J= 2.2 Hz, 4H, O- CH_2), 4.00 (brds, 1H, NH), 6.54 (d, J= 4.1 Hz, 1H, ArH), 6.90 (d, J= 2.8 Hz, 1H, ArH), 7.20 (d, J= 3.2 Hz, 1H, Ar-H), 7.48-7.53 (m, 3H, Ar-H), 7.88 (d, J= 4.2 Hz, 2H, Ar-H), 7.90 (s, 1H, ArH), 7.99 (brds, 1H, NH), 8.32 (d, J= 2.8 Hz, 1H, ArH) ppm; ^{13}C NMR (125 MHz, CDCl_3): $\delta = 22.3$ (CH_3), 25.7 (CH_3), 42.4 (N- CH_2), 55.92 (N- CH_2), 62.4 (O- CH_2), 63.9 (CH_2), 68.5 (O- CH_2), 109.0 (CAr), 110.3 (CAr), 119.4 (CAr), 123.9 (CAr), 125.0 (Cq), 126.9 (3xCAR), 129.5 (2xCAR), 130.8 (CAr), 133.6 (Cq), 133.8 (Cq), 136.5 (Cq), 156.0 (Cq), 165.4 (Cq), 165.5 (C=O), 168.4 (Cq) ppm; HRMS (ESI⁺) m/z calcd for $[\text{C}_{25}\text{H}_{28}\text{N}_4\text{O}_2] + \text{H}^+$ 417.5234, found 417.5270 $[(\text{C}_{25}\text{H}_{28}\text{N}_4\text{O}_2) + \text{H}]^+$.

2.1.5.6. *N*-(4-Methyl-3-((4-methylpyridin-2-yl)amino)phenyl)-4-((4-(2,3,4-trimethoxybenzyl)piperazin-1-yl)methyl)benzamide (Compound 10)

Orange-brownish gummy solid, (This compound was purified by flash column chromatography using DCM/MeOH 7:1 as eluent, Rf: 0.54 (7:1 DCM/MeOH), yield 44.6%, m.p.87°C); IR (ATR) n_{max} 3295 (NH), 2936, 2811, 1652 (C=O), 1140, 1008

cm⁻¹; ¹H NMR (500 MHz, CDCl₃): δ = 2.24 (s, 3H, CH₃), 2.41 (s, 3H, CH₃), 2.53 (brds, 8H, N-CH₂), 3.45 (s, 2H, CH₂), 3.54 (s, 2H, CH₂), 3.85 (s, 3H, O-CH₃), 3.86 (s, 3H, O-CH₃), 3.88 (s, 3H, O-CH₃), 6.49 (d, J = 5.0 Hz, 1H, Ar-H), 6.59 (d, J = 5.0 Hz, 1H, Ar-H), 6.62 (d, J = 8.5 Hz, 1H, Ar-H), 6.92 (brds, 1H, NH), 7.01 (d, J = 8.5 Hz, 1H, Ar-H), 7.16 (d, J = 8.3 Hz, 1H, Ar-H), 7.40 (d, J = 8.1 Hz, 1H, Ar-H), 7.44 (d, J = 7.3 Hz, 2H, Ar-H), 7.79 (d, J = 8.1 Hz, 2H, Ar-H), 8.03 (brds, 1H, NH), 8.26 (d, J = 5.0 Hz, 1H, Ar-H), 8.33 (d, J = 1.9 Hz, 1H, Ar-H) ppm; ¹³C NMR (125 MHz, CDCl₃): δ = 20.6 (CH₃), 24.1 (CH₃), 53.0 (2xN-CH₂), 55.9 (OCH₃), 56.3 (2xCH₂), 60.3 (OCH₃), 61.1 (OCH₃), 62.5 (2xN-CH₂), 106.9 (CAr), 109.8 (CAr), 112.3 (CAr), 112.7 (CAr), 114.9 (CAr), 123.5 (Cq), 125.3 (CAr), 127.0 (3xCAr), 129.3 (2xCAr), 130.8 (CAr), 134.0 (Cq), 136.5 (Cq), 138.0 (Cq), 142.2 (Cq), 142.4 (Cq), 150.2 (2xCq), 157.4 (CAr), 160.1 (Cq), 165.5 (Cq), 168.3 (C=O) ppm; HRMS (ESI+) m/z calcd for [C₃₅H₄₁N₅O₄]+H⁺ 596.7391, found 596.7520 ([C₃₅H₄₁N₅O₄]+H)⁺.

2.2. Cell Culture

2.2.1. Chemicals and Instruments

K562, Jurkat, Molt-4, and Nalm-6 cell lines were cultured in RPMI-1640 medium (ECM2001, Euroclone), Reh cell line was cultured in DMEM medium (LM-D1111- Biosera) Hek293T cell line was cultured in IMDM medium (AL070A - HiMedia) supplemented with 10% heat-inactivated fetal bovine serum (F7524-Merck & Co., USA), penicillin and streptomycin (P4333-Sigma Aldrich). K562, Jurkat and Molt-4 cell lines were seeded as 4x10⁵/ml, Reh and Nalm-6 cell lines were seeded 5x10⁵/ml, Hek293T cell line was seed as 2x10⁵/ml. All cells were incubated at 5% CO₂ and 37 °C. All cell lines were kindly provided by Dr. M. Sayitoglu and Dr. Ö. Hatirnaz-Ng from Acibadem University.

2.2.1.1. In vitro toxicity assay

MTT assay [37] was used to evaluate the growth inhibition percentage of the newly synthesized imatinib compounds against different types of leukemia cell lines (K562, Nalm-6, Molt4, Reh and Jurkat) and control cell line non-leukemia cell line (Hek293T).

MTT assay is a 3-day test. On the first day, cell count was performed in Bio Rad TC-20 device with the help of trypan blue, each cell line was prepared by diluting to the specified concentrations and seeded in a 96-well plate as 100µL to each well and incubated for 1 day.

Each compound was solved in DMSO, their stock solutions (33.3, 10, 5, 1 mM, and 300 µM) were prepared by diluting with the same solvent and they were stored under -20°C when they were not used.

On the second day, stock solutions were subsequently diluted to various concentrations (0.3–200 µM) with related medium prior to experiments. Specified concentrations of the compounds were seeded in a 96-well plate as 100µL to each well and incubated for 24 h.

After incubation (on the third day), to precipitate leukemia cells, the cell plate was centrifuged at 1500 rpm for 5 min. Then, 100 µL of supernatant was removed from each well carefully and 10 µL of MTT solution (5 mg/mL) was added to each well and incubated at 37 °C for 4 h. The 50 µL of supernatant was discarded from each well and 100 µL of DMSO was added to dissolve the formazan. Plates were shaken for 45 min to dissolve the dye. Then the optical density of each well was measured by using Thermo VarioSkan Flush Multimode Reader Quantum ST5-1100 at 570 nm wavelength.

Subsequently, viability rate of the cells at each concentration, as percentage, was determined by following formula (1):

$$\text{Viability rate (\%)} = 100 - \left[\frac{(\text{OD}_{(\text{control})} - \text{OD}_{(\text{sample})})}{\text{OD}_{(\text{control})}} \times 100 \right].$$

OD = Optical Density

2.2.1.2. Statistical Analyses for IC₅₀

The IC₅₀ values were calculated by using GraphPad Prism. All the data presented as the mean of 6 replicates. Results were analyzed and illustrated with Graph Pad Prism (version 5; GraphPad Software, San Diego, CA, USA). Statistical analysis was performed using dose-response inhibition, log(inhibitor) vs response-variable slope, least squares (ordinary) fit.

2.3. ABL1 Expression analysis

Raw data generated using Affymetrix Human Gene 1.0 ST Array were collected from GEO (Gene Expression Omnibus) using the accession numbers GSE139094 (Hek293T), GSE48558 (Jurkat, K562, Nalm-6 and Reh) and GSE26790 (Molt-4). The raw data were processed using the RMA (Robust Multi-array Average) method, which is part of the R package oligo [38] and the batch effect was removed using the limma package [39]. The Affymetrix Probe IDs were mapped to Ensembl IDs with the help of hugene10sttranscriptcluster.db annotation package in R. The normalized and log₂-transformed expression values for the gene ABL1 were extracted using the Ensembl ID ENSG0000097007. To assess whether a difference exists in the expression level of ABL1 among the cell lines, we performed one-way ANOVA (analysis of variance) assuming unequal variances.

2.4. Molecular Docking

2.4.1. Prediction of Target Protein

Putative targets for the newly synthesized imatinib analogs were predicted using SEA (Similarity Ensemble Approach, <https://sea.bkslab.org/>) online search tool provided by Shoichet Laboratory in the Department of Pharmaceutical Chemistry at the University of California [40]. For this, SMILES (Simplified Molecular-Input Line-Entry System) representations for the derivatives were generated and used as search keys to the SEA server that uses chemical similarity to find protein targets (see Table-S3).

2.3.2. Crystal Structures and Docking Procedure

In order to assess which conformation of ABL1 and BRAF kinases our newly synthesized compounds bind to, we performed molecular docking simulations using 8 and 7 different crystal structures of kinase domains of wild type ABL1 and BRAF respectively. The properties of the structures used in this study together with the original ligands that are bound to the structures are given in Table S4 and Table S6.

We used the chemical toolbox Open Babel 2.4.1[41] in order to build the initial conformations of the compounds from their SMILES representations. The target protein structures (see Table S5) and compounds were prepared for docking using the AutoDock Tools version 1.5.6 [42]. AutoTors utility of AutoDock Tools was used for definition of the torsions of the compounds. All torsions except for amide and ring torsions were treated as flexible. Gasteiger atomic charges [43] were assigned to both the protein and the compounds. The nonpolar hydrogen atoms were merged while the polar hydrogen atoms were kept explicit.

Extensive docking simulations were performed using the program AutoDock 4.2 [42]. Grid maps were generated with 0.375Å spacing by the AutoGrid program. The grid center was chosen to coincide with the center of the original ligand in the crystal structure. Grid dimensions (70Å x 70Å x 70Å) that span the binding pocket in three dimensions were computed.

Standard Lamarckian genetic algorithm protocol was used with default settings, except for the number of energy evaluations and the number of independent runs, which were increased to obtain more reliable results. We started molecular docking simulations with 25 million energy evaluations for imatinib and its newly synthesized 6 analogs. We assessed the convergence of a docking simulation by performing clustering analysis of the resulting docking conformations where we used a root mean square deviation of 2 Å as cut-off. We assumed that the docking simulation was converged when 20% of the 100 independent runs resulted in the same binding conformation. When this condition was not met, we increased the maximum number of energy evaluations gradually. Due to their relatively high number of torsions (10 for compound 6 and 11 for compound 10), we performed additional docking simulations for the compounds 6 and 10 where we set the maximum number of energy evaluations to 30, 40, and 50 million. For the docking simulations of imatinib, Compound 5, Compound 7, Compound 8 and Compound 9; 25 million of maximum number of energy evaluations sufficed. However, for all reported results, a maximum number of energy evaluations of 40 million was used. The starting point of the ligand was generated randomly, in all docking simulations.

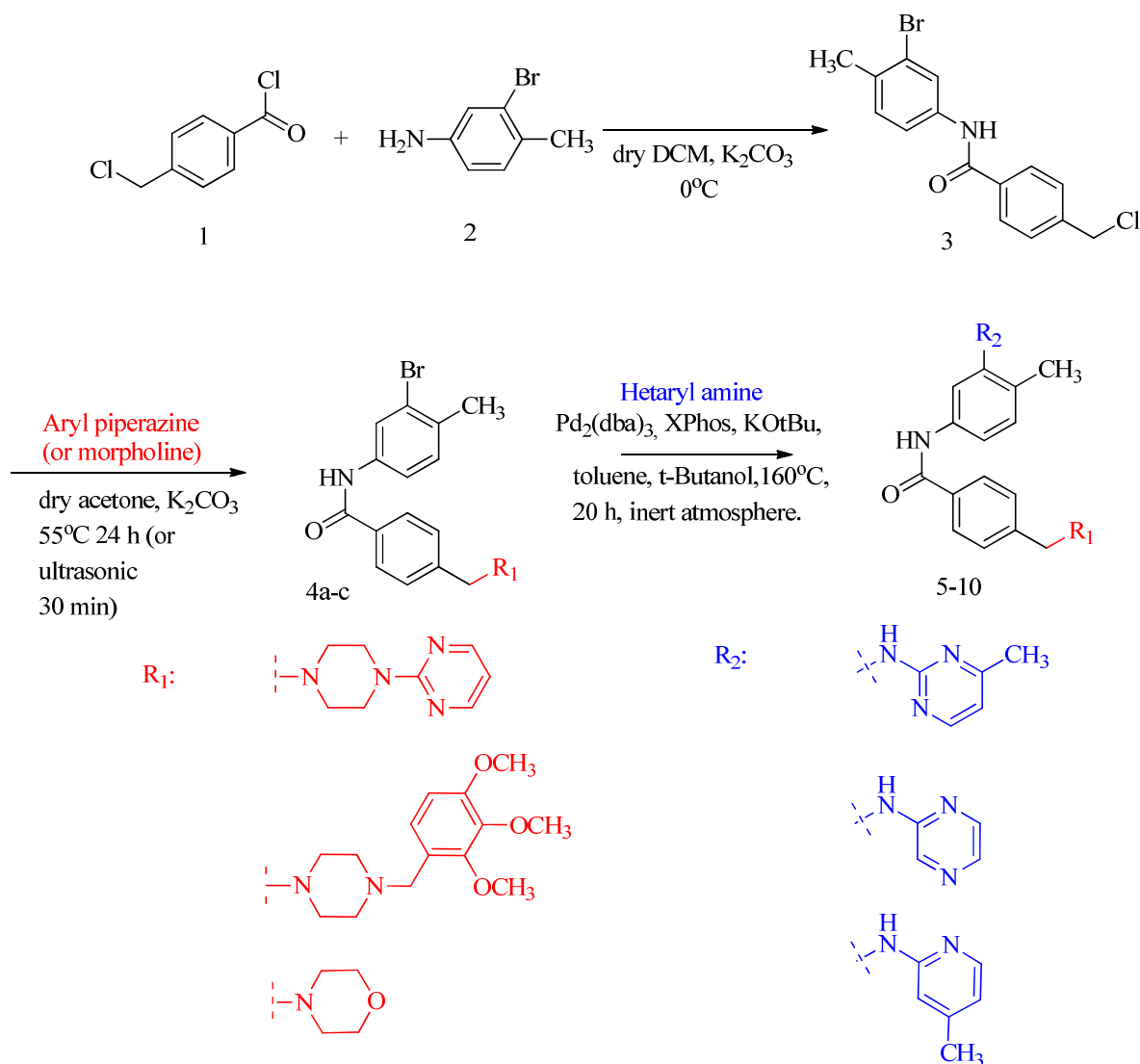
3. Results and Discussion

3.1. Chemistry

3-step synthesis of novel imatinib derivatives was performed by a substitution reaction (S_N2) with Compound-3 [20-21] and various cyclic secondary amine compounds and then the obtained bromobenzamide intermediates (Compound 4a-c) were reacted with different hetaryl primary amines in the conditions of Buchwald Hardwing coupling reaction and Compound 5-10 were obtained at 40.0%–58.1% yields. The general procedure was outlined in Scheme (see Table S1). The structures of the target compounds 5-10 were elucidated by FT-IR, ^1H NMR and ^{13}C NMR, and HRMS (ESI⁺) analyses (see Figure S1-S43).

For preparation of compound 4a, 2-(1-piperazinyl)pyrimidine was used as an aryl piperazine group in synthesis of compound 5 and 7; because pyrimidine and its derivatives are found in nucleobases which composed DNA and RNA and they have broad spectrum of biological activities including anticancer activity [44]. For preparation of compound 4b, 1-(2,3,4-trimethoxybenzyl)piperazine dihydrochloride (called also as Trimetazidine dihydrochloride) was used as an aryl piperazine group, in synthesis of compounds 6 and 10. It was selected due to its antineoplastic [45] properties. For preparation of compound 4c, morpholine was used as cyclic secondary amine group, because morpholine moiety also plays critical role in several inhibition activities and used as anticancer agents [46–48].

The FTIR spectrum of compounds 5-10 showed characteristic NH and C=O peaks at 3200 and 1650 cm^{-1} , respectively. This situation confirms that there was a benzamide structure in the molecules.



Scheme. Synthesis route of novel imatinib derivatives (compound 5-10).

When the results of the 1H NMR spectra were examined, the peaks of the $-CH_3$ (methyl) groups on the pyridine, pyrimidine and benzene rings were observed individually between 2.28–2.39 ppm. The broad peak observed around 2.50 ppm belongs to the $-N-CH_2$ that form the piperazine and morpholine rings. However, the peaks observed at 3.50 ppm indicate $-N-CH_2$, the part of the piperazine and morpholine rings attached to the benzamide molecule. Also in the same circles indicates $-CH_2$ where the trimethoxyphenyl ring is attached to the piperazine (compounds 6 and 10).

The peaks of $-OCH_3$, which were substituents of the same compounds, were around 3.80–3.95 ppm. The two NH peaks in the molecules were observed between 3.48–4.02 and 6.75–6.92 ppm. Multiple peaks were appeared in the range 7.00–8.33 ppm due to aromatic hydrogen atoms.

In ^{13}C NMR spectra, the peaks belong to aliphatic ($-CH_3$, $-CH_2-$) parts were observed between 20–65 ppm and the peaks of the aromatic parts were upward 100 ppm. Carbonyl peak of amide was seen around 165 ppm.

3.2. Characteristics of Newly Synthesized Compound According to Lipinski's Rule of Five

Because oral using of pharmaceutical compounds is easier, the new molecules were evaluated by Lipinski Rule of 5, using Medchem Designer program and <https://www.molinspiration.com>, comparing with imatinib, (see Table 1) Compound-6 and 10 slightly exceed the rules due to MW > 500 g/mole and RB is higher than 10 for compound-10.

Note: Calculation of Molecular Properties and Bioactivity Score [online]. Website <https://www.molinspiration.com/cgi-bin/properties>. [accessed 10 May 2021]

Table 1. Values of synthesized compounds found according to Lipinski rules.

Compound	Molecular weight (g/mole)	MlogP ^(a)	HBA ^(b)	HBD ^(c)	T_PSA (Å ²) ^(d)	RB ^(e)
4a	466.388	3.726	6	1	61.36	5
4b	568.52	2.939	7	1	63.27	9
4c	389.22	3.166	4	1	41.57	4
5	494.603	3.191	9	2	99.17	7
6	596.734	2.377	10	2	101.08	10
7	480.576	2.18	9	2	99.17	7
8	417.514	2.862	7	2	79.38	6
9	416.526	3.017	6	2	66.49	6
10	595.746	2.477	9	2	88.19	11
imatinib	493.615	2.907	8	2	86.28	7

(a) Moruguchi octanol: water partition coefficient, (b) hydrogen bond acceptor, (c) hydrogen bond donor, (d) topological polar surface area, (e) rotatable bonds.

3.3. In vitro anti-proliferative activity

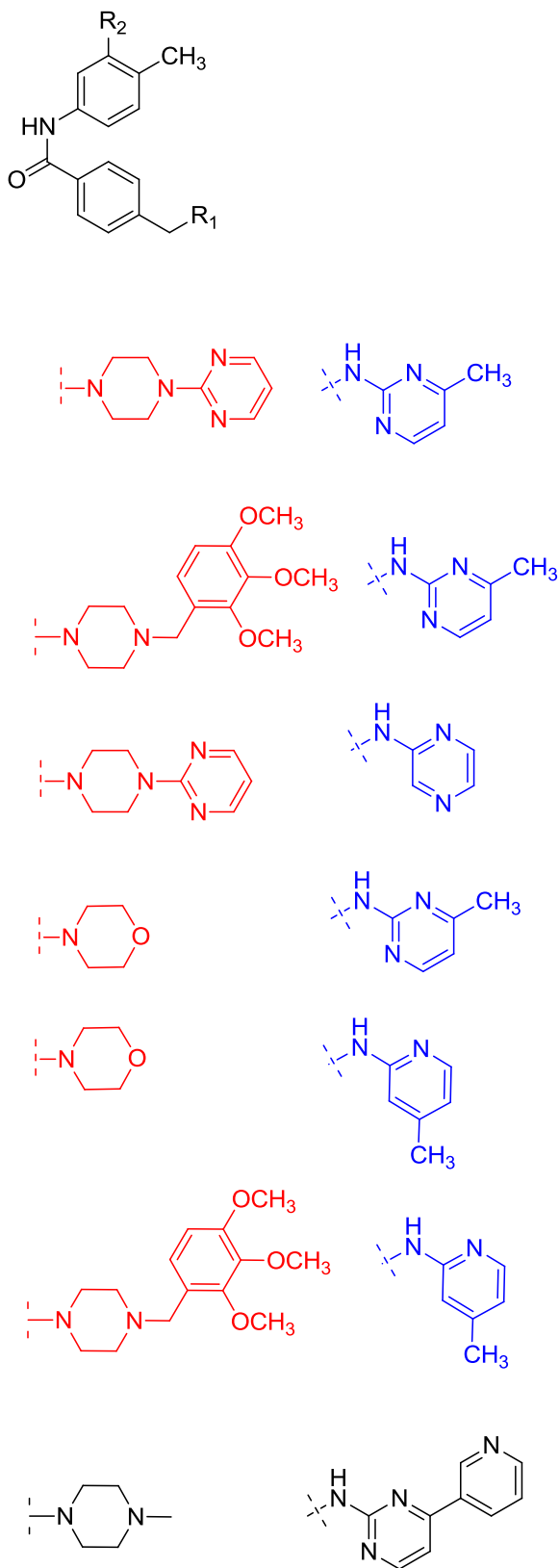
To evaluate in-vitro anti-cancer activity of the newly synthesized compounds, they were tested by using the MTT assay in the BCR-ABL positive leukemic cell line (K562), BCR-ABL negative leukemic cell lines (Nalm-6, Molt-4, Reh and Jurkat), and non-leukemic human embryonic kidney tissue (Hek293T) cell line. All cells were incubated with various concentrations (between 0.3 and 200 μM) of the derivatives for 24 h, and imatinib was used as the reference compound. The viability rate of each concentration was calculated by the formula stated in material and methods, the viability rate results for each cell were presented in Table S2 and Figure S44. Accordingly, after the test, only the compounds viability rate less than 50% were considered for calculation IC₅₀. The corresponding results for IC₅₀ values presented in Table 2. And viability rate (at 200 μM) graphics in different cell lines were shown in Figure 2.

In K562 cells, after 24 h incubation with the compounds, the lowest viability rate was observed with imatinib, around 30% (29.7%). Among the newly synthesized derivatives, only compound 10 (38.7%), and in less extent compound 9 (45.0%), were also able to achieve lower viability rate in the K562 cell line. Moreover, the IC₅₀ value of compound 10 (35.04 μM) is lower compared to imatinib (78.37 μM) indicating K562 cell line is more sensitive to the newly synthesized derivative than the reference compound. The other derivatives were significant less effective in reducing the number of living cells compared to imatinib.

In BCR-ABL negative cell lines, a decrease in the number of viable cells was also observed with drug administration. In consistent with K562 cells, compound 6, 9, and 10 exhibited anti-proliferative activities in nearly all BCR-ABL negative cell lines. In Nalm-6 and Jurkat cell lines, 50% decrease was observed in the viable cells. Especially for Nalm-6, after incubation with compound-6 and compound-9 percentage of viable cells was calculated as 42.8% and 39.2%. The IC₅₀ values were 47.96 μM and 1.639 μM respectively. The observed viability rate values of compound 10 and imatinib were very close to each other, compound-10-administered cells showed viability as 28.7% with IC₅₀ of 28.73 μM and imatinib-administered cells showed viability as 29.0% with IC₅₀ of 16.09 μM in Nalm6 cells. The effects of imatinib and its derivatives on Jurkat cells were similar to the results obtained with Nalm-6 cells. Again, the best decrease in the number of viable cells was obtained with imatinib (16.6% viability). In Molt-4 the reduction in the number of viable cells was moderate or low for all the compounds. Interestingly, only compound-10, showed less 50% viability on Molt-4 cells. Reh cells appear to be less sensitive to the newly synthesized derivatives. Up to about 60% viability was seen in Reh cells, including imatinib (see Figure S44).

In general, according to MTT assay results, the compounds with 2,3,4-trimethoxybenzyl in aryl piperazine group (R1, Scheme), (compound 6 and 10) exhibited high anticancer activity on all cell lines, except Reh. Whereas, instead of aryl piperazine ring, morpholine substituted analogs (compound 8 and 9) displayed somewhat relatively lower activity, and the analogs with pyrimidine ring in aryl piperazine group (compound 5 and 7) were characterized by very poor activity.

Also, the results show that there was not so much difference between 2-aminopyrimidine and 2-aminopyrazine heterocyclic ring system (R2, Scheme), (compound 5-7).

Table 2. The chemical structures and IC₅₀ values (μM) of the compounds 5-10 against K562, Nalm6, Molt4, Reh, Jurkat, Hek293T.

All experiments were performed in six replicates in the range of 0.3–200μM.

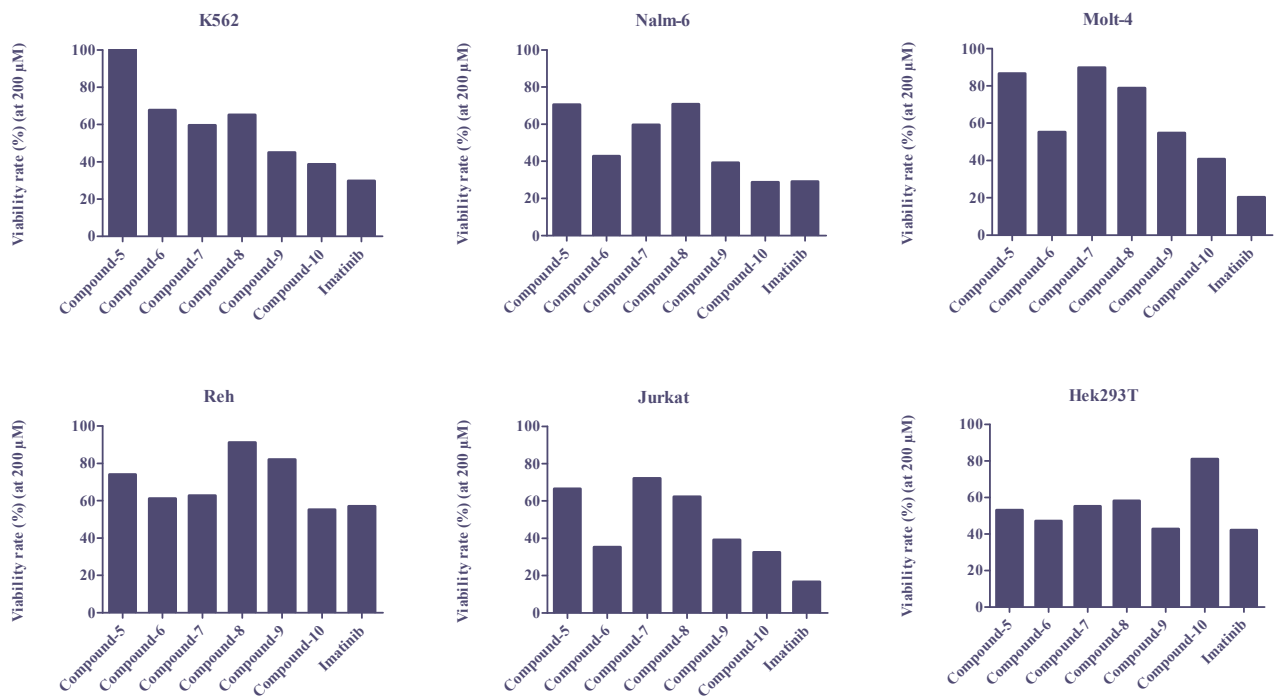


Figure 2. Viability rate of the compound 5-10 and imatinib (at 200 µM) in different cell lines.

High growth inhibitory activity was also obtained for pyrimidine-substituted derivatives. And also, the pyridine linked analogs (compound 9-10) exhibited high anticancer activity than pyrimidine and pyrazine group.

3.4. ABL1 Expression analysis

Although imatinib was specifically designed as a drug for the BCR-ABL fusion gene product, our results showed that it was also effective in BCR-ABL negative cell lines. One explanation can be given that all the compounds, including imatinib mesylate, are targeted to the kinase domain of ABL protein. The ABL protein, encoded by the ABL1-gene, is a non-receptor tyrosine kinase, which is constitutively expressed in all cells. ABL protein is activated in response to several stimuli such as cell adhesion, cytokines, growth factors, DNA damage, and other signals. Activation of ABL protein will result in migration, cell proliferation, differentiation and apoptosis. Although the BCR-ABL negative cell lines do not express the fusion protein, they all expressed the endogenous ABL protein, which can be targeted also by the compounds. To support this, we have compared the gene expression of ABL1 in the cell lines by microarray data available in the literature. Indeed, we observed that ABL1 gene is highly expressed in these cell lines, with the highest in K562 cell line.

Secondly, other tyrosine kinase proteins with similar kinase domain as the ABL1 protein can also be targeted by the compounds as it is predicted with the SEA search tool.

Figure 3 depicts the expression level of the gene ABL1 in the cell lines. The mean expression level for ABL1 varies between 8.3 (Jurkat) and 9.1 (K562). Even though the one-way ANOVA results suggest significant difference (p -value < 0.01), the log₂ fold change values (< 0.8) we obtained from binary comparisons support no difference in ABL1 expression level among the cell lines.

The comparable expression level of ABL1 in the studied cell lines may explain why the compounds 6, 9, and 10 show no cell line specific inhibitory effect.

3.5. Molecular docking

3.5.1. Protein targets for novel imatinib analogs

SEA [40] search tool predicted several proteins as target for the novel imatinib analogs (see Table S4). We picked three most appropriate targets that are common to lists of imatinib and its newly synthesized analogs and decided to further assess them using molecular docking simulations. Among our 3 putative targets, which are Atypical chemokine receptor 3 (P25106), Serine/threonine-protein kinase BRAF (Uniprot ID: P155056) and BCR/ABL p210 fusion protein (A1Z199), Atypical chemokine receptor 3 does not have a crystal structure; hence, we could not perform molecular docking simulations for this protein.

BCR/ABL fusion protein has a constitutively activated ABL tyrosine kinase domain. Imatinib inhibits the catalytic activity of BCR/ABL by binding to an inactive conformation of the ABL kinase domain [49]. Since our newly synthesized

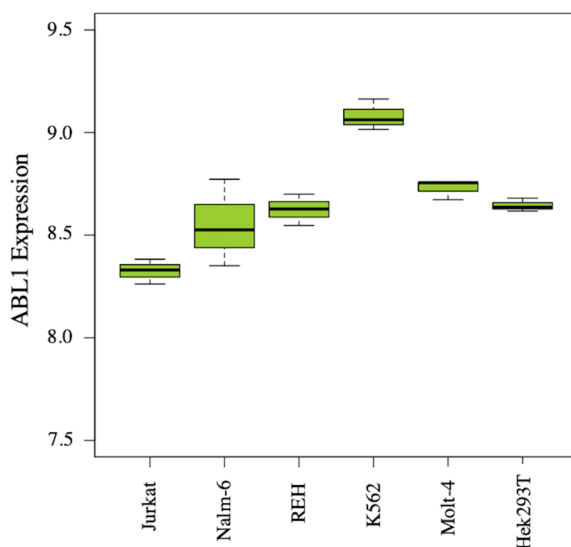


Figure 3. Boxplot of normalized and log₂-transformed expression values for Abl1. The figure was generated using graphics package in R version 3.6.3.

compounds are analogs of imatinib, it is not surprising that ABL kinase is one of the putative targets for our compounds. Superposition of various structures reported, and molecular dynamic simulation studies performed show a great conformational flexibility in ABL protein kinase [49–51]. This conformational plasticity is the reason for the differences in inhibitor binding site, which has been exploited for inhibitor selectivity and affinity optimization. The conformation of the DFG motif has long been known for its effect on the binding pocket. Four main conformations have been reported for the highly conserved DFG motif. Those conformations can be listed as the active conformation, the DFG-out conformation, the DFG-flip conformation and the Src-like inactive conformation. We evaluated all crystal structures of wild-type human ABL kinase domain in the Protein Databank [52–53] and selected 8 of them for molecular docking analysis (see Table S5). These selected structures represent inactive DFG-out conformation [2HYY [51], 2E2B [54], 2HZ0 [51], 3CS9 [55] and 3UE4 [56]], Src-like inactive conformation (4CY8 [57]), intermediate DFG-flip conformation (2HZI [51]) and active conformation (2HZ4 [51]).

Table 3 summarizes the results of the docking simulations of imatinib and its 6 newly synthesized analogs to the 8 different conformations of wild-type human ABL kinase domain. We assessed the reliability of docking results using the percentage of independent runs that converge to the same binding conformation. We assumed a docking simulation result reliable when at least 20% of the independent runs resulted in this particular binding conformation (see Table 3).

This assumption is based on the re-docking calculations that we performed where we docked the original ligands to the protein conformations found in the crystal structures. The sizes of the clusters that we obtained from the re-docking calculations vary between 20 and 100 conformations (see Table S5 and Table S7). Our results presented in Table 3 suggest that imatinib binds to different conformations of ABL however with varying free energies of binding (9.6 – 14.7 kcal/mol). According to the free energies given in the table, imatinib prefers DFG-out conformations of the ABL kinase domain, which is also well reported in the literature [49]. The analog compounds 5, 7, 8, 9 and 10 have a similar tendency with imatinib. However, compound 6 seems to prefer the intermediate conformation where the DFG motif adopts a flipped conformation (see Table 3). Among all the newly synthesized analogs compound 10 has the most favorable free energy of binding (–14.2 kcal/mol) that is closest to the free energy of binding for imatinib (–14.7 kcal/mol). Evaluating molecular docking and MTT assay results together we decided to compare the interactions of imatinib and compound 10 with ABL kinase domain in details. As provided in Figure 4, two molecules adopt overall a similar binding mode despite some local differences. The common rings (the methylbenzene, the benzamide and the N-methylpiperazine rings) between two molecules adopt exactly the same conformation and contribute to the same type of interactions. The overlapping in binding modes is also true for Compound 5, 7, and 8 (see Figure S45, S47 and S48) and partially true for Compound 9 (see Figure S49). However, compared to imatinib, compound 6 adopts a very distinct binding mode (see Figure S46).

Table 3. The results of molecular docking to wild type human ABL1 kinase domain. Binding free energies (ΔG) correspond to the highest-ranking conformation of the largest cluster. The energy values are in kcal/mol. Number in parenthesis shows the percentage of independent runs that resulted in the same docked conformation. Values depicted in gray correspond to the docking simulations that did not meet our convergence criterion.

Structures	ΔG for compounds (kcal/mol)						
	5	6	7	8	9	10	Imatinib
2HYY ^[a]	–13.0 (35%)	–10.1 (15%)	–13.0 (92%)	–12.0 (62%)	–12.1 (98%)	–14.2 (42%)	–14.7 (34%)
2E2B ^[b]	–13.0 (49%)	–10.5 (11%)	–12.8 (90%)	–11.9 (81%)	12.1 (96%)	–13.9 (45%)	–14.5 (57%)
2HZ0 ^[c]	–13.6 (43%)	–9.5 (6%)	–13.3 (75%)	–12.4 (64%)	–12.6 (67%)	–11.6 (9%)	–14.6 (78%)
3CS9 ^[d]	–9.4 (33%)	–9.6 (12%)	–12.9 (49%)	–10.9 (59%)	–11.3 (79%)	–12.8 (30%)	–13.1 (38%)
3UE4 ^[e]	–9.8 (20%)	–10.5 (8%)	–8.2 (13%)	–9.1 (42%)	–8.9 (47%)	–11.2 (21%)	–10.1 (34%)
4YC8 ^[f]	–10.1 (15%)	–10.2 (8%)	–9.7 (36%)	–9.0 (35%)	–8.9 (46%)	–9.9 (22%)	–9.6 (25%)
2HZI ^[g]	–11.3 (23%)	–11.8 (20%)	–11.2 (22%)	–11.2 (91%)	–10.1 (38%)	–11.1 (21%)	–12.1 (51%)
2HZ4 ^[h]	–8.7 (15%)	–11.0 (12%)	–9.2 (29%)	–9.3 (66%)	–8.8 (39%)	–9.7 (26%)	–9.9 (56%)

[a] Human Abl kinase domain in complex with imatinib, [b] Crystal structure of the c-Abl kinase domain in complex with INNO-406, [c] Abl kinase domain in complex with NVP-AEG082, [d] Human ABL kinase in complex with nilotinib, [e] Structural and spectroscopic analysis of the kinase inhibitor bosutinib binding to the Abl tyrosine kinase domain, [f] C-Helix-Out Binding of Dasatinib Analog to c-Abl Kinase, [g] Abl kinase domain in complex with PD180970, [h] Abl kinase domain unligated and in complex with tetrahydrostaurosporine.

Similar to ABL kinase, for BRAF kinase different conformational states reported in literature as well; inactive DFG-out conformation [1UWH[59], 4KSP[60] and 4JVG[61]], Src-like inactive conformation [3C4C[62] and 5CSW[63]] and active conformation [2FB8[64] and 3D4Q[65]]. The results of molecular docking to wild type human BRAF kinase domain is tabulated in Table 4. As seen in the table, the new imatinib analogs have lower affinities for BRAF kinase compared to ABL kinase.

4. Conclusion

The anti-proliferative activities in vitro showed that compound 10 gives close results to imatinib. Although imatinib was specifically designed as a drug for the BCR-ABL fusion gene, our results showed that it was also effective for Jurkat and

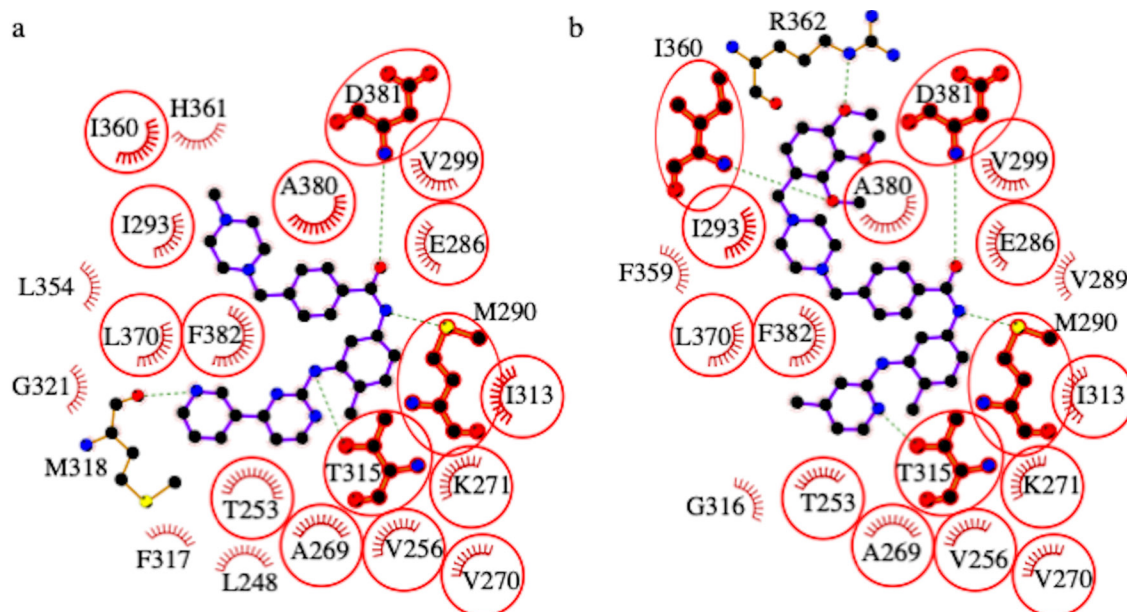


Figure 4. Detailed interactions of ABL1 kinase domain with imatinib (a) and Compound 10 (b). The common contact residues are highlighted with red circles. Hydrogen bonds are indicated by dashed lines, while the hydrophobic interactions are represented by an arc with spokes. The figure was generated using LigPlot+ v.2.2 [58].

Table 4. The results of molecular docking to wild type human BRAF kinase domain. Binding free energies (ΔG) correspond to the highest-ranking conformation of the largest cluster. The energy values are in kcal/mol. Number in parenthesis shows the percentage of independent runs that resulted in the same docked conformation. Values depicted in gray correspond to the docking simulations that did not meet our convergence criterion.

ΔG for compounds (kcal/mol)						
Structures	5	6	7	8	9	10
1UWH ^[a]	-11.7 (39%)	-10.7 (11%)	-12.0 (32%)	-10.5 (56%)	-11.2 (76%)	-11.3 (10%)
4KSP ^[b]	-11.1 (10%)	-9.8 (16%)	-10.1 (52%)	-10.0 (45%)	10.7 (52%)	-11.5 (20%)
4JVG ^[c]	-10.8 (56%)	-8.7 (9%)	-11.0 (55%)	-10.2 (27%)	-9.8 (54%)	-10.3 (14%)
3C4C ^[d]	-8.9 (22%)	-10.4 (15%)	-10.2 (20%)	-7.6 (23%)	-9.5 (43%)	-9.5 (24%)
5C5W ^[e]	-8.7 (29%)	-10.8 (16%)	-11.3 (6%)	-8.5 (52%)	-9.6 (86%)	-11.5 (45%)
2FB8 ^[f]	-9.7 (35%)	-8.9 (11%)	-9.0 (15%)	-8.7 (42%)	-8.8 (50%)	-9.5 (8%)
3D4Q ^[g]	-9.3 (24%)	-9.8 (16%)	-9.5 (13%)	-9.6 (37%)	-8.6 (30%)	-8.4 (13%)

[a] Solution structure of the DEP domain of mouse pleckstrin, [b] Crystal Structure of Human B-raf bound to a DFG-out Inhibitor TAK-632, [c] B-Raf Kinase in Complex with Birb796, [d] B-Raf Kinase in Complex with PLX4720, [e] 1.25 Å resolution structure of an RNA 20-mer, [f] Structure of the B-Raf kinase domain bound to SB-590885, [g] Pyrazole-based inhibitors of B-Raf kinase.

Nalm-6 cells, which are BCR-ABL negative cells. We also found that Compound 6 and 9 were relatively effective in Nalm-6 and Jurkat cells.

Except for compound 6, the newly synthesized imatinib analogs prefer a DGF-out conformation of ABL kinase. Among all newly synthesized analogs, compound 10 has the highest affinity for ABL kinase domain which is comparable to the affinity of imatinib for the ABL kinase domain. Analysis of molecular interactions revealed similarities between binding patterns of compound 10 and imatinib. Despite predicted to be a potential target, the new imatinib analogs have lower affinities for BRAF kinase compared to ABL kinase.

To sum up, this study introduces a novel successful design for imatinib derivatives as the potential antitumor agents. These compounds possess a simple molecular structure and are easy to synthesize, which makes them very attractive for further exploration as kinase inhibitors with application in cancer.

Acknowledgements

We would like to offer special thanks to Prof. Dr. Nuket Ocal, who, unfortunately, is no longer with us, for her valuable contribution to this project. This study was supported by the Research Fund of Yıldız Technical University (Project Number: FYL-2017-3173).

References

1. Tuğlu MM, Melli M. İmatinib: Etki Mekanizması ve Direnç Geliştirme Mekanizmaları. Ankara Üniversitesi Tıp Fakültesi Mecmuası 2012; 65 (2): 77-82. doi: 10.1501/Tıpfak_000000813
2. Sacha T. Imatinib in Chronic Myeloid Leukemia: an Overview. Mediterranean Journal of Hematology and Infectious Diseases 2014; 6 (1): e2014007. doi: 10.4084/MJHID.2014.007
3. Waclaw J, Sacha T, Stoklosa T. Imatinib in the treatment of chronic myeloid leukemia: current perspectives on optimal dose. Blood and Lymphatic Cancer: Targets and Therapy 2015; 5: 101–108. doi: 10.2147/BLCTT.S58845
4. Lopes LF, Bacchi CE. Imatinib treatment for gastrointestinal stromal tumour (GIST). Journal of Cellular and Molecular Medicine 2010; 14 (1-2): 42–50. doi: 10.1111/j.1582-4934.2009.00983.x
5. Murray M, Hatcher H, Jessop F, Williams D, Carroll N et al. Treatment of wild-type gastrointestinal stromal tumor (WT-GIST) with imatinib and sunitinib. Pediatric Blood & Cancer 2008; 50 (2): 386-388. doi: 10.1002/pbc.21312
6. Paul MK, Mukhopadhyay AK. Tyrosine kinase - Role and significance in Cancer. International Journal of Medical Sciences 2004; 1 (2): 101-115. doi: 10.7150/ijms.1.101
7. Rossari F, Minutolo F, Orciuolo E. Past, present, and future of Bcr-Abl inhibitors: from chemical development to clinical efficacy. Journal of Hematology & Oncology 2018; 11: 84-97. doi: 10.1186/s13045-018-0624-2
8. Xing L, Xungui H, Wang Y, Bekhazi M, Krivonos S et al. Imatinib production process. World Intellectual Property Organization International Bureau Patent 2008; 2008135980.
9. (a) Zimmermann, J. Pyrimidine derivatives and processes for their preparation. European Patent 1993; PT564409E. (b) Zimmermann, J. Pyrimidine derivatives and processes for the preparation thereof. U.S. Patent 1996; 5521184A. (c) Zimmermann J, Buchdunger E, Mett H, Meyer T, Lydon NB et al. (Phenylamino)pyrimidine (PAP) derivatives: a new class of potent and highly selective PDGF-receptor autophosphorylation inhibitors. Bioorganic & Medicinal Chemistry Letters 1996; 6 (11): 1221–1226. doi: 10.1016/0960-894X(96)00197-7
10. Kompella A, Bhujanga Rao AKS, Venkaiah Chowdary NWO. A Facile Total Synthesis for Large-Scale Production of Imatinib Base. Organic Process Research & Development 2012; 16 (11): 1794–1804. doi: 10.1021/op300212u
11. Szczepek W, Luniewski W, Kaczmarek L, Zagrodski B, Samson-Lazinska D et al. A process for preparation of imatinib base. World Intellectual Property Organization International Bureau Patent 2006; 2006071130.
12. Loiseleur O, Kaufmann D, Abel S, Buerger HM, Meisenbach M et al. N-phenyl-2-pyrimidine-amine derivatives. World Intellectual Property Organization International Bureau Patent 2003; WO 03/066613 A1.
13. Zhang X, Sun J, Chen T, Yang C, Yu LA. A Practical Preparation of Imatinib Base. Synlett 2016; 27: 2233-2236. doi: 10.1055/s-0035-1562498
14. Kang J, Lee JY, Park JH, Chang DJ. Synthesis of imatinib, a tyrosine kinase inhibitor, labeled with carbon-14. Journal of Label Compounds and Radiopharmaceuticals 2020; 63: 174–182. doi: 10.1002/jlcr.3830
15. Macdonald P and Rossetto P. Process for the preparation of imatinib. World Intellectual Property Organization International Bureau Patent 2008; WO2008051597A1.

16. Ivanov S, Shishkov SV. Synthesis of imatinib: a convergent approach revisited. *Monatshefte für Chemie - Chemical Monthly* 2009; 140: 619–623. doi: 10.1007/s00706-008-0105-3
17. Zhao Y, Li Z, Liu G, Liu C, Xu L. Method for preparing imatinib. Chinese Patent 2013; CN101921260B.
18. Yan R, Yang H, Hou W, Xu Y. Convenient and quick method for preparing high-purity imatinib and mesylate thereof. Chinese Patent 2011; CN101985442B.
19. Kamath AA, Pai GG, Ujagare AM, He X, Wu S et al. Process for the preparation of imatinib and salts thereof. World Intellectual Property Organization International Bureau Patent 2011; 2011070588.
20. Hopkin MD, Baxendale IR, Ley SV. A flow-based synthesis of Imatinib: the API of Gleevec. *Chemical Communications* 2010; 46: 2450-2. doi: 10.1039/C001550D
21. Hopkin MD, Baxendale IR, Ley SV. An expeditious synthesis of imatinib and analogues utilising flow chemistry methods. *Organic & Biomolecular Chemistry* 2013; 11: 1822-39. doi: 10.1039/C2OB27002A
22. Ingham RJ, Riva E, Nikbin N, Baxendale IR, Ley SV. A “Catch–React–Release” Method for the Flow Synthesis of 2-Aminopyrimidines and Preparation of the Imatinib Base. *Organic Letters* 2012; 14: 3920–3. doi: 10.1021/ol301673q
23. Leonetti F, Capaldi C, Carotti A. Microwave-assisted solid phase synthesis of Imatinib, a blockbuster anticancer drug. *Tetrahedron Letters* 2007; 48: 3455–8. doi: 10.1016/j.tetlet.2007.03.033
24. Heo Y, Hyun D, Kumar MR, Jung HM, Lee S. Preparation of copper (II) oxide bound on polystyrene beads and its application in the aryl aminations: synthesis of Imatinib. *Tetrahedron Letters* 2012; 53 (49): 6657-61. doi: 10.1016/j.tetlet.2012.09.097
25. Lee SH, Ryu JC, El-Deeb IM. Synthesis of new N-arylpurimidin-2-amine derivatives using a palladium catalyst. *Molecules* 2008; 13 (4): 818–830. doi: 10.3390/molecules13040818
26. Fors BP, Watson DA, Biscoe MR, Buchwald SL. A highly active catalyst for Pd-catalyzed amination reactions: cross-coupling reactions using aryl mesylates and the highly selective monoarylation of primary amines using aryl chlorides. *Journal of American Chemical Society* 2008; 130 (41): 13552-4. doi: 10.1021/ja8055358
27. Maiti D, Fors BP, Henderson JL, Nakamura Y, Buchwald SL. Palladium-catalyzed coupling of functionalized primary and secondary amines with aryl and heteroaryl halides: two ligands suffice in most cases. *Chemical Science* 2011; 2: 57-68. doi: 10.1039/C0SC00330A
28. Yaghmaie M, Yeung CCS. Molecular Mechanisms of Resistance to Tyrosine Kinase Inhibitors. *Current Hematological Malignancy Reports* 2019; 14 (5): 395–404. doi: 10.1007/s11899-019-00543-7
29. Bitencourt R, Zalberg I, Louro ID. Imatinib resistance: a review of alternative inhibitors in chronic myeloid leukemia. *Revista Brasileira de Hematologia e Hemoterapia* 2011; 33 (6): 470-475. doi: 10.5581/1516-8484.20110124
30. Huang M, Dorsey JF, Epling-Burnett PK, Nimmanapalli R, Landowski TH et al. Inhibition of Bcr-Abl kinase activity by PD180970 blocks constitutive activation of Stat5 and growth of CML cells. *Oncogene* 2002; 21: 8804-16. doi: 10.1038/sj.onc.1206028
31. Warmuth M, Simon N, Mitina O, Mathes R, Fabbro D et al. Dual-specific Src and Abl kinase inhibitors, PP1 and CGP76030, inhibit growth and survival of cells expressing imatinib mesylate-resistant Bcr-Abl kinases. *Blood* 2003; 101 (2): 664-672. doi: 10.1182/blood-2002-01-0288
32. Shah NP, Tran C, Lee FY, Chen P, Norris D et al. Overriding Imatinib Resistance with a Novel ABL Kinase Inhibitor. *Science* 2004; 305 (5682): 399-401. doi: 10.1126/science.1099480
33. Weisberg E, Manley P, Mestan J, Cowan-Jacob S, Ray A et al. AMN107 (nilotinib): a novel and selective inhibitor of BCR-ABL. *British Journal of Cancer* 2006; 94 (12): 1765-9. doi: 10.1038/sj.bjc.6603170
34. O'Hare T, Shakespeare WC, Zhu X, Eide CA, Rivera VM et al. AP24534, a pan-BCR-ABL inhibitor for chronic myeloid leukemia, potently inhibits the T315I mutant and overcomes mutation-based resistance. *Cancer Cell* 2009; 16 (5): 401-412. doi: 10.1016/j.ccr.2009.09.028
35. Hoover RR, Mahon FX, Melo JV, Daley GQ. Overcoming STI571 resistance with the farnesyl transferase inhibitor SCH66336. *Blood* 2002; 100 (3): 1068-71. doi: 10.1182/blood.v100.3.1068
36. Manley PW, Stie N, Cowan-Jacob SW, Kaufman S, Mestan J et al. Structural resemblances and comparisons of the relative pharmacological properties of imatinib and nilotinib. *Bioorganic & Medicinal Chemistry* 2018; 26 (15), 4537-43. doi: 10.1016/j.bmc.2010.08.026
37. Cory AH, Owen TC, Barltrop JA, Cory JG. Use of an aqueous soluble tetrazolium/formazan assay for cell growth assays in culture. *Cancer Communications* 1991; 3 (7): 207-212. doi: 10.3727/095535491820873191
38. Carvalho BS, Irizarry RA. A framework for oligonucleotide microarray preprocessing. *Bioinformatics* 2010; 26 (19): 2363-7. doi: 10.1093/bioinformatics/btq431
39. Ritchie ME, Phipson B, Wu D, Hu Y, Law CW et al. limma powers differential expression analyses for RNA-sequencing and microarray studies. *Nucleic Acids Research* 2015; 43(7): e47. doi: 10.1093/nar/gkv007

40. Keiser MJ, Roth BL, Armbruster BN, Ernsberger P, Irwin JJ et al. Relating protein pharmacology by ligand chemistry. *Nature Biotechnology* 2007; 25 (2): 197-206. doi: 10.1038/nbt1284
41. O'Boyle NM, Banck M, James CA, Morley C, Vandermeersch T et al. Open Babel: An open chemical toolbox. *Journal of Cheminformatics* 2011; 3 (33): 1-14. doi: 10.1186/1758-2946-3-33
42. Morris GM, Huey R, Lindstrom W, Sanner MF, Belew RK et al. AutoDock4 and AutoDockTools4: Automated Docking with Selective Receptor Flexibility. *Journal of Computational Chemistry* 2009; 30 (16): 2785-2791. doi: 10.1002/jcc.21256
43. Gasteiger J, Marsili MA. A new model for calculating atomic charges in molecules. *Tetrahedron Letters* 1978; 19 (34): 3181-3184. doi: 10.1016/S0040-4039(01)94977-9
44. Kumar S, Deep A, Narasimhan B. A Review on Synthesis, Anticancer and Antiviral Potentials of Pyrimidine Derivatives. *Current Bioactive Compounds* 2019; 15 (3): 289-303. doi: 10.2174/1573407214666180124160405
45. Gatta L, Vitiello L, Gorini S, Chianotto S, Costelli P et al. Modulating the metabolism by trimetazidine enhances myoblast differentiation and promotes myogenesis in cachectic tumorbearing c26 mice. *Oncotarget* 2017; 8 (69): 113938-56. doi: 10.18632/oncotarget.23044
46. Jakubowska J, Wasowska-Lukawska M, Czyz M. STI571 and morpholine derivative of doxorubicin collaborate in inhibition of K562 cell proliferation by inducing differentiation and mitochondrial pathway of apoptosis. *European Journal of Pharmacology* 2008; 596 (1-3): 41. doi:10.1016/j.ejphar.2008.08.021
47. Hamidian H, Aziz S. Synthesis of novel compounds containing morpholine and 5(4H)-oxazolone rings as potent tyrosinase inhibitors. *Bioorganic & Medicinal Chemistry* 2015; 23 (21): 7089-7094. doi: 10.1016/j.bmc.2015.09.015
48. Goud NS, Pooladanda V, Mahammad GS, Jakkula P, Gatreddi S et al. Synthesis and biological evaluation of morpholines linked coumarin-triazole hybrids as anticancer agents. *Chemical Biology & Drug Design* 2019; 94: 1919-29. doi: 10.1111/cbdd.13578
49. Manley PW, Cowan-Jacob SW, Buchdunger E, Fabbro D, Fendrich G et al. Imatinib: a selective tyrosine kinase inhibitor. *European Journal of Cancer* 2002; 38 (S5): S19-S27. doi: 10.1016/S0959-8049(02)80599-8
50. Levinson NM, Kuchment O, Shen K, Young MA, Koldobskiy M et al. A Src-like inactive conformation in the Abl tyrosine kinase domain. *Plos Biology* 2006; 4 (5): 753-767. doi: 10.1371/journal.pbio.0040144
51. Cowan-Jacob SW, Fendrich G, Floersheimer A, Furet P, Liebetanz J et al. Structural biology contributions to the discovery of drugs to treat chronic myelogenous leukaemia. *Acta Crystallographica, Section D, Biological Crystallography* 2007; 63 (Pt 1): 80-93. doi: 10.1107/S0907444906047287
52. Bernstein FC, Koetzle TF, Williams GJ, Meyer Jr EF, Brice MD et al. Protein Data Bank - Computer-Based Archival File for Macromolecular Structures. *Journal of Molecular Biology* 1977; 112 (3): 535-542. doi: 10.1016/s0022-2836(77)80200-3
53. Berman HM, Westbrook J, Feng Z, Gilliland G, Bhat TN et al. The Protein Data Bank. *Nucleic Acids Research* 2000; 28 (1): 235-242. doi: 10.1093/nar/28.1.235
54. Horio T, Hamasaki T, Inoue T, Wakayama T, Itou S et al. Structural factors contributing to the Abl/Lyn dual inhibitory activity of 3-substituted benzamide derivatives. *Bioorganic & Medicinal Chemistry Letters* 2007; 17 (10): 2712-2717. doi: 10.1016/j.bmcl.2007.03.002
55. Weisberg E, Manley PW, Breitenstein W, Brügger J, Cowan-Jacob SW et al. Characterization of AMN107, a selective inhibitor of native and mutant Bcr-Abl. *Cancer Cell* 2005; 7 (2): 129-141. doi: 10.1016/j.ccr.2005.01.007
56. Levinson NM, Boxer SG. Structural and Spectroscopic Analysis of the Kinase Inhibitor Bosutinib and an Isomer of Bosutinib Binding to the Abl Tyrosine Kinase Domain. *Plos One*. 2012; 7 (4): e29828. doi: 10.1371/journal.pone.0029828
57. Jensen CN, Mielke T, Farrugia JE, Frank A, Man H et al. Structures of the Apo and FAD-Bound Forms of 2-Hydroxybiphenyl 3-monooxygenase (HbpA) Locate Activity Hotspots Identified by Using Directed Evolution. *Chembiochem*. 2015; 16 (6): 968-976. doi: 10.1002/cbic.201402701
58. Laskowski RA, Swindells MB. LigPlot+: multiple ligand-protein interaction diagrams for drug discovery. *Journal of Chemical Information and Modelling* 2011; 51 (10): 2778-86. doi:10.1021/ci200227u
59. Wan PTC, Garnett MJ, Roe SM, Lee S, Niculescu-Duvaz D et al. Mechanism of activation of the RAF-ERK signaling pathway by oncogenic mutations of B-RAF. *Cell* 2004; 116 (6): 855-86. doi: 10.1016/s0092-8674(04)00215-6
60. Okaniwa M, Hirose M, Arita T, Yabuki M, Nakamura A et al. Discovery of a Selective Kinase Inhibitor (TAK-632) Targeting Pan-RAF Inhibition: Design, Synthesis, and Biological Evaluation of C-7-Substituted 1,3-Benzothiazole Derivatives. *Journal of Medicinal Chemistry* 2013; 56 (16): 6478-6494. doi: 10.1021/jm400778d
61. Lavoie H, Thevakumaran N, Gavory G, Li JJ, Padeganeh A et al. Inhibitors that stabilize a closed RAF kinase domain conformation induce dimerization. *Nature Chemical Biology* 2013; 9 (7): 428-436. doi: 10.1038/nchembio.1257
62. Tsai J, Lee JT, Wang W, Zhang J, Cho H et al. Discovery of a selective inhibitor of oncogenic B-Raf kinase with potent antimelanoma activity. *Proceedings of the National Academy of Sciences* 2008; 105 (8): 3041-6. doi: 10.1073/pnas.0711741105

63. Waizenegger IC, Baum A, Steurer S, Stadtmüller H, Bader G et al. A Novel RAF Kinase Inhibitor with DFG-Out-Binding Mode: High Efficacy in BRAF-Mutant Tumor Xenograft Models in the Absence of Normal Tissue Hyperproliferation. *Molecular Cancer Therapeutics* 2016; 15 (3): 354-365. doi: 10.1158/1535-7163.MCT-15-0617
64. King AJ, Patrick DR, Batorsky RS, Ho ML, Do HT et al. Demonstration of a genetic therapeutic index for tumors expressing oncogenic BRAF by the kinase inhibitor SB-590885. *Cancer Research* 2006; 66 (23): 11100-11105. doi: 10.1158/0008-5472.CAN-06-2554
65. Hansen JD, Grina J, Newhouse B, Welch M, Topalov G et al. Potent and selective pyrazole-based inhibitors of B-Raf kinase. *Bioorganic & Medicinal Chemistry Letters* 2008; 18 (16): 4692-4695. doi: 10.1016/j.bmcl.2008.07.002

Supplementary Information

Synthesis, molecular modeling and biological evaluation of novel imatinib derivatives as anticancer agents

Fulya GUNAY^{1,2}, Sevcan BALTA¹, Yuk Yin NG², Ozlem ULUCAN², Zuhale TURGUT¹ and

Omer Tahir GUNKARA^{1*}

¹ Department of Chemistry, Faculty of Arts and Science, Yildiz Technical University, Istanbul,
Turkey

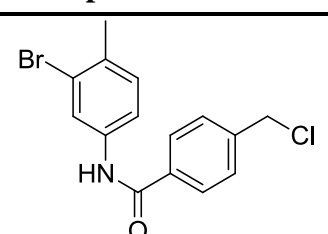
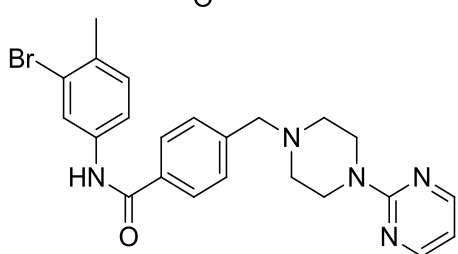
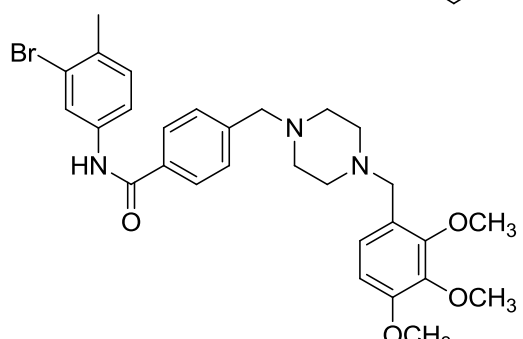
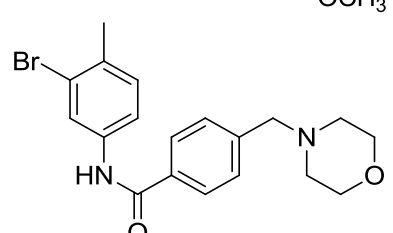
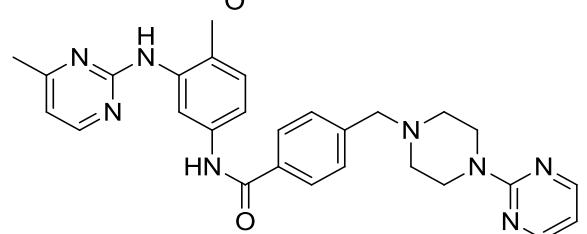
² Department of Genetics and Bioengineering, Faculty of Engineering and Natural
Sciences, Istanbul Bilgi University, Istanbul, Turkey

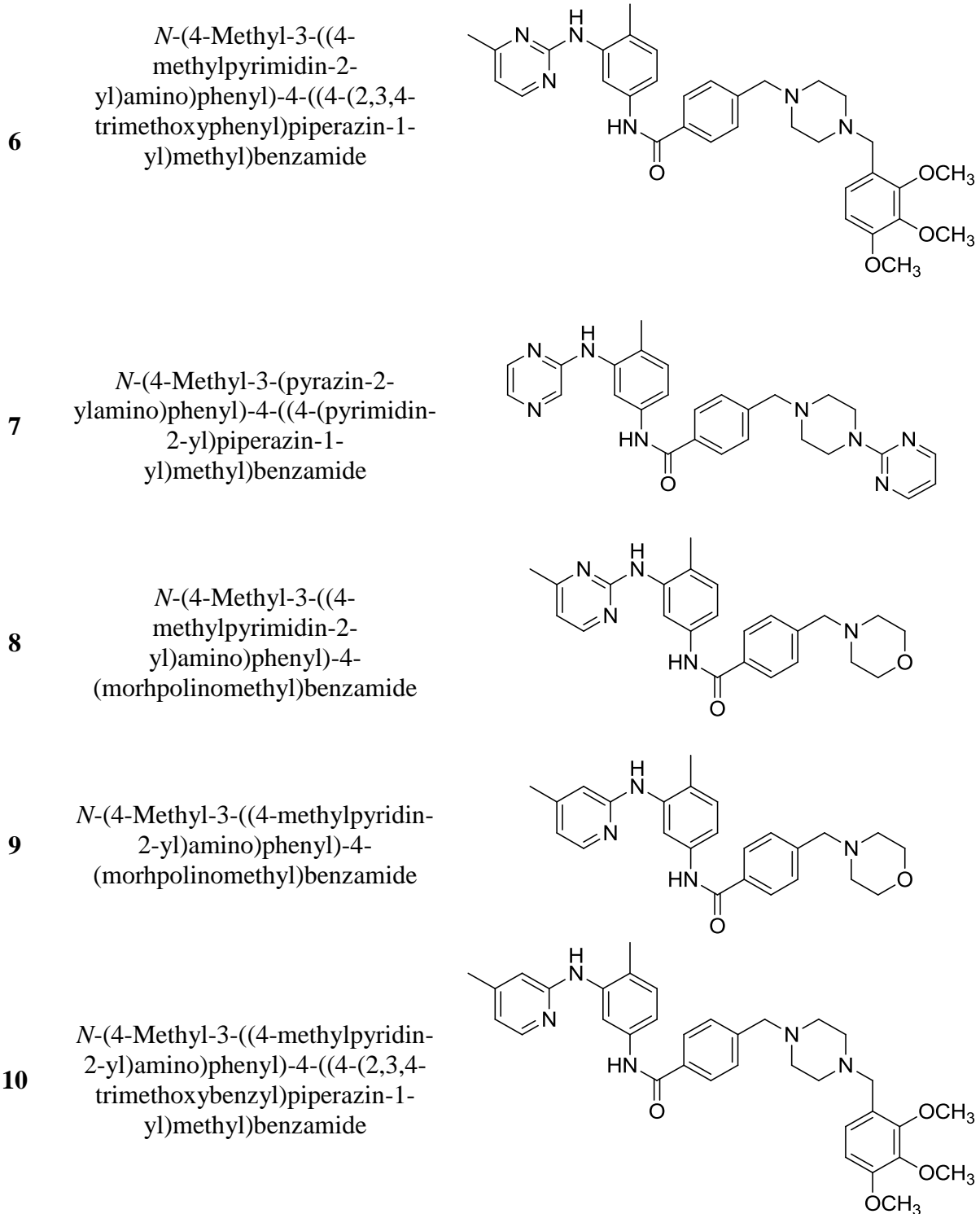
*Correspondence: gunkara@yildiz.edu.tr

Table of Contents	Page
Table S1. New imatinib derivatives list	S4-S5
Figure S1. IR spectrum of Compound 3	S6
Figure S2. ¹ H-NMR spectrum of Compound 3	S6
Figure S3. APT spectrum of Compound 3	S7
Figure S4. IR spectrum of Compound 4a	S8
Figure S5. ¹ H-NMR spectrum of Compound 4a	S8
Figure S6. APT spectrum of Compound 4a	S9
Figure S7. HRMS Spectrum of Compound 4a	S9
Figure S8. IR spectrum of Compound 4b	S10
Figure S9. ¹ H-NMR spectrum of Compound 4b	S10
Figure S10. ¹ H-NMR spectrum of Compound 4b	S11
Figure S11. ¹ H-NMR spectrum of Compound 4b	S11
Figure S12. APT spectrum of Compound 4b	S12
Figure S13. HRMS Spectrum of Compound 4b	S12
Figure S14. IR spectrum of Compound 4c	S13
Figure S15. ¹ H-NMR spectrum of Compound 4c	S14
Figure S16. APT spectrum of Compound 4c	S14
Figure S17. HRMS Spectrum of Compound 4c	S15
Figure S18. IR spectrum of Compound 5	S16
Figure S19. ¹ H-NMR spectrum of Compound 5	S16
Figure S20. APT spectrum of Compound 5	S17
Figure S21. HRMS Spectrum of Compound 5	S17
Figure S22. IR spectrum of Compound 6	S18
Figure S23. ¹ H-NMR spectrum of Compound 6	S18
Figure S24. ¹ H-NMR spectrum of Compound 6	S19
Figure S25. ¹ H-NMR spectrum of Compound 6	S19
Figure S26. APT spectrum of Compound 6	S20
Figure S27. HRMS Spectrum of Compound 6	S20
Figure S28. IR spectrum of Compound 7	S21
Figure S29. ¹ H-NMR spectrum of Compound 7	S21
Figure S30. APT spectrum of Compound 7	S22
Figure S31. HRMS Spectrum of Compound 7	S22
Figure S32. IR spectrum of Compound 8	S23
Figure S33. ¹ H-NMR spectrum of Compound 8	S24
Figure S34. APT spectrum of Compound 8	S24
Figure S35. HRMS Spectrum of Compound 8	S25
Figure S36. IR spectrum of Compound 9	S26
Figure S37. ¹ H-NMR spectrum of Compound 9	S26
Figure S38. APT spectrum of Compound 9	S27
Figure S39. HRMS Spectrum of Compound 9	S27
Figure S40. IR spectrum of Compound 10	S28
Figure S41. ¹ H-NMR spectrum of Compound 10	S28
Figure S42. APT spectrum of Compound 10	S29
Figure S43. HRMS Spectrum of Compound 10	S29
Table S2. Concentration (μM)- viability rate (%) values according to MTT assay in different cell lines.	S30-S32

Figure S44. Comparison between imatinib and compound-6-9-10 in all cell-lines	S33
Table S3. Values of synthesized molecules related to target proteins	S34
Table S4. Cristal structures of ABL1	S35
Table S5. Redocking the original ligands to the crystal structures of wild type ABL1	S35
Table S6. Cristal structures of BRAF	S36
Table S7. Redocking of the original ligands to the crystal structures of BRAF	S37
Figure S45. Comparison of ABL-imatinib (background) and ABL-Compound 5 (foreground) interactions. Imatinib and its contact residues are depicted in gray, while the common contact residues are marked with red circles.	S38
Figure S46. Comparison of ABL-imatinib (background) and ABL-Compound 6 (foreground) interactions. Imatinib and its contact residues are depicted in gray, while the common contact residues are marked with red circles.	S39
Figure S47. Comparison of ABL-imatinib (background) and ABL-Compound 7 (foreground) interactions. Imatinib and its contact residues are depicted in gray, while the common contact residues are marked with red circles.	S40
Figure S48. Comparison of ABL-imatinib (background) and ABL-Compound 8 (foreground) interactions. Imatinib and its contact residues are depicted in gray, while the common contact residues are marked with red circles.	S41
Figure S49. Comparison of ABL-imatinib (background) and ABL-Compound 9 (foreground) interactions. Imatinib and its contact residues are depicted in gray, while the common contact residues are marked with red circles.	S42

Table S1: New imatinib derivatives list

Entry	Compound Name	Compound Structure
3	<i>N</i> -(3-Bromo-4-methylphenyl)-4-(chloromethyl)benzamide	
4a	<i>N</i> -(3-Bromo-4-methylphenyl)-4-((4-(pyrimidin-2-yl)piperazin-1-yl)methyl)benzamide	
4b	<i>N</i> -(3-Bromo-4-methylphenyl)-4-((4-(2,3,4-trimethoxybenzyl)piperazin-1-yl)methyl)benzamide	
4c	<i>N</i> -(3-Bromo-4-methylphenyl)-4-(morpholinomethyl)benzamide	
5	<i>N</i> -(4-Methyl-3-((4-methylpyrimidin-2-yl)amino)phenyl)-4-((4-(pyrimidin-2-yl)piperazin-1-yl)methyl)benzamide	



Compound 3

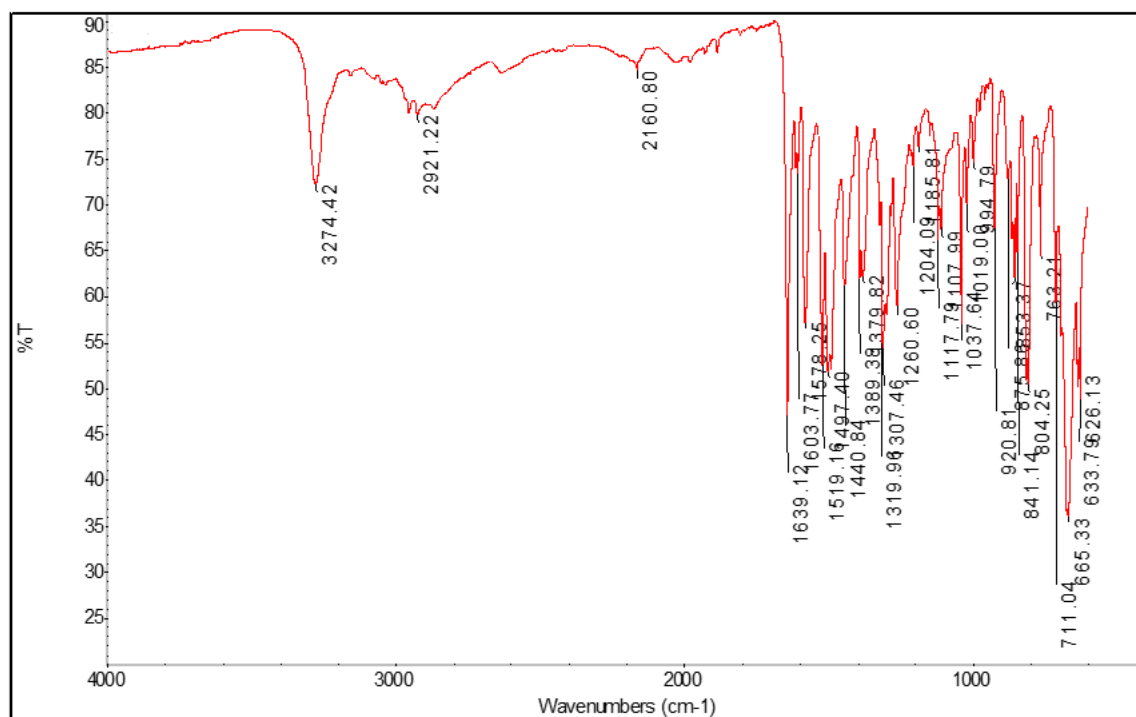


Figure S1. IR spectrum of Compound 3.

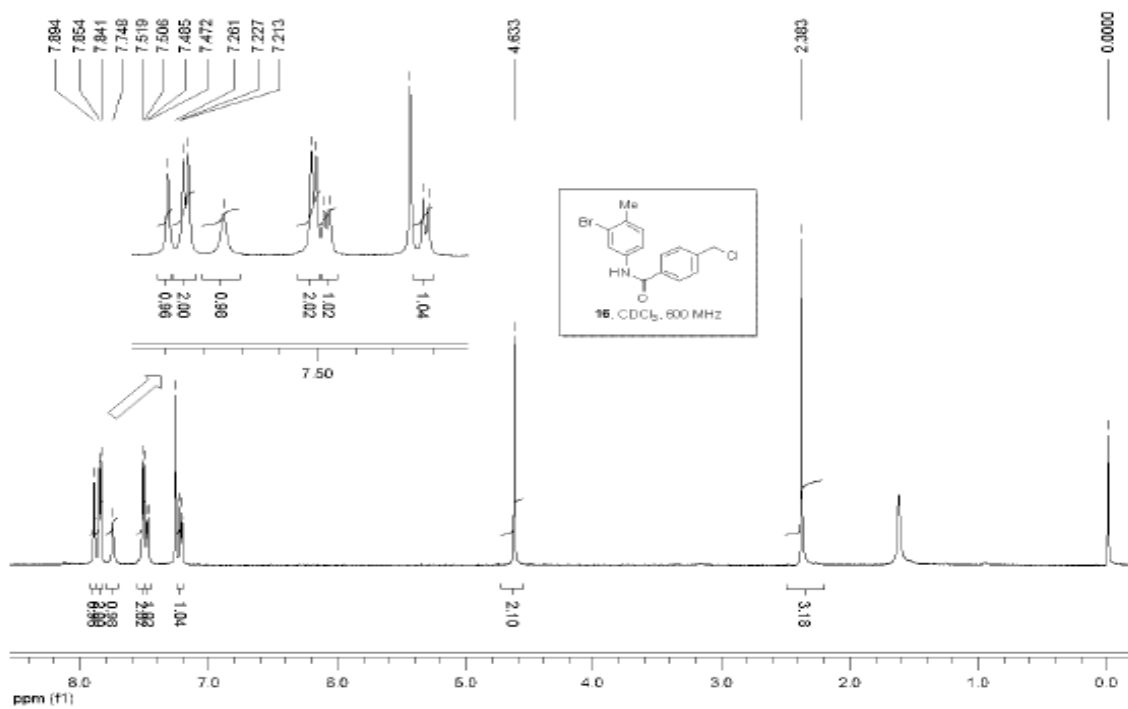


Figure S2. ¹H-NMR spectrum of Compound 3 (Reference-13).

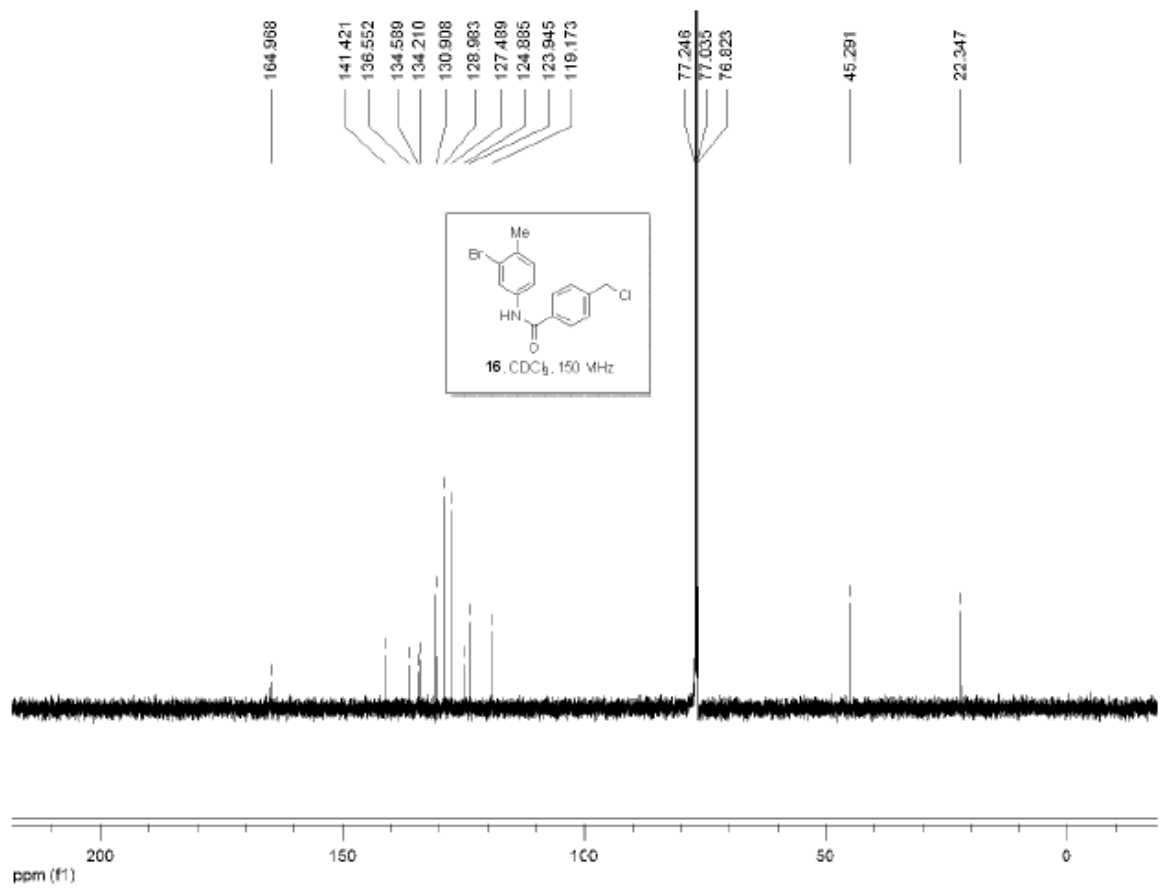


Figure S3. ¹³C-NMR spectrum of Compound 3 (Reference-13).

Compound 4a

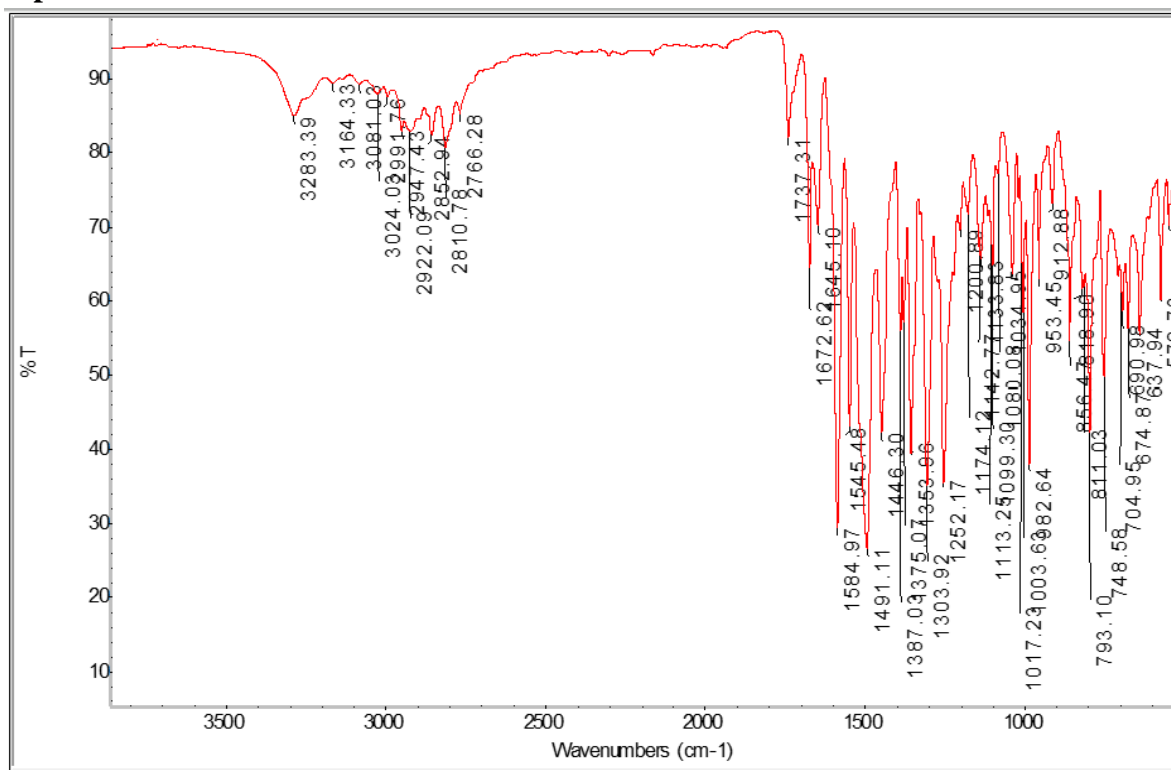


Figure S4. IR spectrum of Compound 4a.

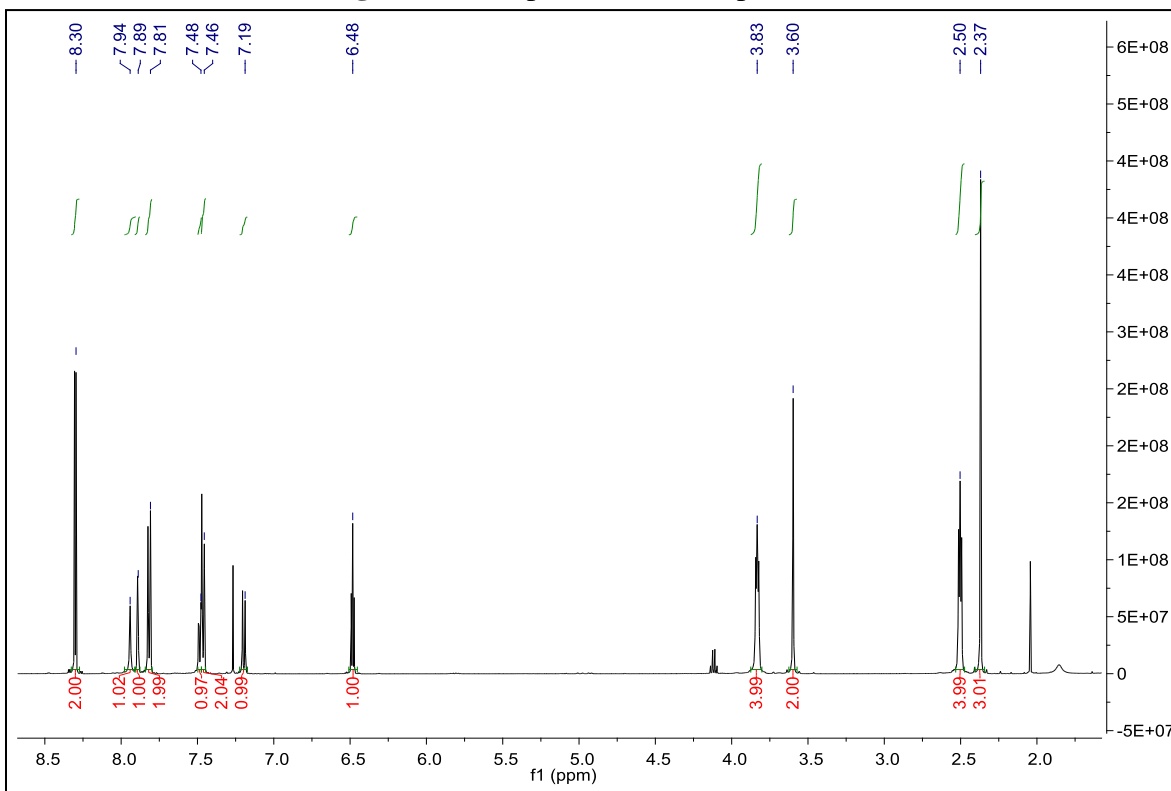


Figure S5. ¹H-NMR spectrum of Compound 4a.

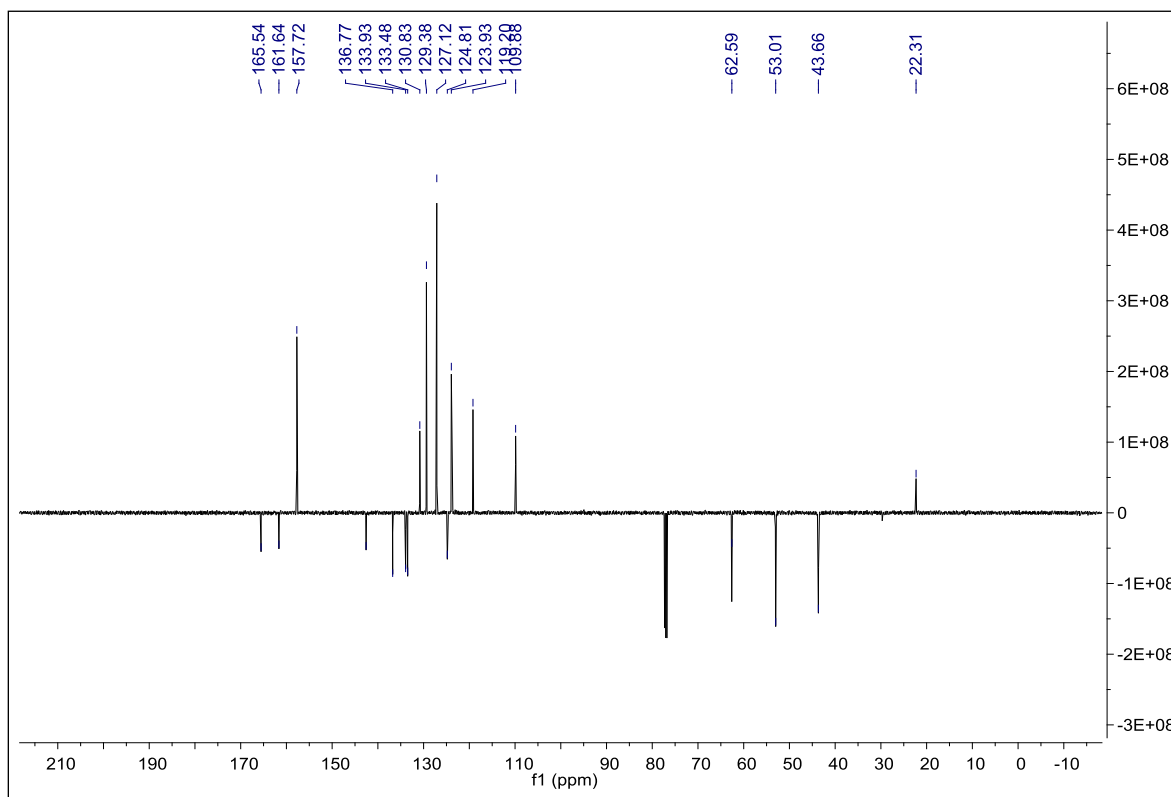


Figure S6. APT spectrum of Compound 4a.

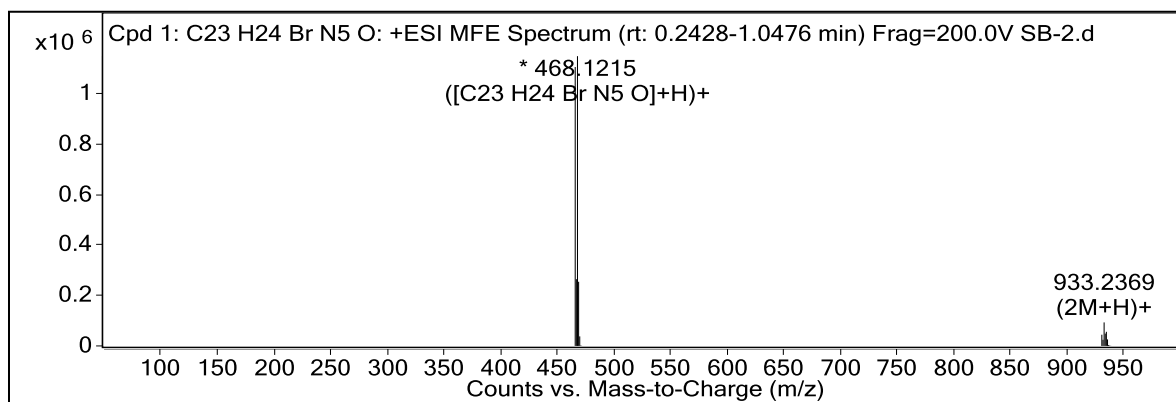


Figure S7. HRMS Spectrum of Compound 4a.

Compound 4b

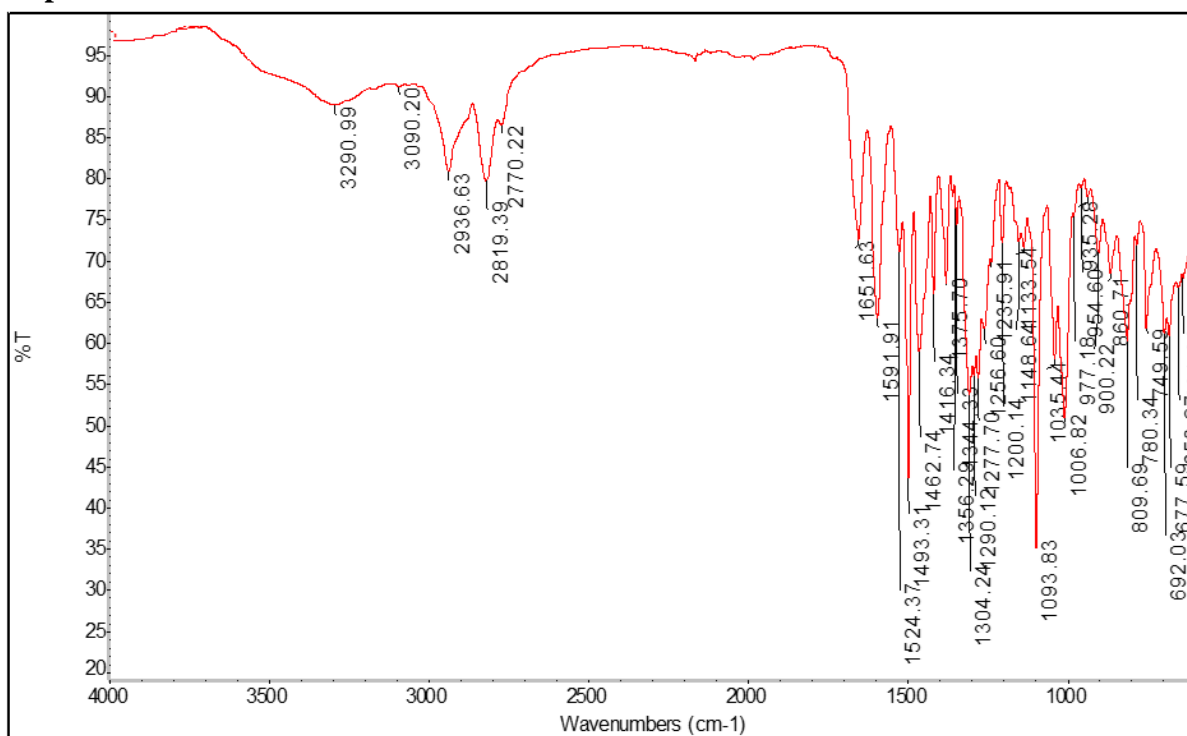


Figure S8. IR spectrum of Compound 4b.

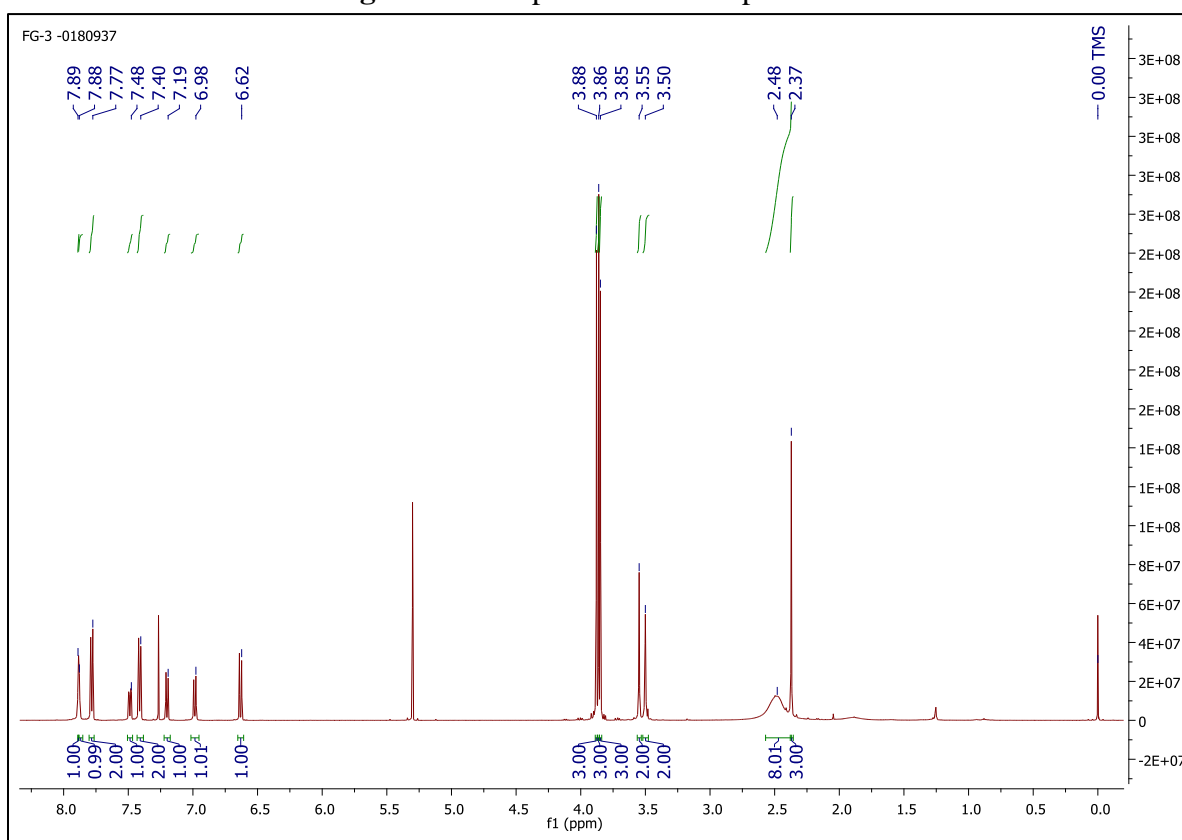


Figure S9. ¹H-NMR spectrum of Compound 4b.

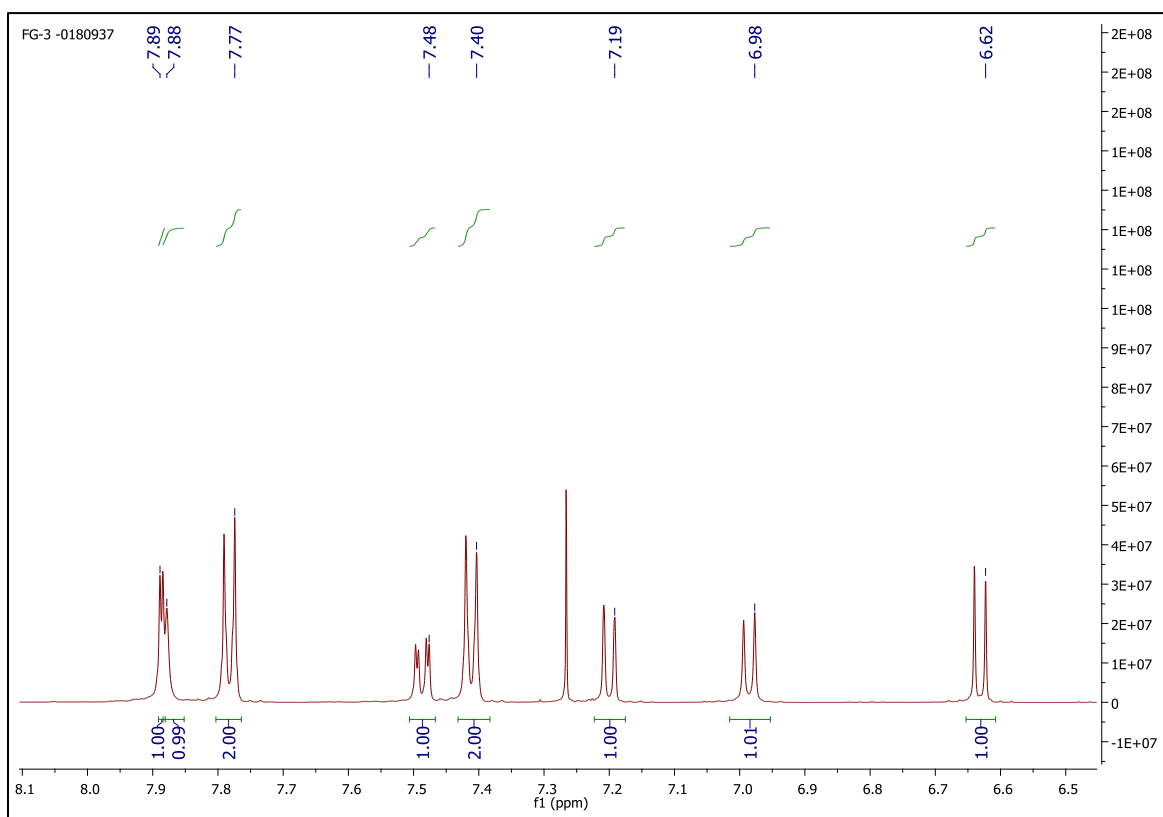
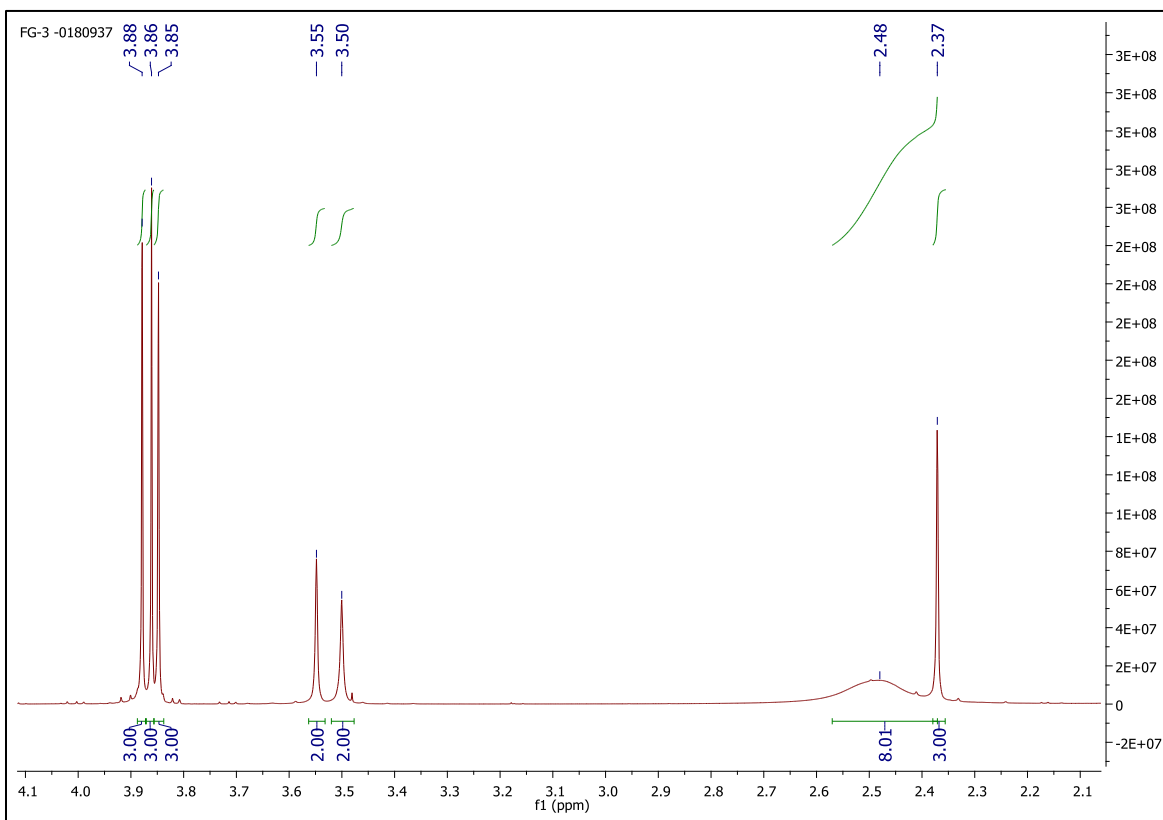


Figure S10-S11. $^1\text{H-NMR}$ spectrum of Compound 4b.

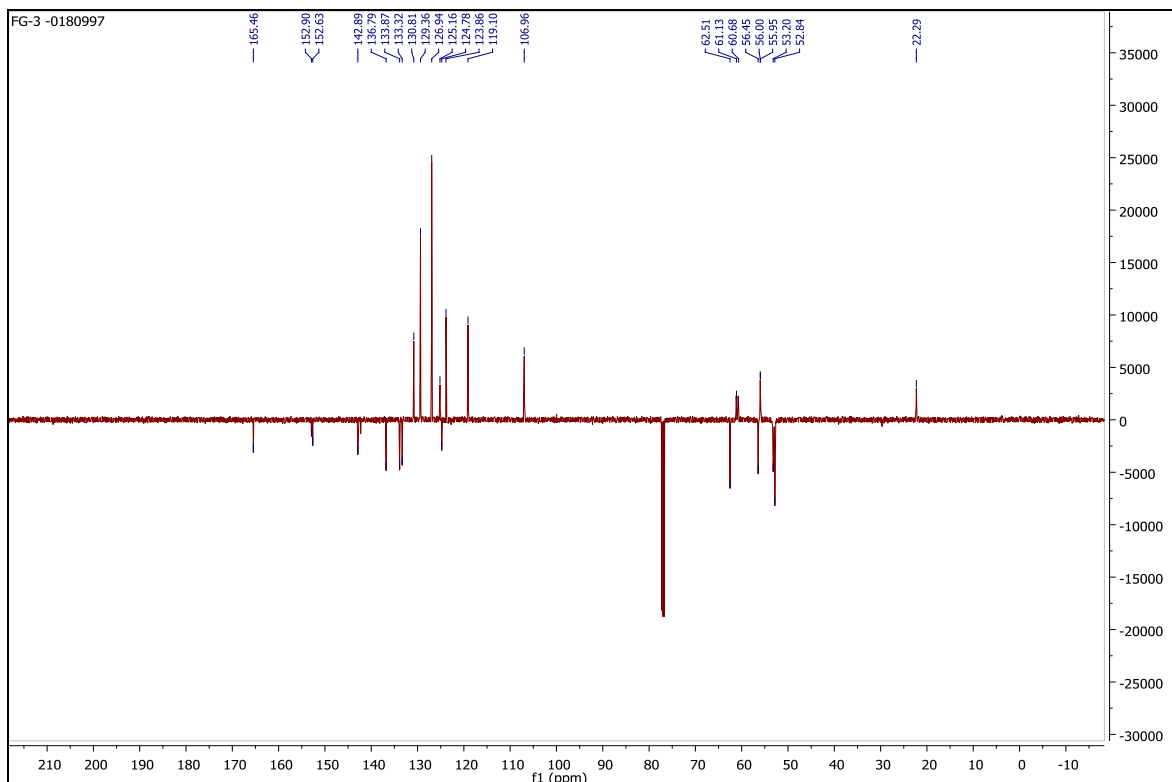


Figure S12. APT spectrum of Compound 4b.

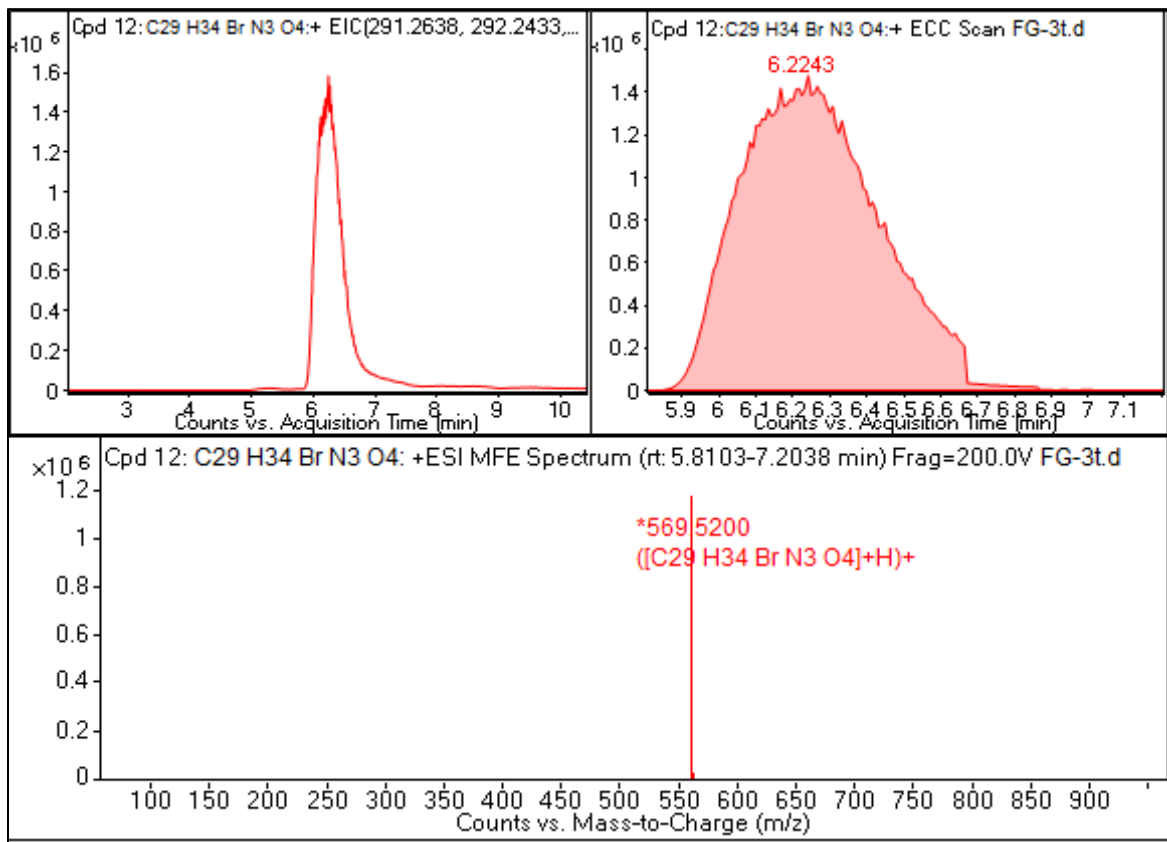


Figure S13. HRMS Spectrum of Compound 4b.

Compound 4c

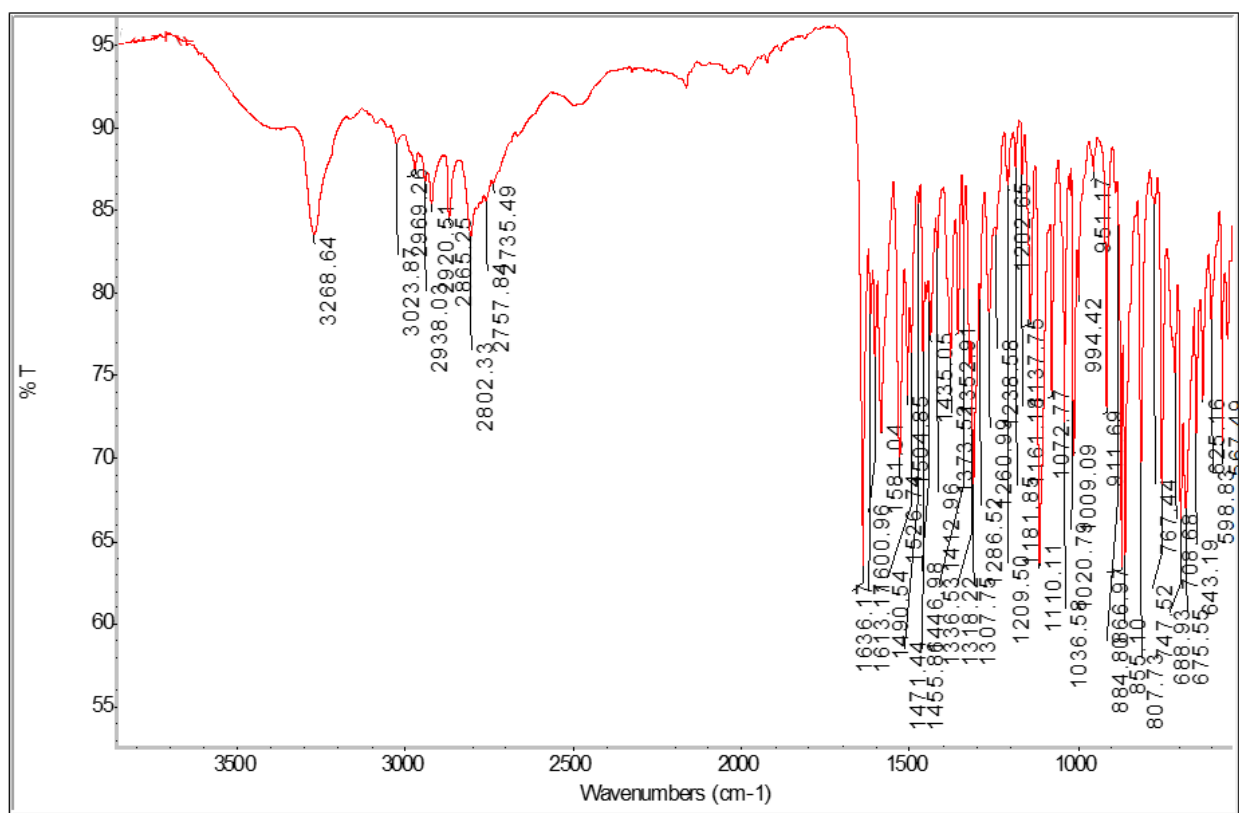


Figure S14. IR Spectrum of Compound 4c.

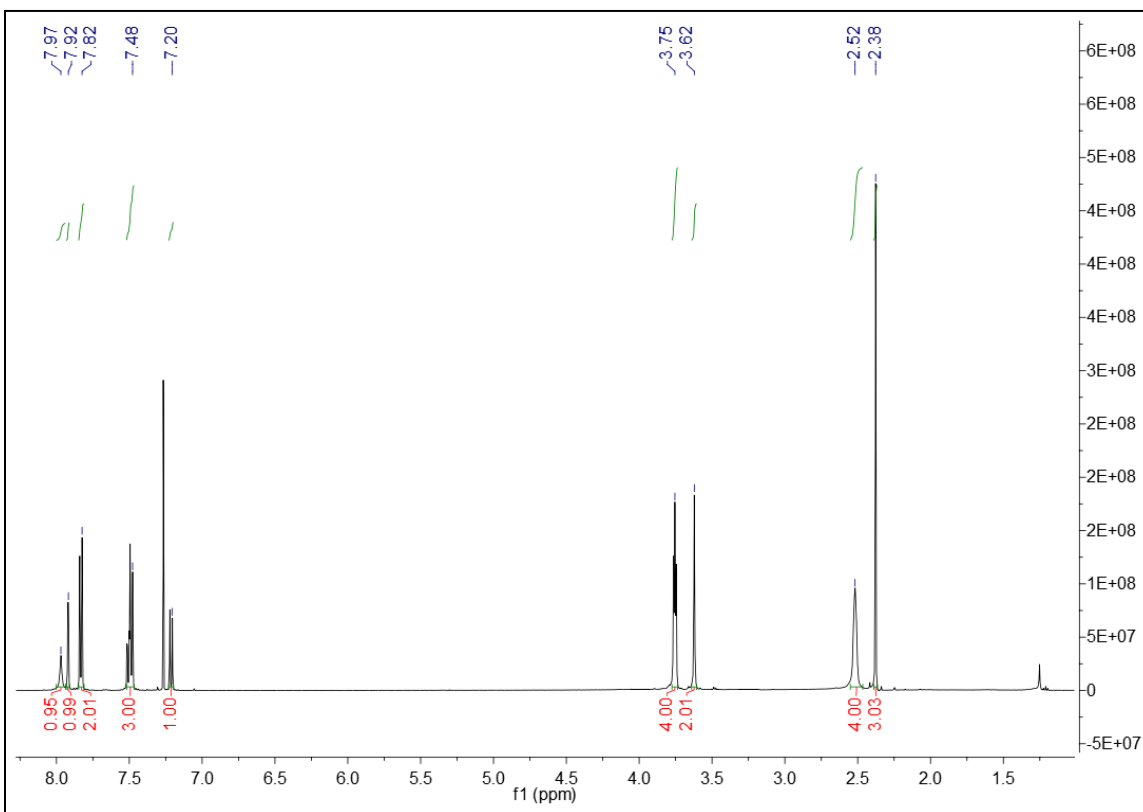


Figure S15. $^1\text{H-NMR}$ spectrum of Compound 4c.

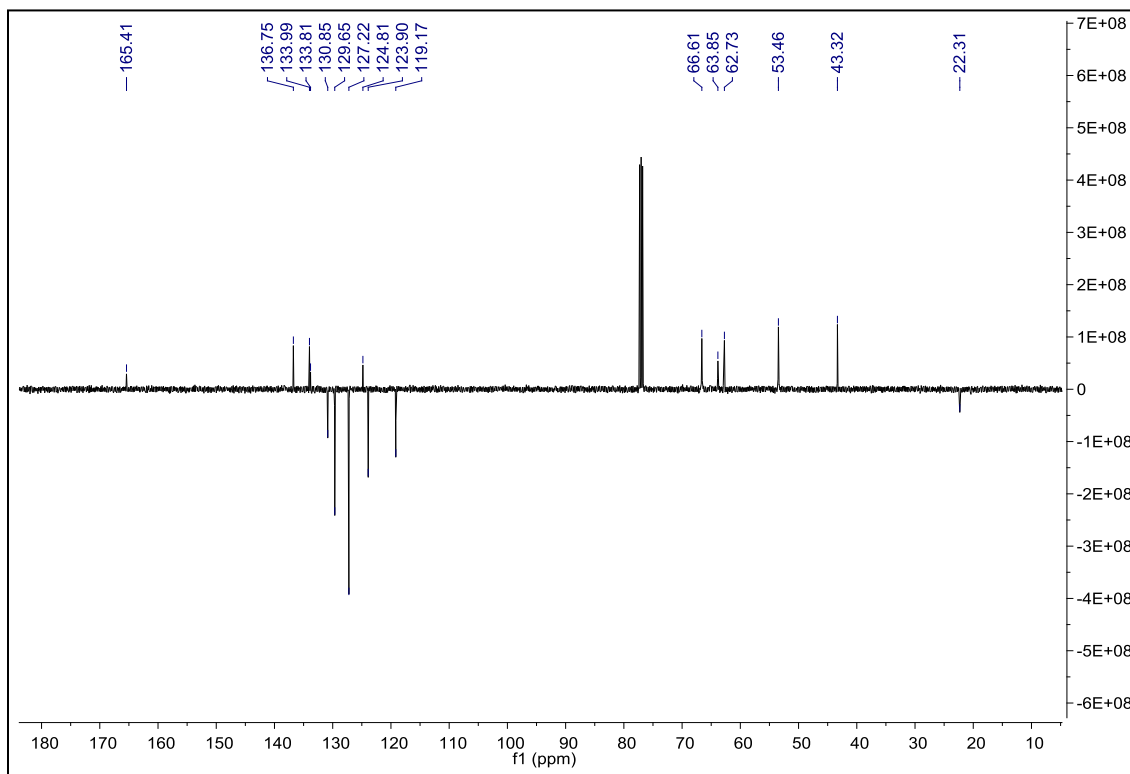


Figure S16. APT spectrum of Compound 4c.

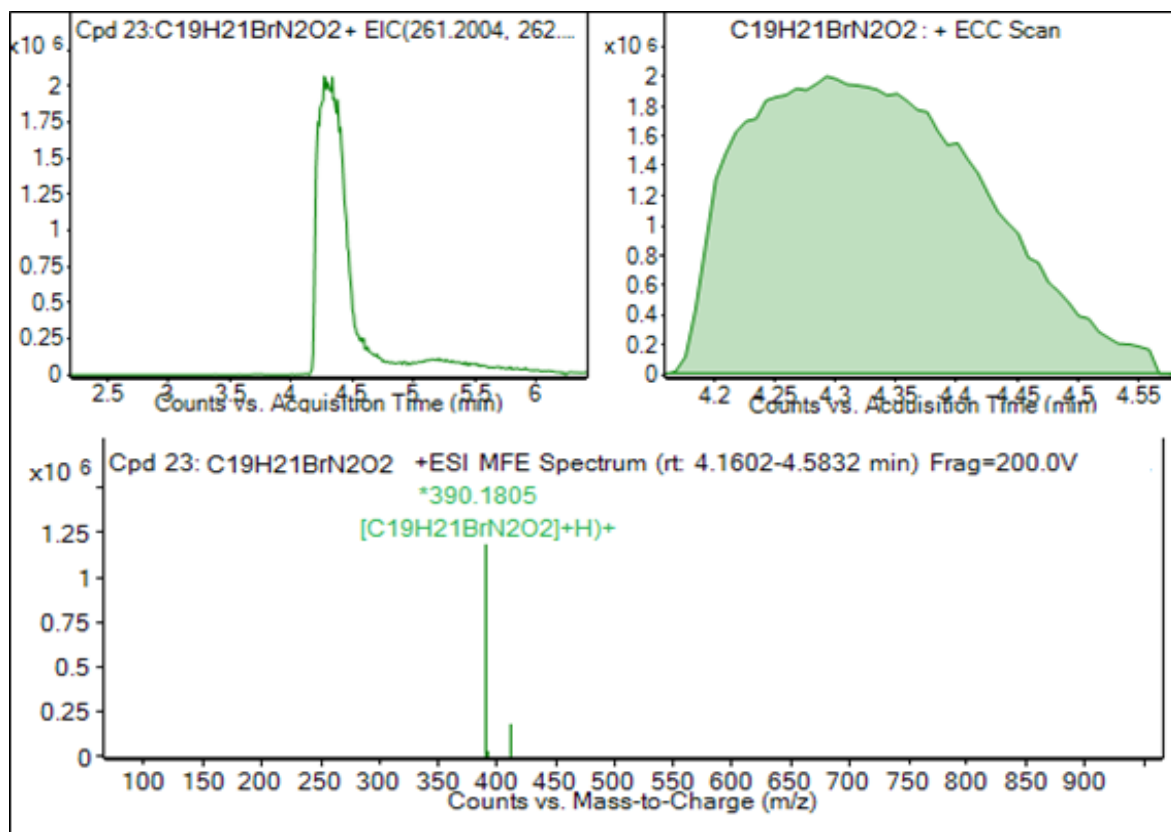


Figure S17. HRMS Spectrum of Compound 4c.

Compound 5

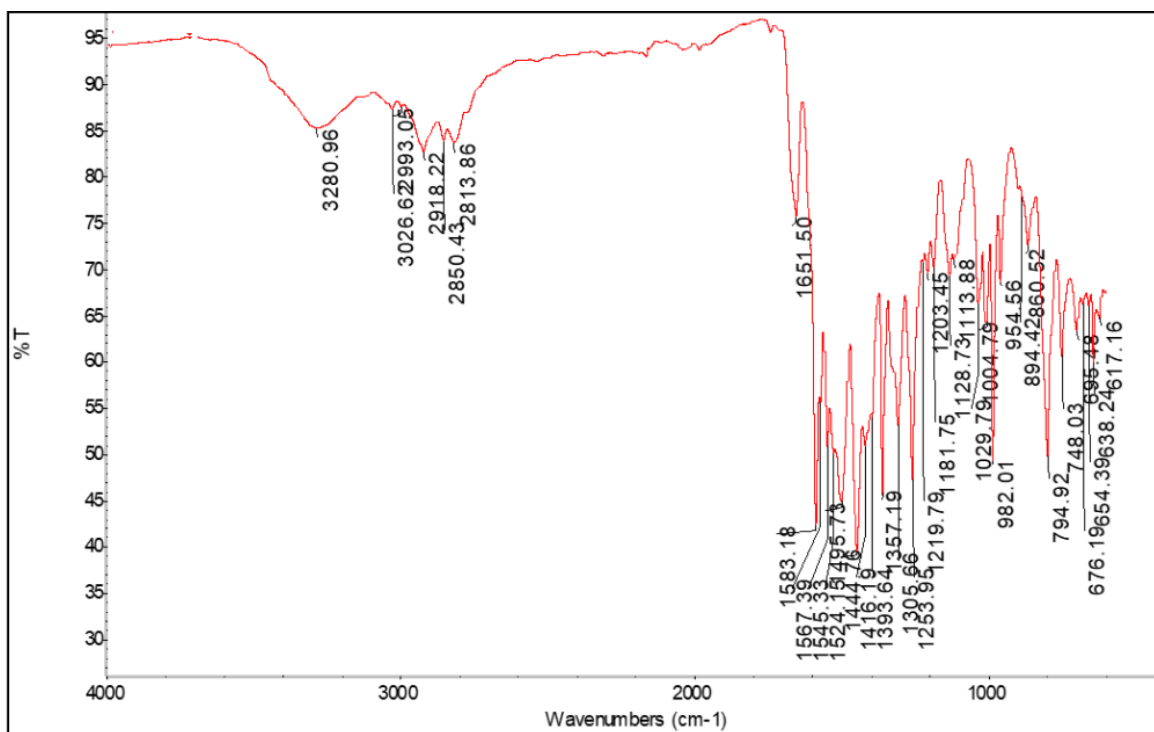


Figure S18. IR Spectrum of Compound 5.

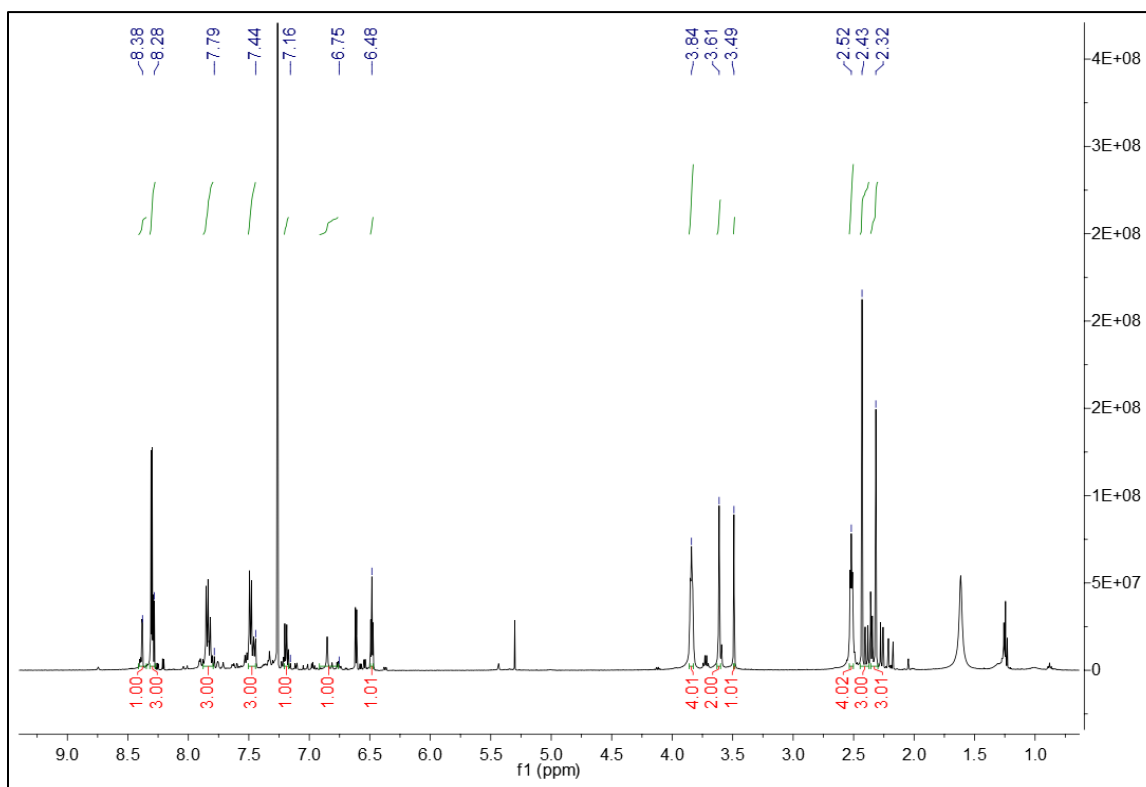


Figure S19. ¹H-NMR spectrum of Compound 5.

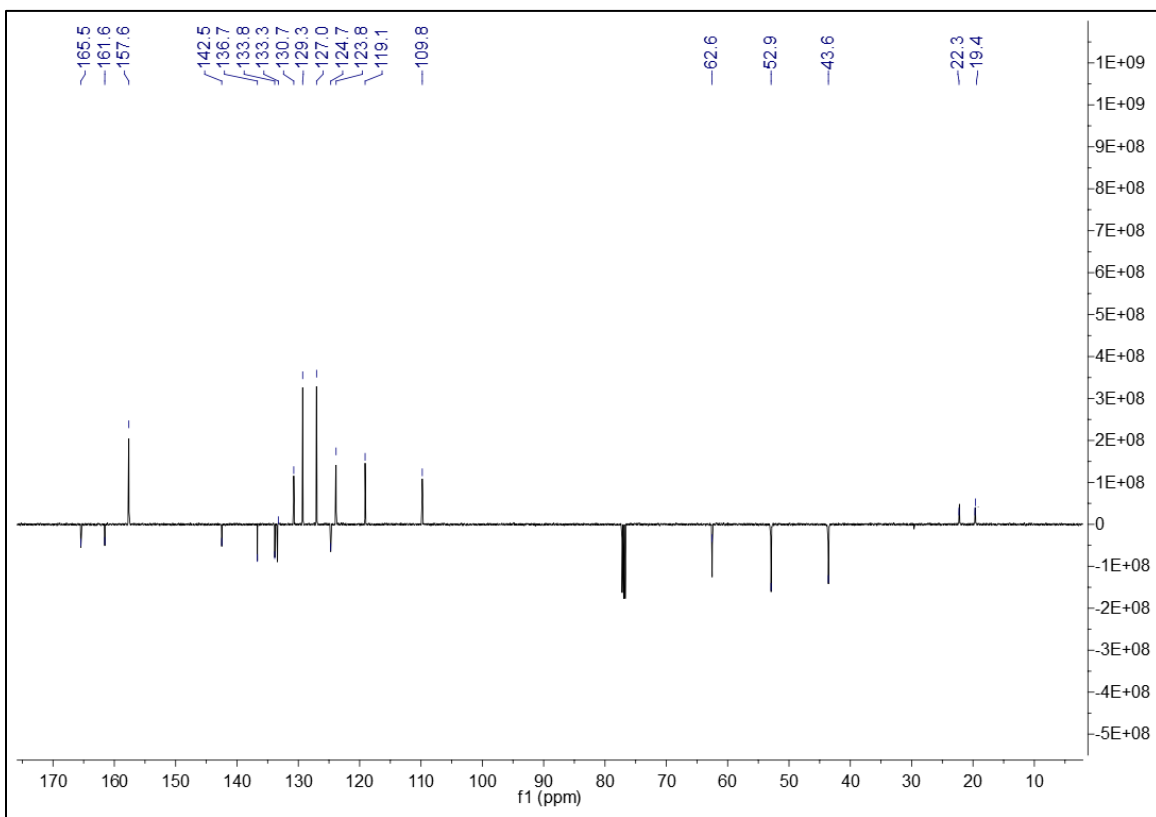


Figure S20. APT spectrum of Compound 5.

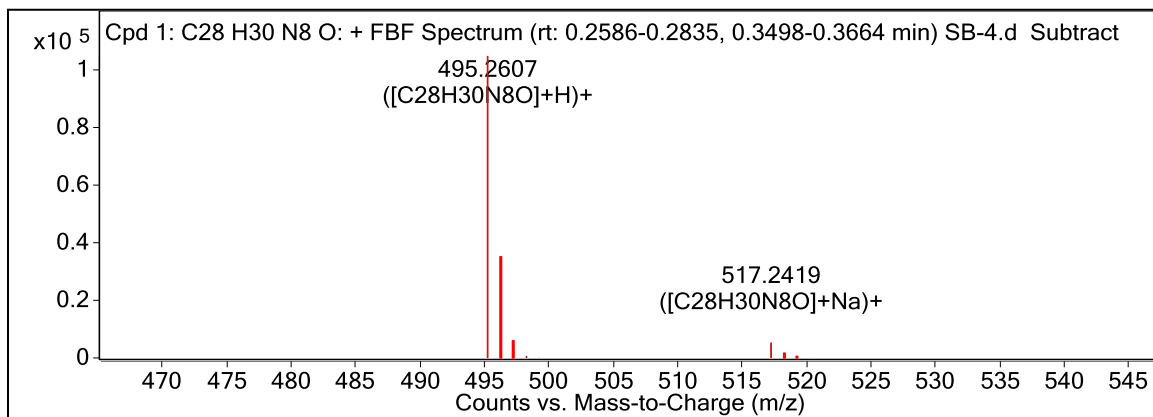


Figure S21. HRMS Spectrum of Compound 5.

Compound 6

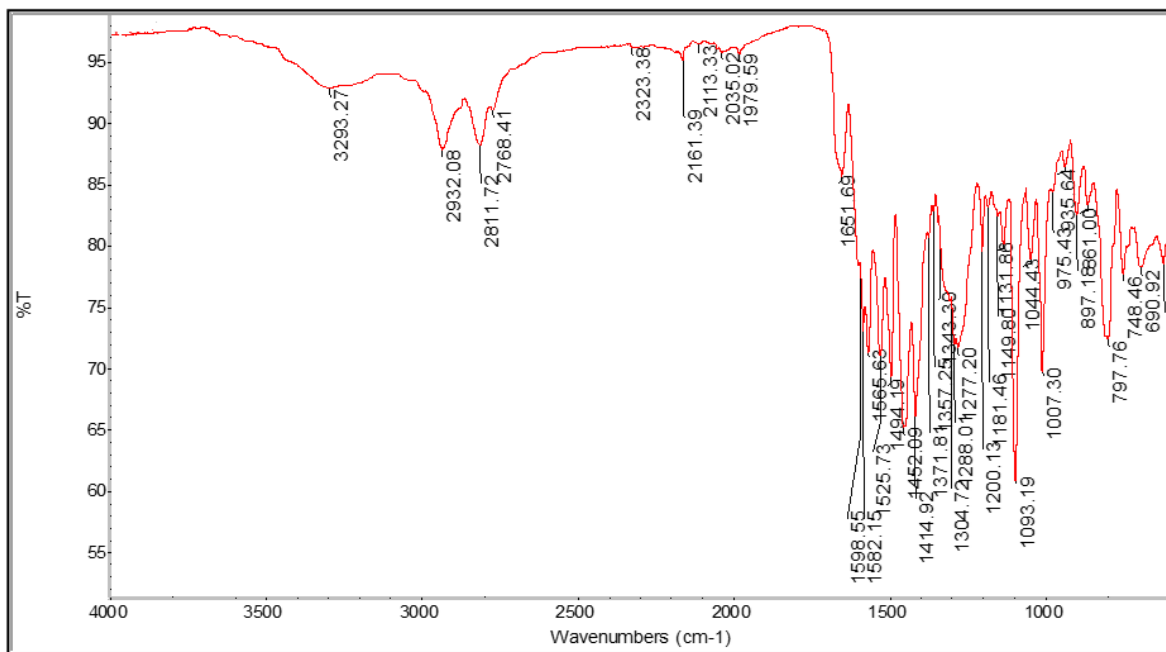
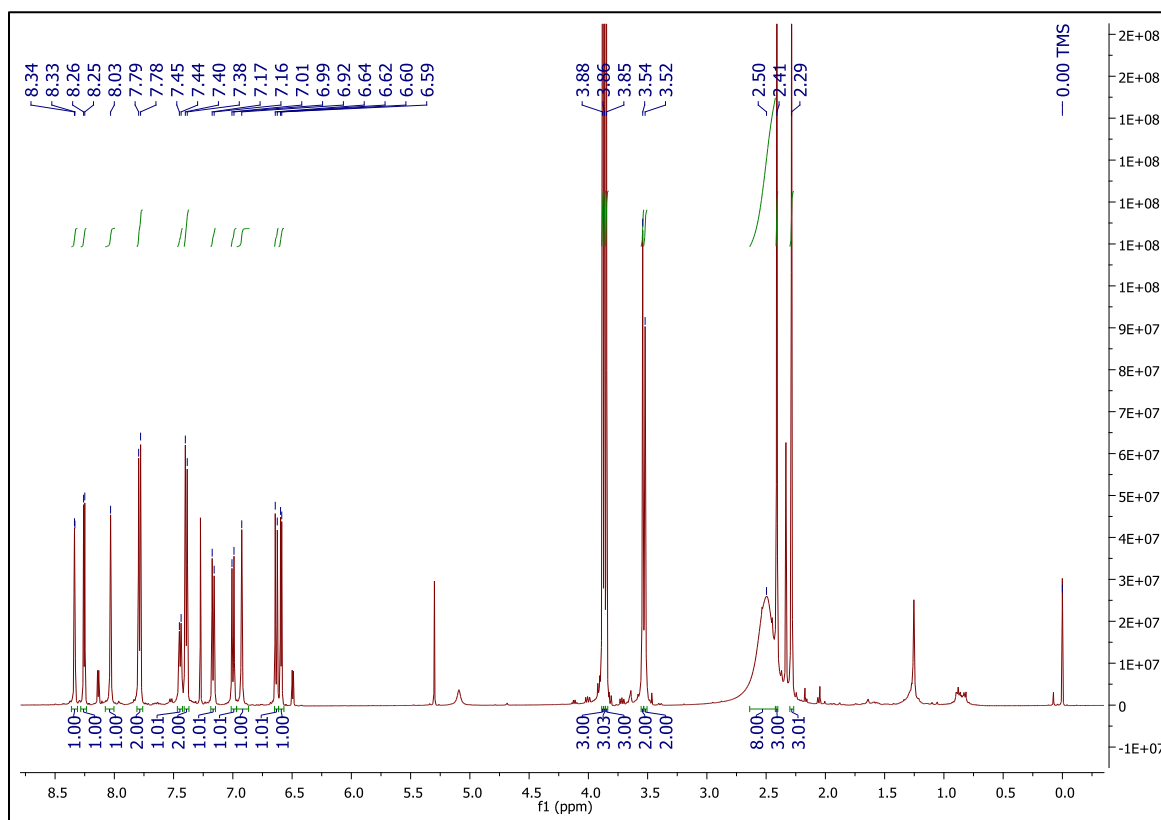


Figure S22. IR spectrum of Compound 6.



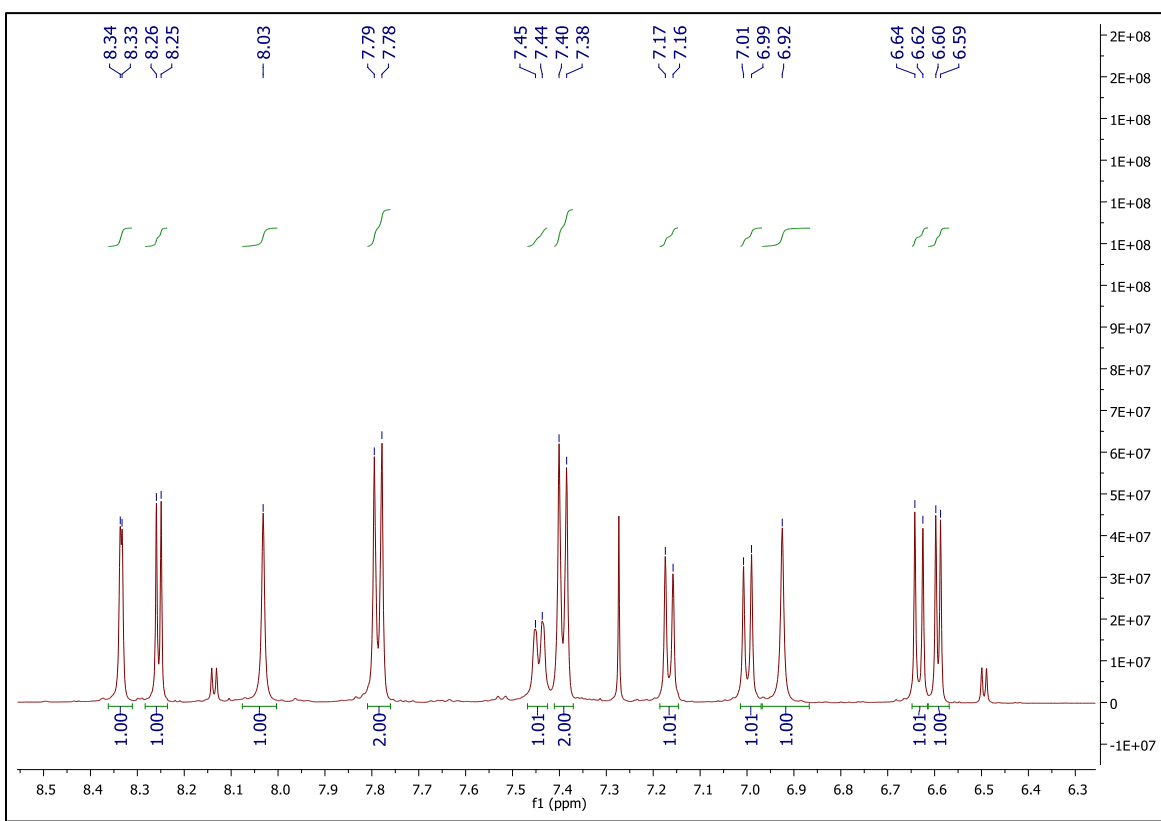
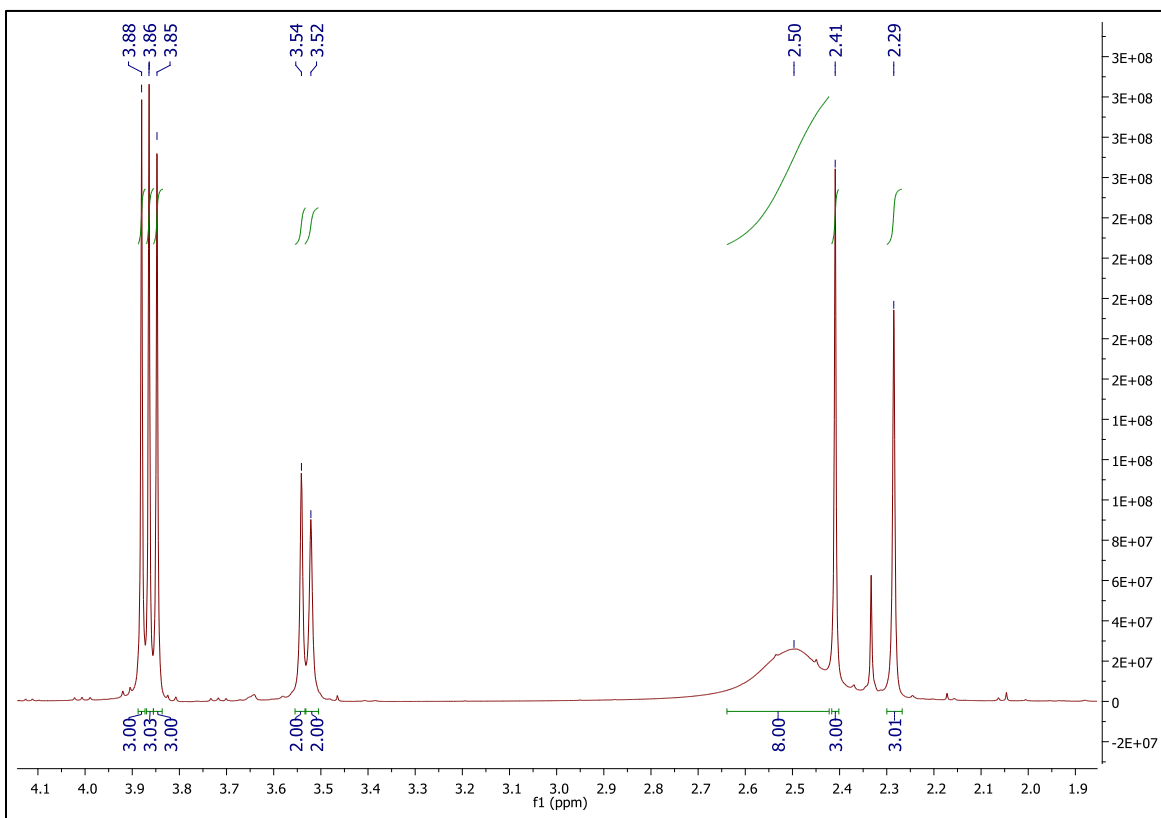


Figure S23-S24-S25. ¹H-NMR spectrum of Compound 6.

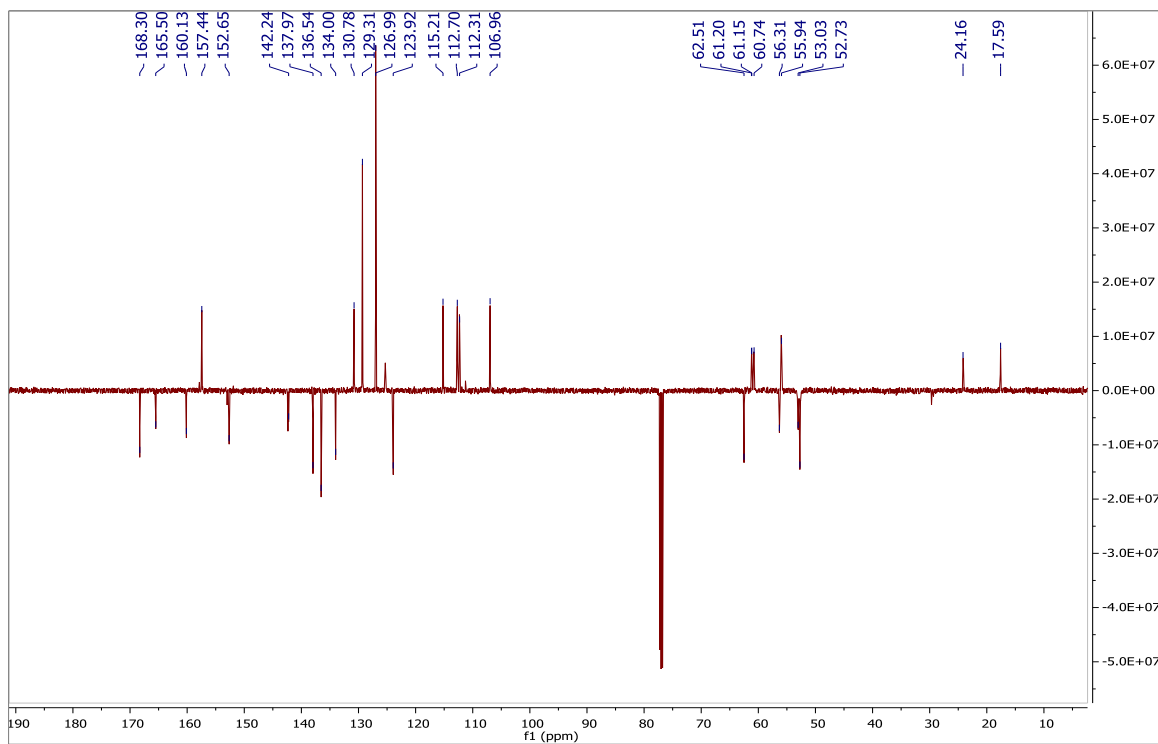


Figure S26. APT spectrum of Compound 6.

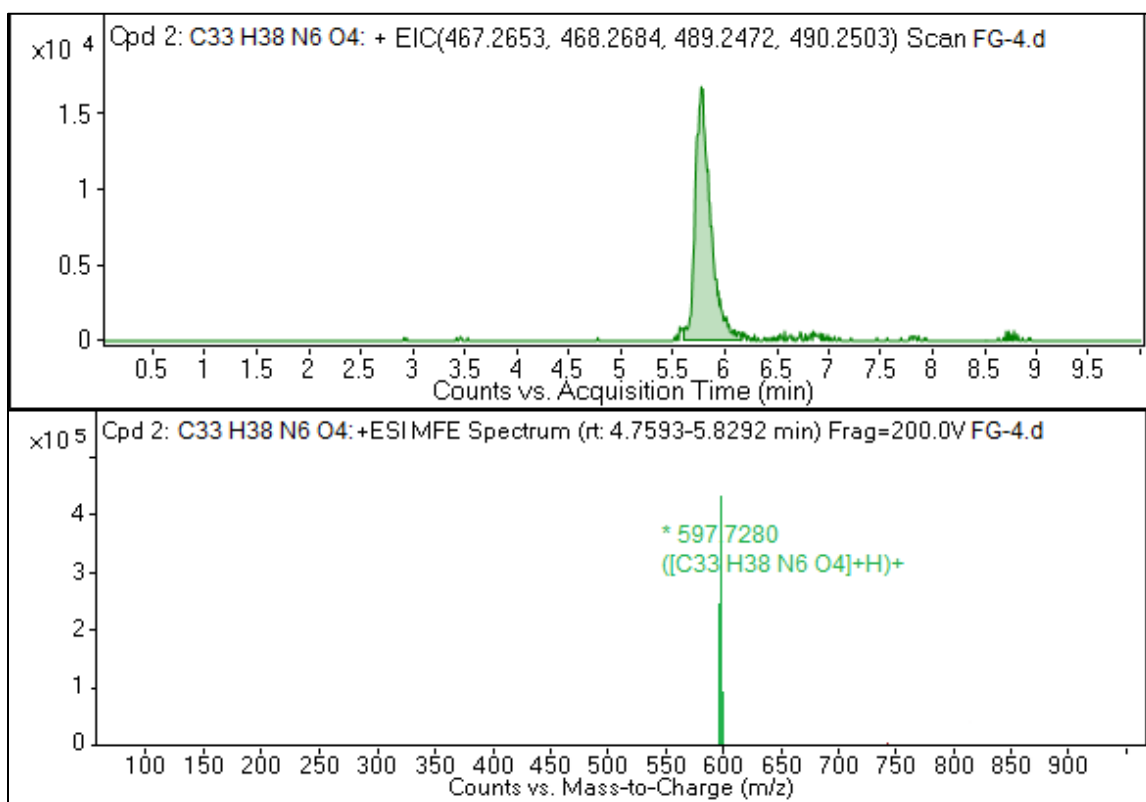


Figure S27. HRMS Spectrum of Compound 6.

Compound 7

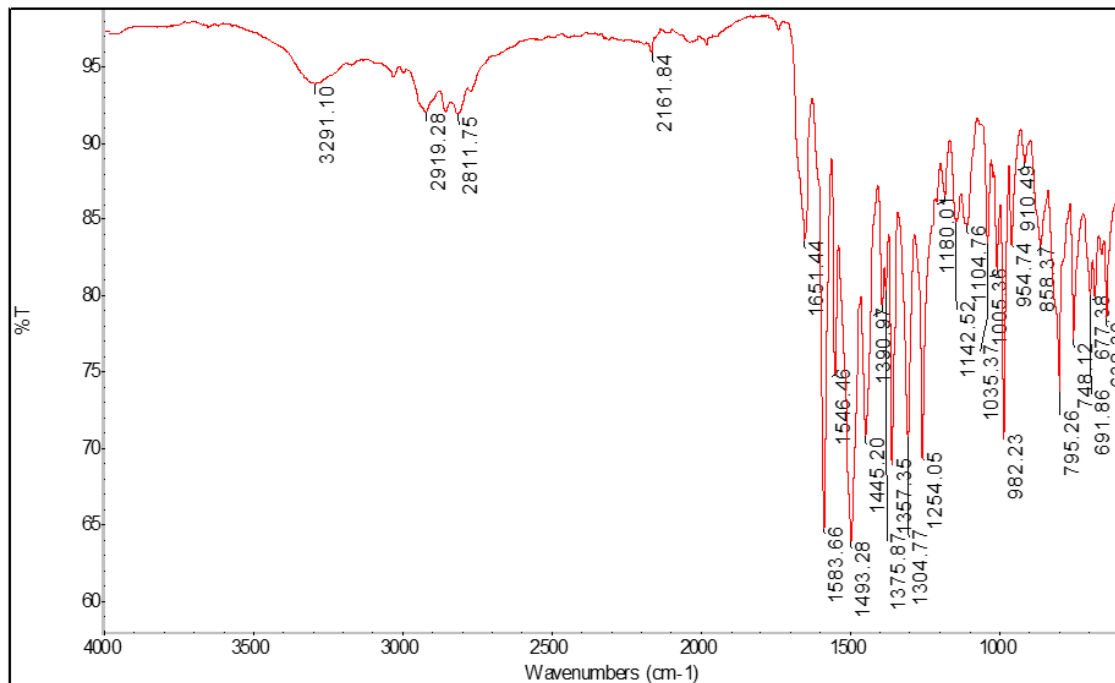


Figure S28. IR spectrum of Compound 7.

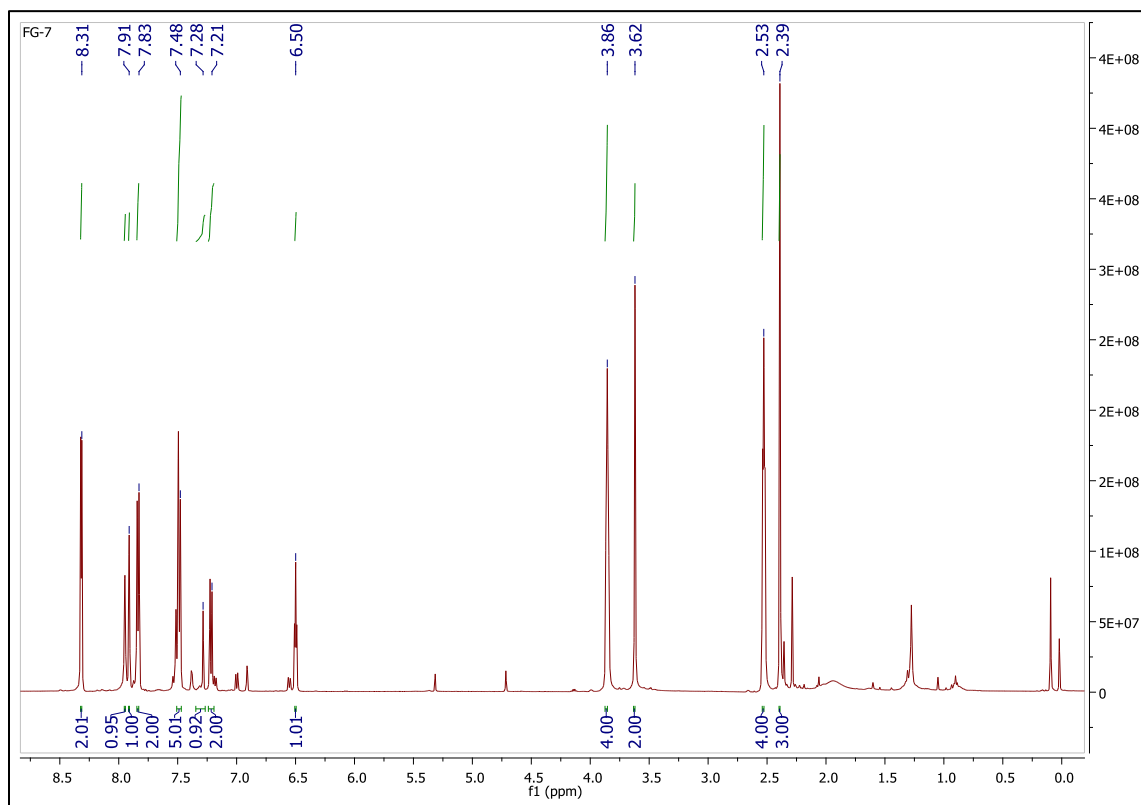


Figure S29. ¹H-NMR spectrum of Compound 7.

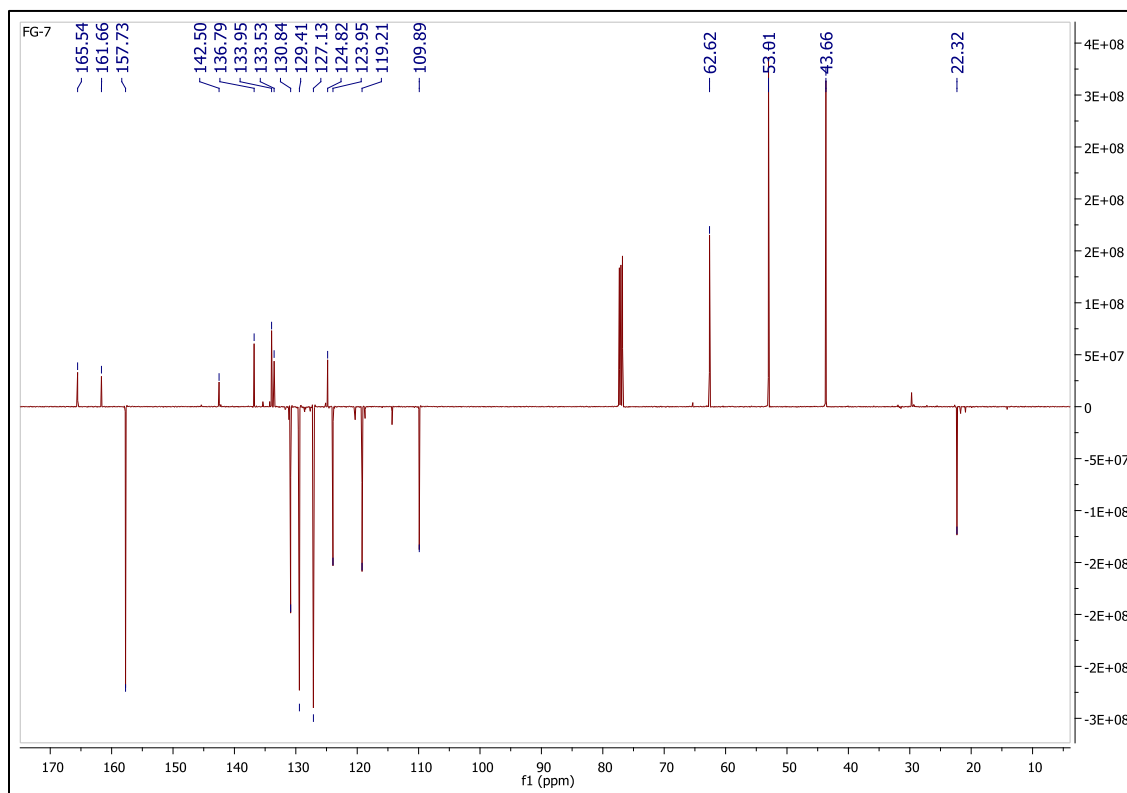


Figure S30. APT spectrum of Compound 7.

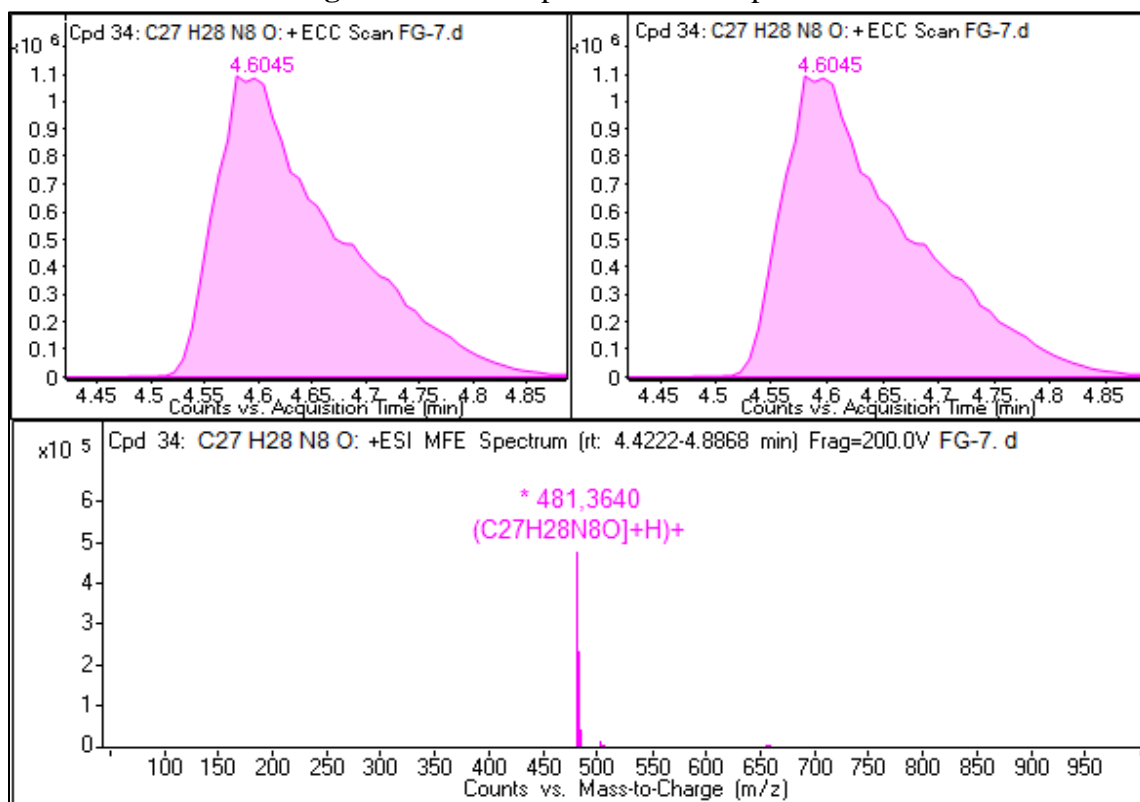


Figure S31. HRMS Spectrum of Compound 7.

Compound 8

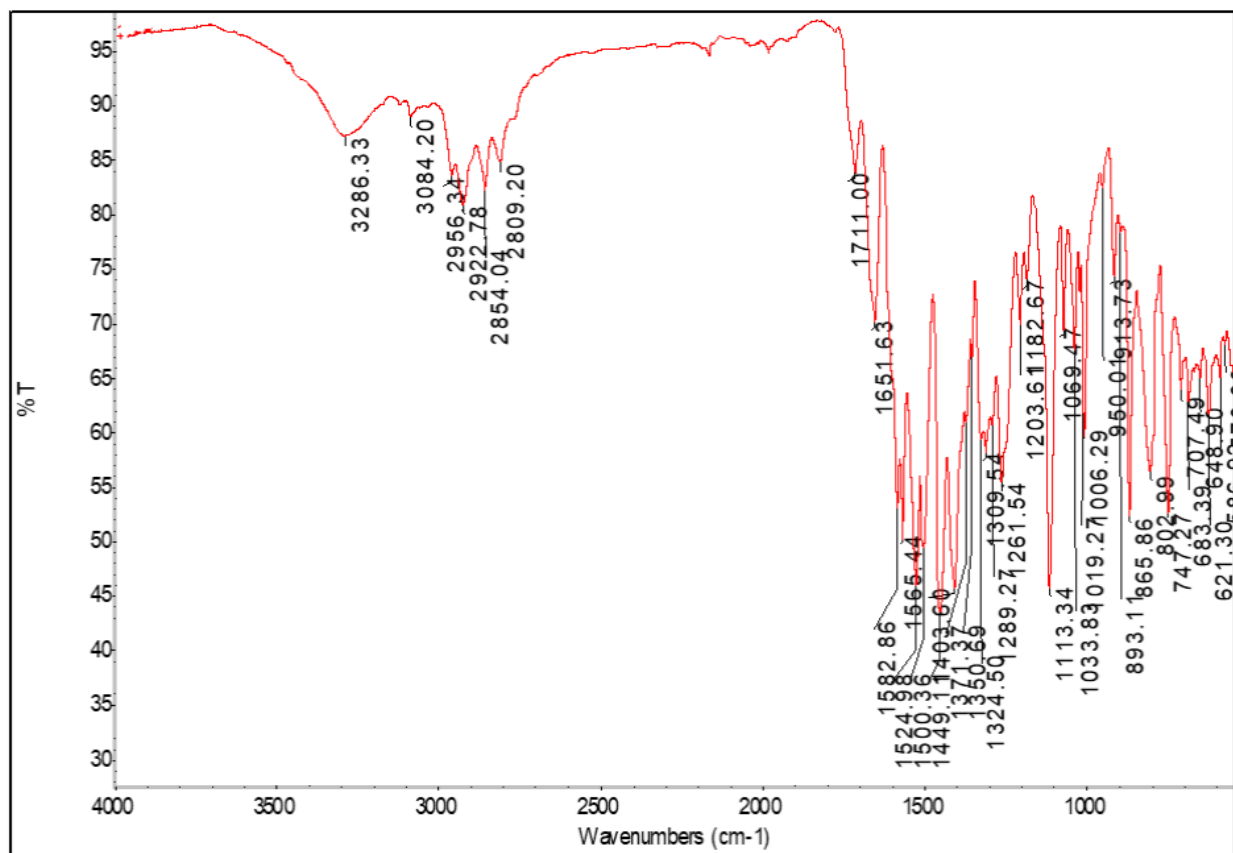


Figure S32. IR spectrum of Compound 8.

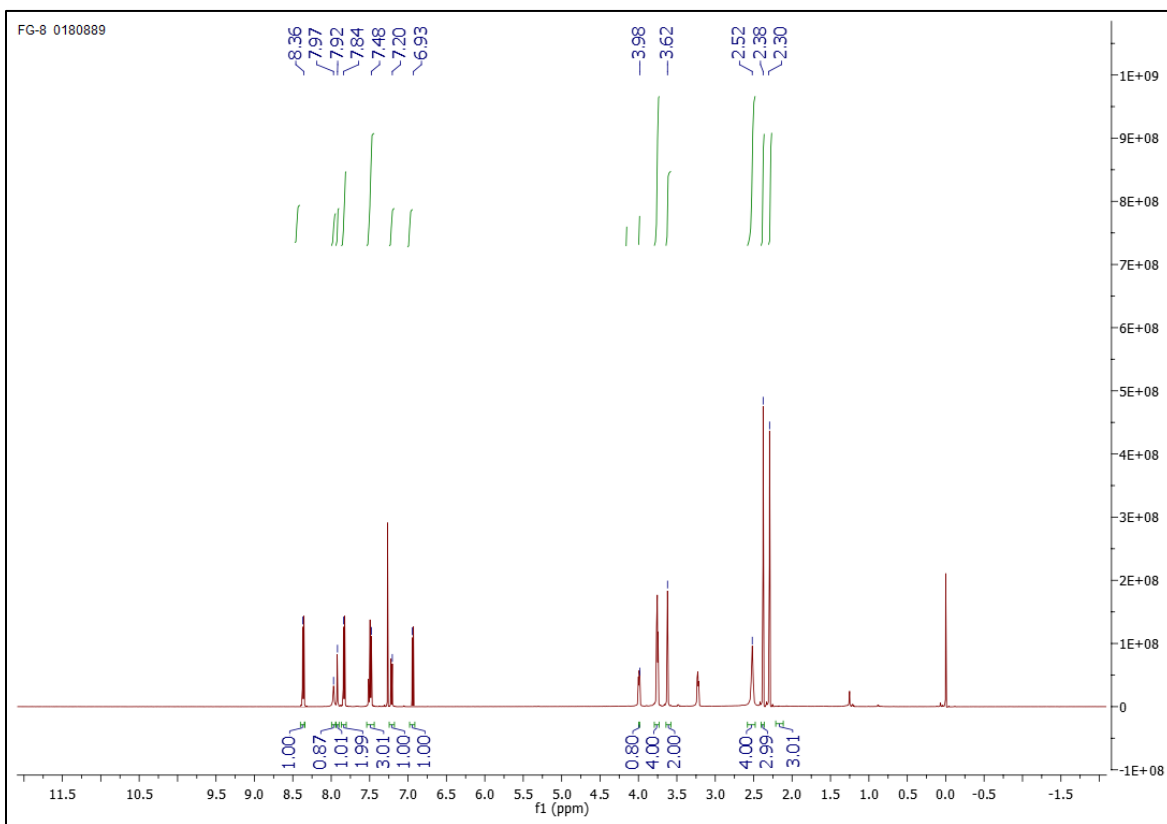


Figure S33. $^1\text{H-NMR}$ spectrum of Compound 8.

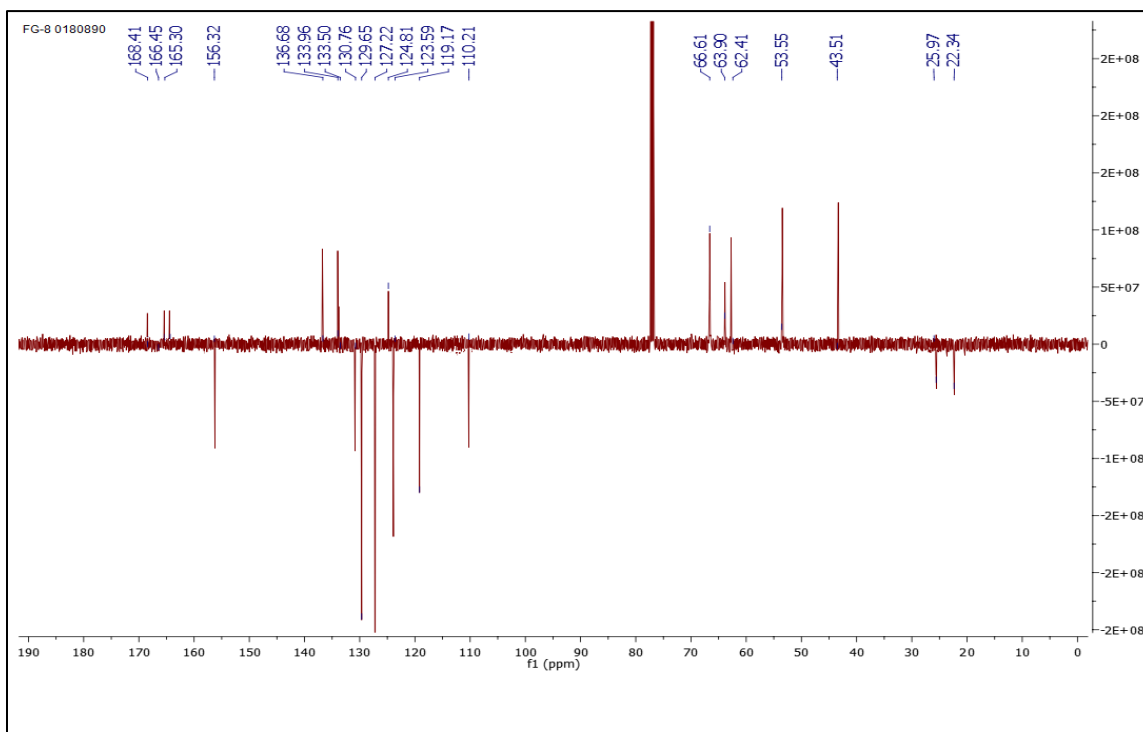


Figure S34. APT spectrum of Compound 8.

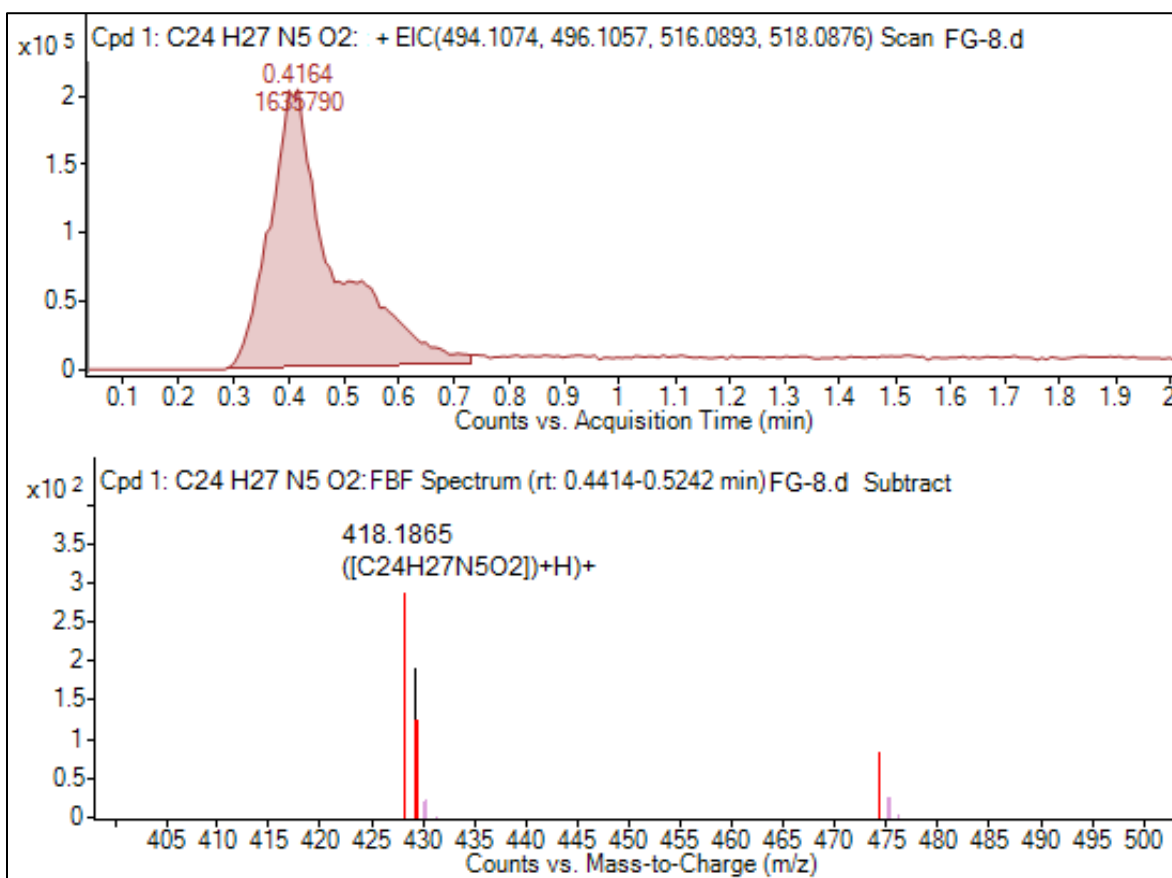


Figure S35. HRMS Spectrum of Compound 8.

Compound 9

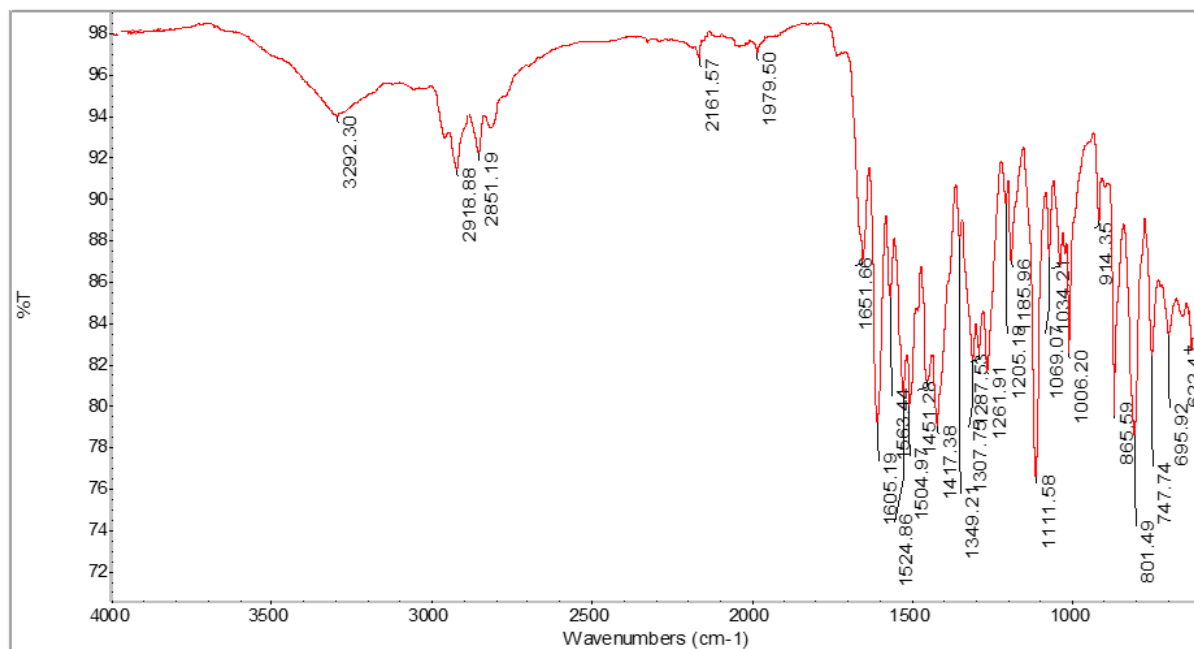


Figure S36. IR spectrum of Compound 9.

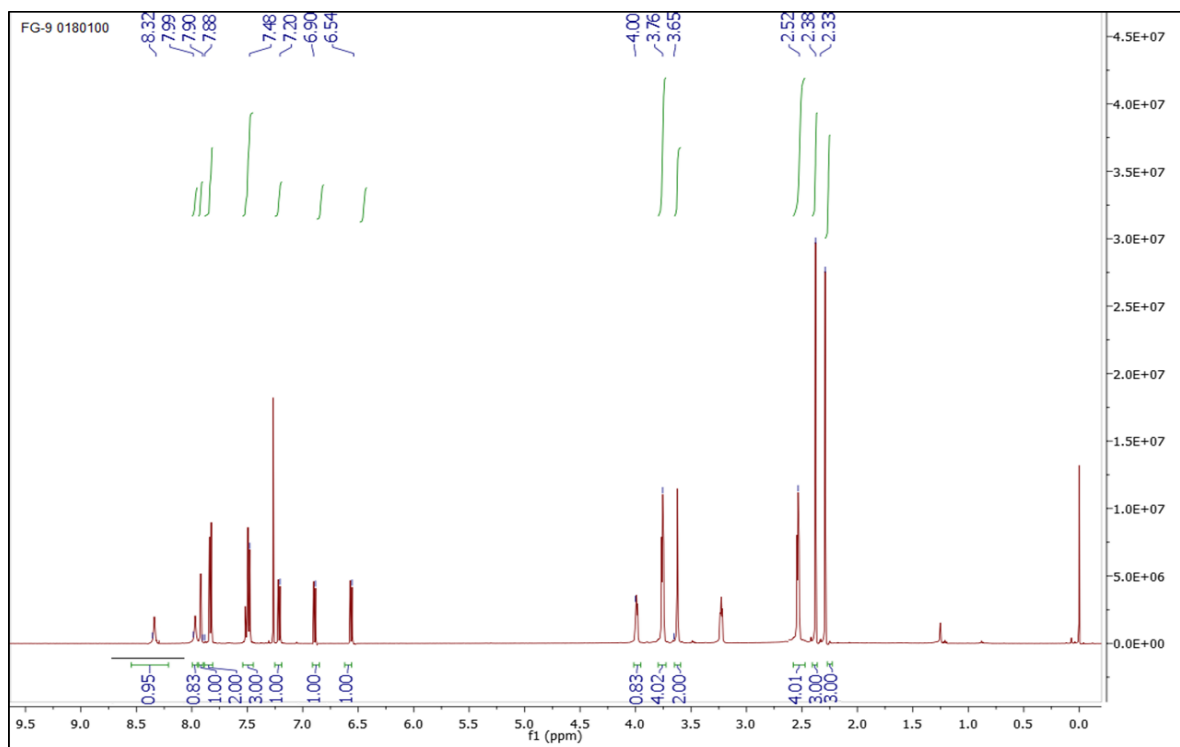


Figure S37. ¹H-NMR spectrum of Compound 9.

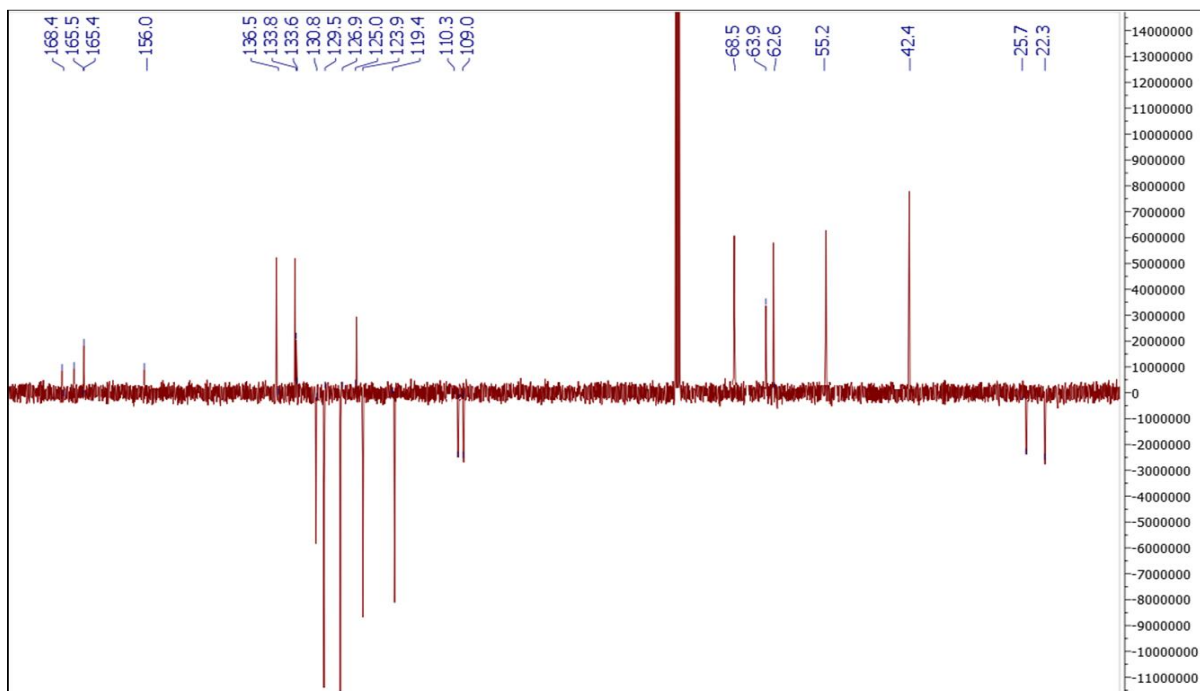


Figure S38. APT spectrum of Compound 9.

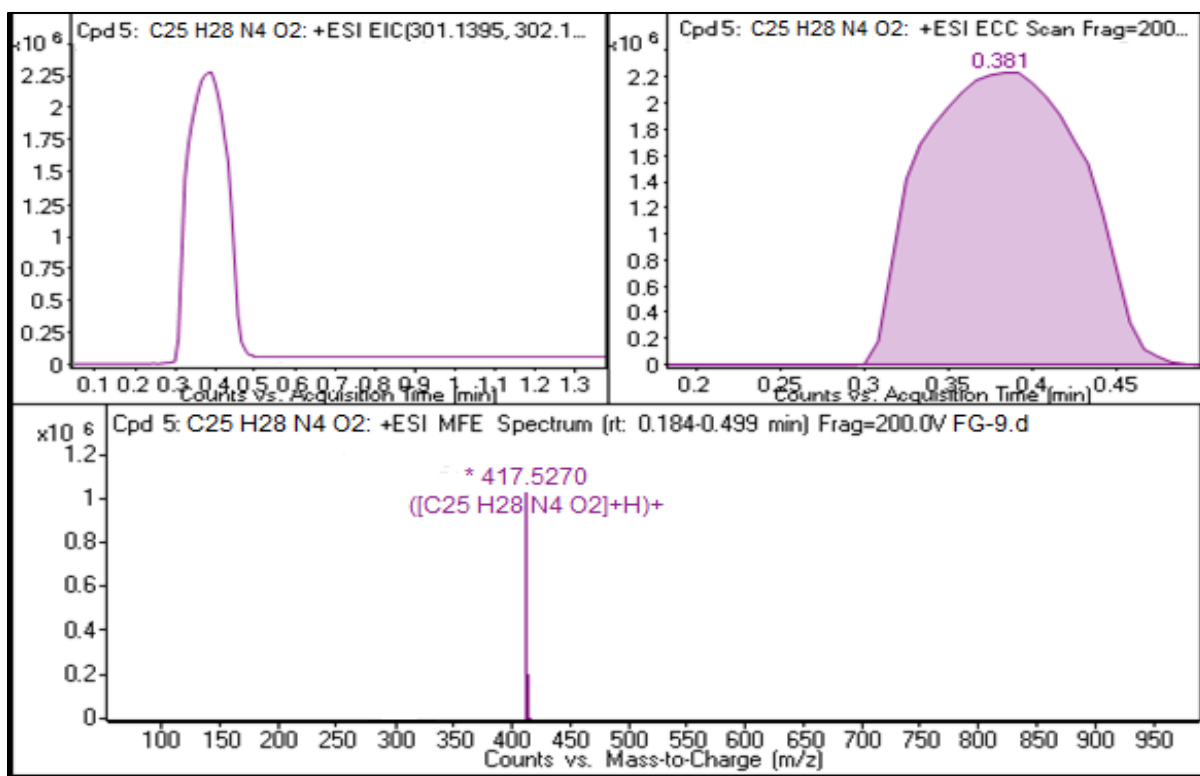


Figure S39. HRMS Spectrum of Compound 9.

Compound 10

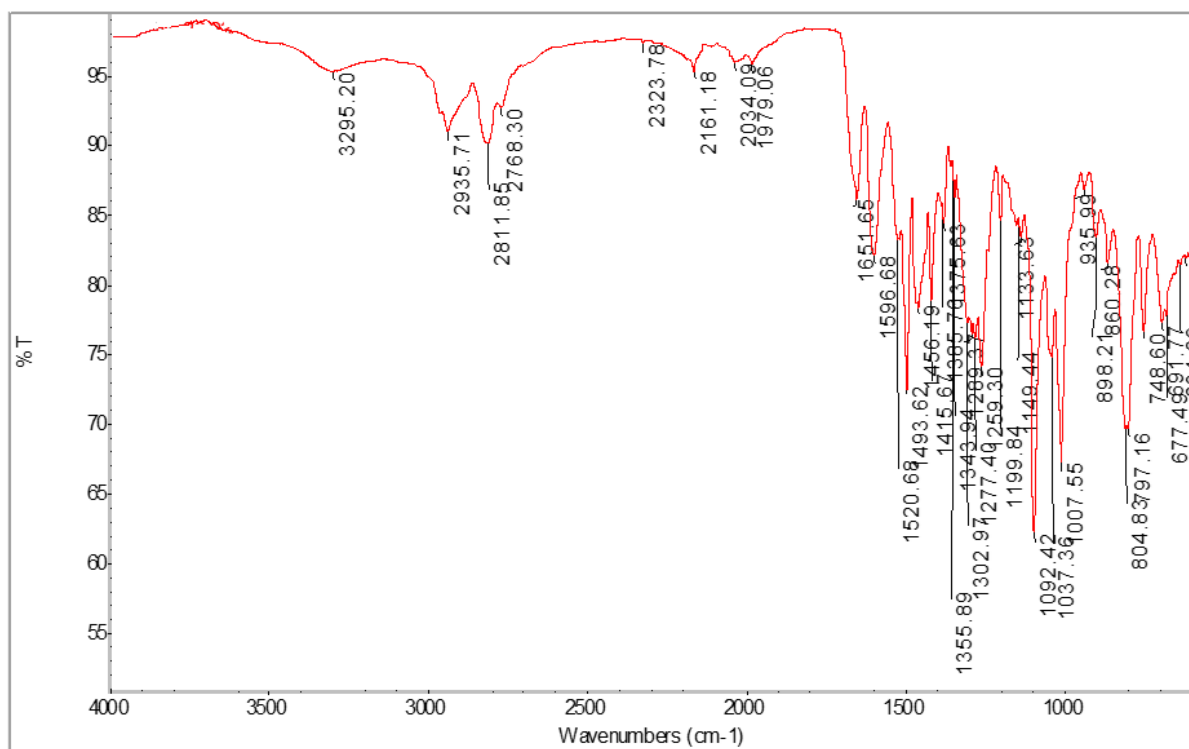


Figure S40. IR spectrum of Compound 10.

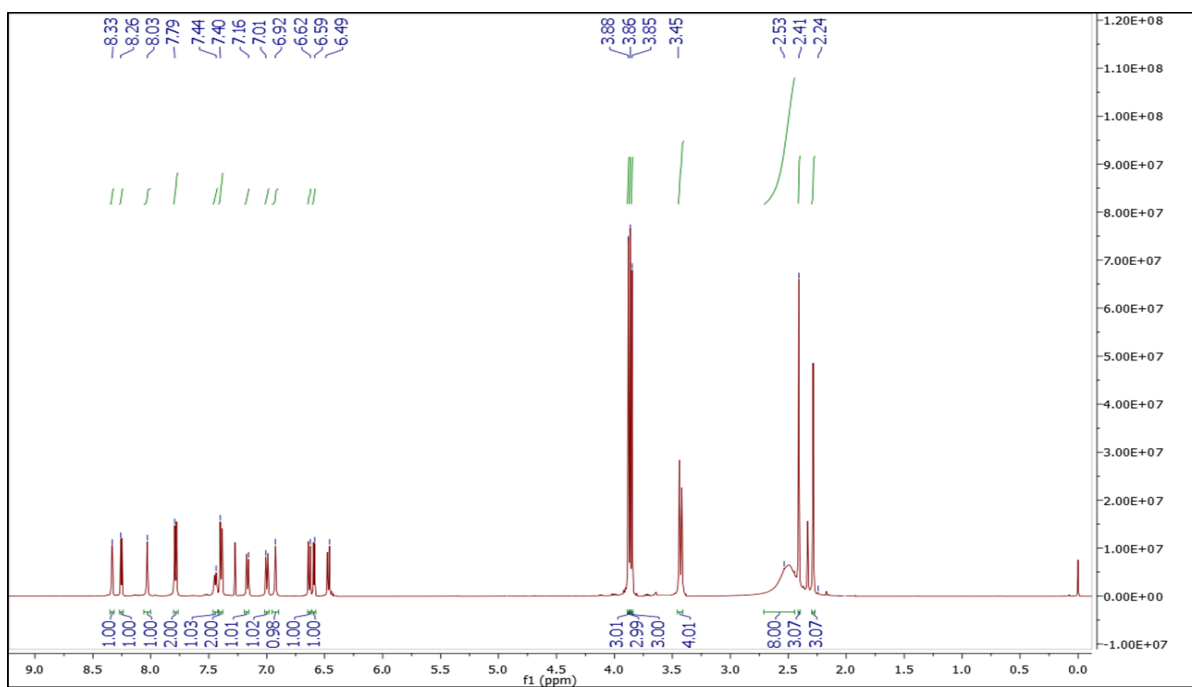


Figure S41. ¹H-NMR spectrum of Compound 10.

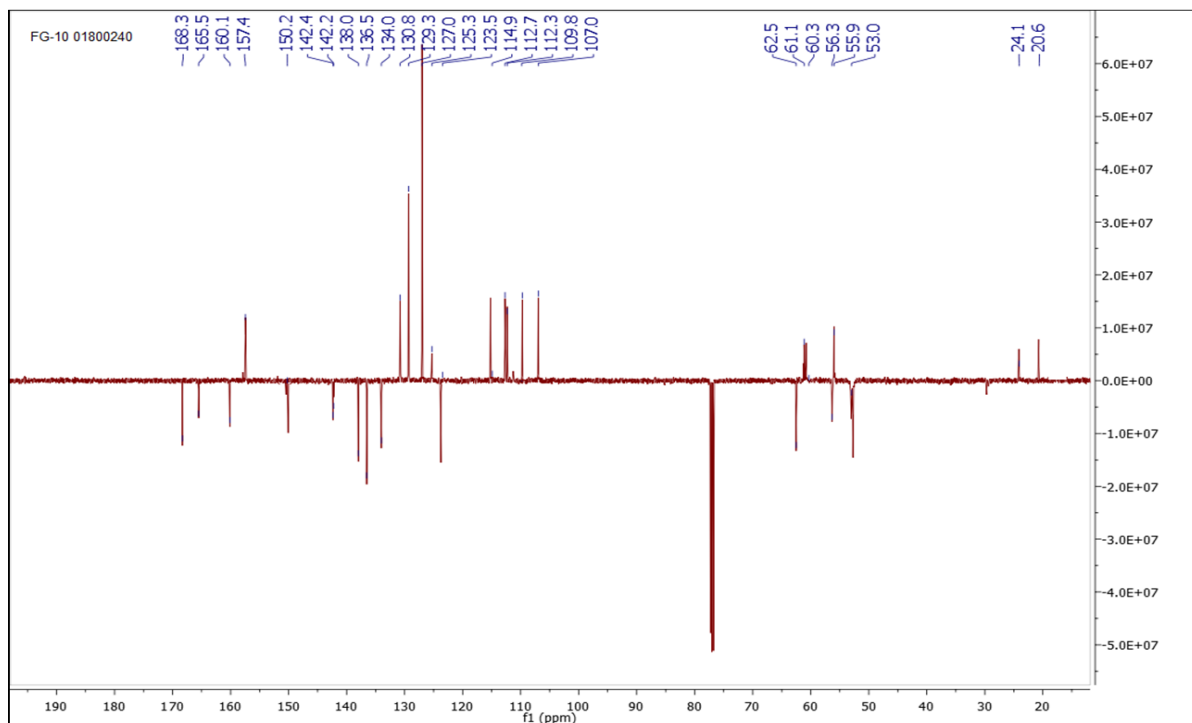


Figure S42. APT spectrum of Compound 10.

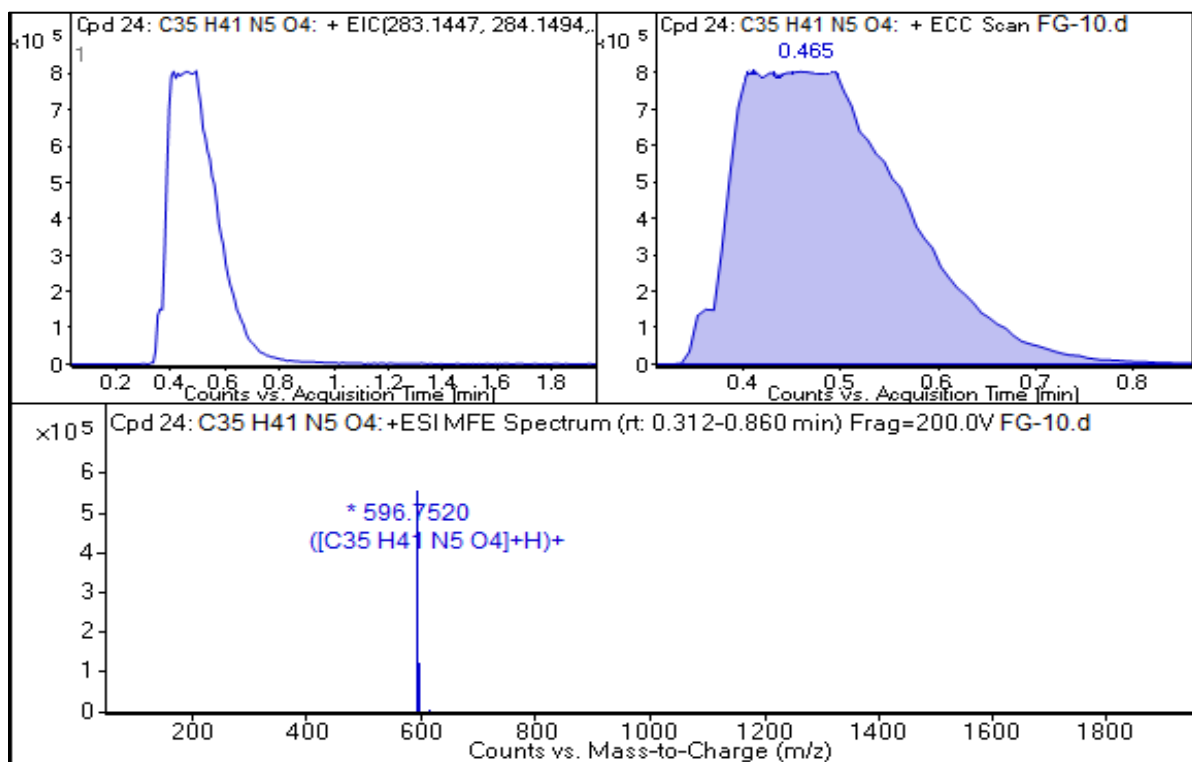


Figure S43. HRMS Spectrum of Compound 10.

Table S1

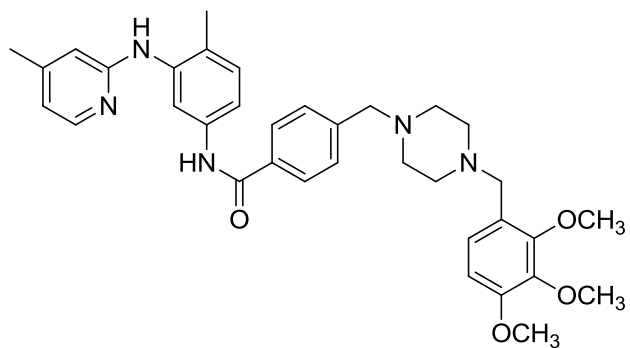
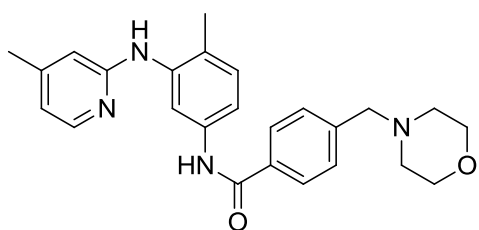
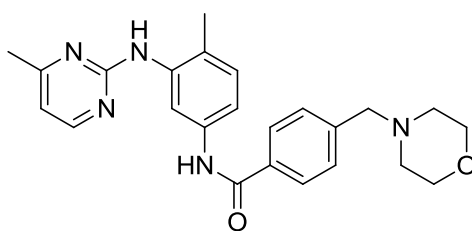
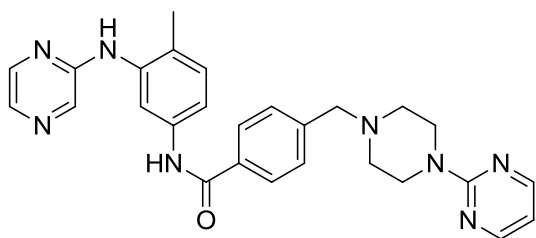
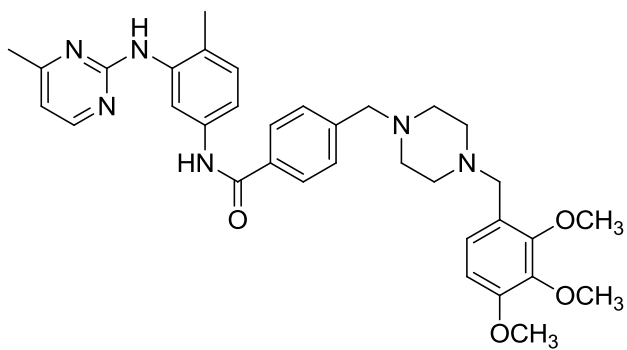
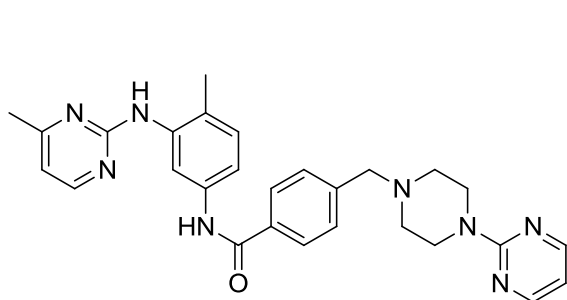
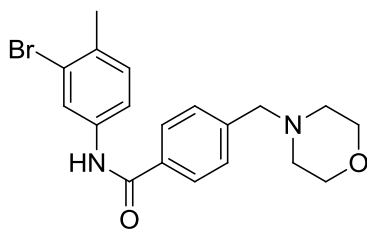
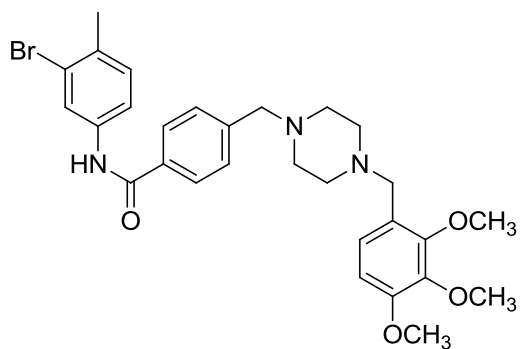
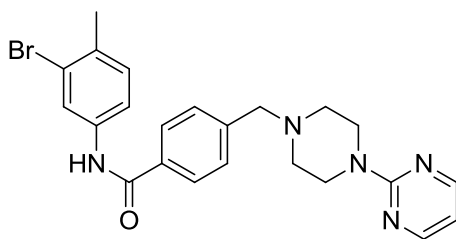
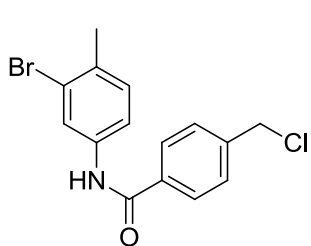


Table S2 Concentration (μM)- viability rate (%) values according to MTT assay in different cell lines.

For K562

Concentration (μM)- Viability rate (%)														
Compd	0.3	0.5	1	3	5	10	15	20	30	50	70	100	150	200
5	-	-	103.1 \pm 0.07	98.7 \pm 0.08	99.7 \pm 0.06	97.0 \pm 0.05	99.5 \pm 0.12	106.5 \pm 0.04	102.7 \pm 0.05	101.6 \pm 0.12	100.1 \pm 0.08	104.6 \pm 0.10	104.3 \pm 0.10	102.1 \pm 0.14
6	92.5 \pm 0.11	91.8 \pm 0.06	91.8 \pm 0.04	88.7 \pm 0.05	87.6 \pm 0.05	87.3 \pm 0.11	87.3 \pm 0.10	86.5 \pm 0.07	85.5 \pm 0.10	78.1 \pm 0.10	68.5 \pm 0.05	67.5 \pm 0.03	67.3 \pm 0.02	67.2 \pm 0.03
7	84.6 \pm 0.15	84.5 \pm 0.08	84.4 \pm 0.08	84.5 \pm 0.10	82.9 \pm 0.12	81.6 \pm 0.05	80.1 \pm 0.06	64.0 \pm 0.07	63.9 \pm 0.04	62.9 \pm 0.06	62.3 \pm 0.07	62.2 \pm 0.05	61.6 \pm 0.05	59.5 \pm 0.07
8	86.2 \pm 0.09	85.3 \pm 0.03	84.7 \pm 0.05	84.7 \pm 0.06	76.8 \pm 0.11	76.7 \pm 0.05	76.7 \pm 0.08	76.6 \pm 0.04	75.6 \pm 0.09	72.5 \pm 0.07	72.6 \pm 0.08	66.4 \pm 0.02	65.3 \pm 0.06	65.2 \pm 0.06
9	79.9 \pm 0.09	78.5 \pm 0.03	77.3 \pm 0.08	77.0 \pm 0.04	75.4 \pm 0.09	73.2 \pm 0.08	72.0 \pm 0.06	69.1 \pm 0.03	69.7 \pm 0.07	61.2 \pm 0.08	58.1 \pm 0.10	51.3 \pm 0.06	49.7 \pm 0.05	45.0 \pm 0.08
10	104.1 \pm 0.07	103.4 \pm 0.06	98.9 \pm 0.05	98.7 \pm 0.04	98.6 \pm 0.06	98.9 \pm 0.09	98.6 \pm 0.08	79.2 \pm 0.06	78.9 \pm 0.10	56.1 \pm 0.03	38.5 \pm 0.02	38.7 \pm 0.01	38.9 \pm 0.01	38.7 \pm 0.01
imatinib	98.0 \pm 0.03	97.4 \pm 0.06	95.4 \pm 0.07	95.3 \pm 0.05	95.4 \pm 0.09	94.8 \pm 0.09	88.5 \pm 0.10	87.0 \pm 0.04	72.8 \pm 0.06	60.8 \pm 0.10	60.0 \pm 0.07	51.3 \pm 0.05	35.1 \pm 0.01	29.7 \pm 0.01

For Nalm-6

Concentration (μM)- Viability rate (%)														
Compd	0.3	0.5	1	3	5	10	15	20	30	50	70	100	150	200
5	-	-	95.8 \pm 0.01	95.0 \pm 0.02	92.4 \pm 0.03	90.1 \pm 0.02	84.1 \pm 0.01	80.1 \pm 0.02	78.6 \pm 0.01	74.1 \pm 0.01	71.9 \pm 0.01	70.3 \pm 0.01	70.2 \pm 0.01	70.5 \pm 0.01
6	100.7 \pm 0.01	100.5 \pm 0.02	100.1 \pm 0.03	100.0 \pm 0.04	98.8 \pm 0.04	98.0 \pm 0.02	95.6 \pm 0.02	82.6 \pm 0.02	71.6 \pm 0.01	55.2 \pm 0.01	43.5 \pm 0.01	42.6 \pm 0.01	42.9 \pm 0.01	42.8 \pm 0.02
7	97.9 \pm 0.06	95.1 \pm 0.03	95.1 \pm 0.03	96.0 \pm 0.03	95.6 \pm 0.02	95.1 \pm 0.02	95.9 \pm 0.03	96.4 \pm 0.03	96.5 \pm 0.05	72.3 \pm 0.02	71.8 \pm 0.02	71.3 \pm 0.02	70.2 \pm 0.01	59.7 \pm 0.02
8	102.8 \pm 0.04	101.8 \pm 0.04	102.7 \pm 0.02	99.6 \pm 0.04	102.5 \pm 0.02	100.6 \pm 0.03	100.0 \pm 0.03	94.2 \pm 0.07	95.9 \pm 0.07	91.9 \pm 0.06	87.7 \pm 0.02	87.4 \pm 0.02	81.3 \pm 0.02	70.8 \pm 0.01
9	86.4 \pm 0.05	85.2 \pm 0.05	72.7 \pm 0.04	64.5 \pm 0.02	62.6 \pm 0.04	53.2 \pm 0.03	50.1 \pm 0.03	49.2 \pm 0.01	48.1 \pm 0.01	43.9 \pm 0.01	42.8 \pm 0.01	42.5 \pm 0.01	42.5 \pm 0.01	39.2 \pm 0.01
10	92.7 \pm 0.08	88.6 \pm 0.06	87.3 \pm 0.07	86.5 \pm 0.02	85.5 \pm 0.06	84.8 \pm 0.08	82.2 \pm 0.08	71.9 \pm 0.07	54.2 \pm 0.07	29.8 \pm 0.01	28.8 \pm 0.01	28.7 \pm 0.01	28.5 \pm 0.01	28.7 \pm 0.01
imatinib	91.0 \pm 0.08	90.7 \pm 0.06	90.1 \pm 0.09	84.7 \pm 0.09	84.5 \pm 0.05	72.9 \pm 0.03	57.1 \pm 0.02	52.7 \pm 0.01	50.7 \pm 0.03	39.7 \pm 0.01	32.5 \pm 0.05	32.2 \pm 0.02	32.5 \pm 0.01	29.0 \pm 0.02

For Molt-4

Compd	Concentration (µM)- Viability rate (%)													
	0.3	0.5	1	3	5	10	15	20	30	50	70	100	150	200
5	-	-	95.2 ± 0.08	84.6 ± 0.04	85.1 ± 0.11	84.8 ± 0.03	84.9 ± 0.11	85.8 ± 0.03	85.3 ± 0.06	86.1 ± 0.11	84.6 ± 0.05	83.5 ± 0.12	87.1 ± 0.09	86.6 ± 0.08
6	84.4 ± 0.14	79.7 ± 0.10	78.7 ± 0.09	79.7 ± 0.18	80.5 ± 0.16	81.8 ± 0.07	79.2 ± 0.15	76.0 ± 0.05	75.4 ± 0.08	73.5 ± 0.04	68.9 ± 0.06	61.7 ± 0.02	59.9 ± 0.05	55.2 ± 0.04
7	93.3 ± 0.16	93.8 ± 0.08	89.8 ± 0.07	89.6 ± 0.12	89.7 ± 0.08	89.5 ± 0.06	90.3 ± 0.04	90.2 ± 0.06	90.9 ± 0.06	92.2 ± 0.05	90.6 ± 0.06	85.5 ± 0.06	90.4 ± 0.04	89.8 ± 0.07
8	98.5 ± 0.09	98.5 ± 0.11	95.4 ± 0.11	89.2 ± 0.07	90.7 ± 0.07	90.4 ± 0.07	90.8 ± 0.05	88.3 ± 0.04	85.8 ± 0.04	83.6 ± 0.02	82.6 ± 0.09	81.5 ± 0.09	78.9 ± 0.05	78.8 ± 0.07
9	93.2 ± 0.17	87.8 ± 0.05	78.4 ± 0.11	72.7 ± 0.04	71.7 ± 0.07	69.3 ± 0.04	68.9 ± 0.05	63.5 ± 0.04	62.0 ± 0.03	61.5 ± 0.07	59.8 ± 0.05	59.5 ± 0.08	58.6 ± 0.06	54.7 ± 0.03
10	87.9 ± 0.03	86.8 ± 0.02	87.7 ± 0.01	86.5 ± 0.02	86.2 ± 0.08	89.1 ± 0.03	88.1 ± 0.04	77.0 ± 0.04	65.3 ± 0.03	52.1 ± 0.03	42.8 ± 0.01	40.4 ± 0.01	40.0 ± 0.01	40.7 ± 0.01
imatinib	75.6 ± 0.18	74.9 ± 0.18	75.1 ± 0.19	73.8 ± 0.17	72.7 ± 0.25	70.7 ± 0.21	70.2 ± 0.10	63.4 ± 0.10	63.3 ± 0.06	55.5 ± 0.05	52.1 ± 0.10	41.2 ± 0.06	29.8 ± 0.04	20.3 ± 0.02

For REH

Compd	Concentration (µM)- Viability rate (%)													
	0.3	0.5	1	3	5	10	15	20	30	50	70	100	150	200
5	-	-	96.6 ± 0.01	95.8 ± 0.05	95.7 ± 0.03	95.1 ± 0.04	94.9 ± 0.04	90.2 ± 0.03	87.9 ± 0.04	85.5 ± 0.05	81.4 ± 0.01	79.1 ± 0.01	79.1 ± 0.02	74. ± 0.01
6	109.5 ± 0.02	105.2 ± 0.02	106.8 ± 0.01	107.9 ± 0.02	108.2 ± 0.01	106.9 ± 0.02	106.5 ± 0.02	97.7 ± 0.02	88.6 ± 0.03	85.6 ± 0.02	65.3 ± 0.02	62.2 ± 0.01	61.3 ± 0.01	61.1 ± 0.02
7	110.0 ± 0.02	109.8 ± 0.02	108.7 ± 0.02	103.4 ± 0.02	108.8 ± 0.02	106.5 ± 0.05	100.2 ± 0.02	95.5 ± 0.06	85.4 ± 0.02	66.7 ± 0.02	66.2 ± 0.03	67.7 ± 0.03	66.8 ± 0.02	62.8 ± 0.02
8	100.8 ± 0.03	102.4 ± 0.02	102.0 ± 0.01	104.8 ± 0.02	103.5 ± 0.01	103.1 ± 0.01	100.3 ± 0.01	100.6 ± 0.02	102.4 ± 0.04	99.4 ± 0.02	94.2 ± 0.03	91.1 ± 0.01	91.1 ± 0.02	91.2 ± 0.04
9	103.8 ± 0.01	101.3 ± 0.03	100.4 ± 0.01	100.5 ± 0.02	101.8 ± 0.03	103.4 ± 0.02	100.2 ± 0.02	99.0 ± 0.02	91.4 ± 0.01	88.2 ± 0.02	84.7 ± 0.03	87.1 ± 0.02	85.0 ± 0.01	82.0 ± 0.02
10	93.4 ± 0.02	92.4 ± 0.02	92.4 ± 0.01	92.6 ± 0.02	92.8 ± 0.02	92.3 ± 0.03	92.6 ± 0.02	91.8 ± 0.01	65.6 ± 0.02	59.5 ± 0.03	59.1 ± 0.02	59.6 ± 0.03	57.4 ± 0.03	55.2 ± 0.03
imatinib	97.6 ± 0.03	96.8 ± 0.03	96.4 ± 0.01	95.5 ± 0.02	94.5 ± 0.03	91.3 ± 0.05	82.4 ± 0.02	78.6 ± 0.02	70.9 ± 0.03	63.5 ± 0.04	62.9 ± 0.03	61.2 ± 0.01	60.3 ± 0.03	57.0 ± 0.02

For Jurkat

Compd	Concentration (μ M)- Viability rate (%)													
	0.3	0.5	1	3	5	10	15	20	30	50	70	100	150	200
5	-	-	90.7.1 \pm 0.10	90.1 \pm 0.11	89.7 \pm 0.09	89.6 \pm 0.15	88.8 \pm 0.09	88.8 \pm 0.08	88.1 \pm 0.10	83.4 \pm 0.12	82.5 \pm 0.07	80.8 \pm 0.13	78.7 \pm 0.12	66.5 \pm 0.05
6	-	-	89.6.1 \pm 0.02	79.1 \pm 0.02	69.8 \pm 0.02	69.7 \pm 0.05	69.2 \pm 0.02	68.9 \pm 0.01	68.8 \pm 0.03	59.1 \pm 0.03	47.8 \pm 0.01	44.0 \pm 0.01	36.4 \pm 0.01	35.3 \pm 0.01
7	77.4 \pm 0.09	77.3 \pm 0.07	75.7 \pm 0.03	75.5 \pm 0.05	75.6 \pm 0.03	74.6 \pm 0.06	74.2 \pm 0.05	74.0 \pm 0.06	73.2 \pm 0.07	72.8 \pm 0.03	72.8 \pm 0.03	72.7 \pm 0.04	72.4 \pm 0.09	72.1 \pm 0.06
8	81.7 \pm 0.08	78.7 \pm 0.03	75.8 \pm 0.04	76.8 \pm 0.04	78.8 \pm 0.02	78.5 \pm 0.05	77.6 \pm 0.05	77.6 \pm 0.04	66.1 \pm 0.07	65.4 \pm 0.03	65.3 \pm 0.04	63.0 \pm 0.02	62.4 \pm 0.08	62.3 \pm 0.05
9	82.3 \pm 0.05	82.0 \pm 0.06	82.0 \pm 0.05	81.7 \pm 0.05	83.0 \pm 0.04	81.9 \pm 0.02	80.4 \pm 0.02	79.0 \pm 0.04	72.9 \pm 0.07	68.1 \pm 0.01	65.1 \pm 0.02	49.6 \pm 0.07	46.9 \pm 0.05	39.1 \pm 0.04
10	73.0 \pm 0.10	71.7 \pm 0.10	70.9 \pm 0.08	69.4 \pm 0.03	68.7 \pm 0.05	68.1 \pm 0.09	67.5 \pm 0.07	64.1 \pm 0.15	61.7 \pm 0.07	61.4 \pm 0.05	50.5 \pm 0.02	38.1 \pm 0.20	35.9 \pm 0.12	32.5 \pm 0.03
imatinib	68.4 \pm 0.12	63.9 \pm 0.03	61.5 \pm 0.07	61.3 \pm 0.05	60.7 \pm 0.08	60.6 \pm 0.14	57.9 \pm 0.05	46.8 \pm 0.05	34.5 \pm 0.04	26.2 \pm 0.05	17.8 \pm 0.02	17.5 \pm 0.01	17.3 \pm 0.01	16.6 \pm 0.01

For Hek293T

Compd	Concentration (μ M)- Viability rate (%)													
	0.3	0.5	1	3	5	10	15	20	30	50	70	100	150	200
5	-	-	68.7.1 \pm 0.04	66.5 \pm 0.11	61.0 \pm 0.13	59.4 \pm 0.08	56.6 \pm 0.10	56.2 \pm 0.03	55.8 \pm 0.05	54.1 \pm 0.04	52.7 \pm 0.03	50.5 \pm 0.02	50.4 \pm 0.02	50.0 \pm 0.04
6	91.1 \pm 0.15	90.8 \pm 0.14	87.0 \pm 0.15	81.4 \pm 0.09	78.5 \pm 0.14	78.2 \pm 0.02	70.6 \pm 0.04	65.5 \pm 0.10	57.4 \pm 0.09	50.7 \pm 0.05	48.8 \pm 0.02	47.9 \pm 0.01	47.7 \pm 0.02	47.0 \pm 0.02
7	87.7 \pm 0.06	87.6 \pm 0.07	87.0 \pm 0.08	84.6 \pm 0.05	81.0 \pm 0.09	80.5 \pm 0.06	80.3 \pm 0.04	76.0 \pm 0.03	72.1 \pm 0.02	64.5 \pm 0.02	64.2 \pm 0.02	63.5 \pm 0.07	60.8 \pm 0.03	55.1 \pm 0.02
8	95.7 \pm 0.03	94.8 \pm 0.07	94.3 \pm 0.06	92.9 \pm 0.04	91.2 \pm 0.09	90.8 \pm 0.05	90.1 \pm 0.07	90.0 \pm 0.04	84.9 \pm 0.04	81.3 \pm 0.02	66.9 \pm 0.02	66.4 \pm 0.03	59.4 \pm 0.01	58.2 \pm 0.01
9	91.7 \pm 0.07	89.8 \pm 0.07	89.5 \pm 0.05	87.4 \pm 0.07	86.2 \pm 0.03	79.3 \pm 0.05	78.3 \pm 0.03	76.5 \pm 0.05	68.9 \pm 0.03	62.2 \pm 0.02	56.2 \pm 0.04	54.8 \pm 0.02	46.9 \pm 0.02	42.8 \pm 0.02
10	82.8 \pm 0.02	78.2 \pm 0.01	78.1 \pm 0.01	80.4 \pm 0.02	79.1 \pm 0.01	80.2 \pm 0.02	81.4 \pm 0.01	80.8 \pm 0.01	82.2 \pm 0.03	79.2 \pm 0.03	80.2 \pm 0.02	80.7 \pm 0.01	80.0 \pm 0.01	81.0 \pm 0.02
imatinib	83.4 \pm 0.02	78.6 \pm 0.04	77.7 \pm 0.03	73.1 \pm 0.03	71.5 \pm 0.02	67.9 \pm 0.01	59.6 \pm 0.01	55.7 \pm 0.03	53.5 \pm 0.01	48.5 \pm 0.05	42.9 \pm 0.03	42.7 \pm 0.03	42.5 \pm 0.02	42.1 \pm 0.01

Six replicates were performed for all concentrations.

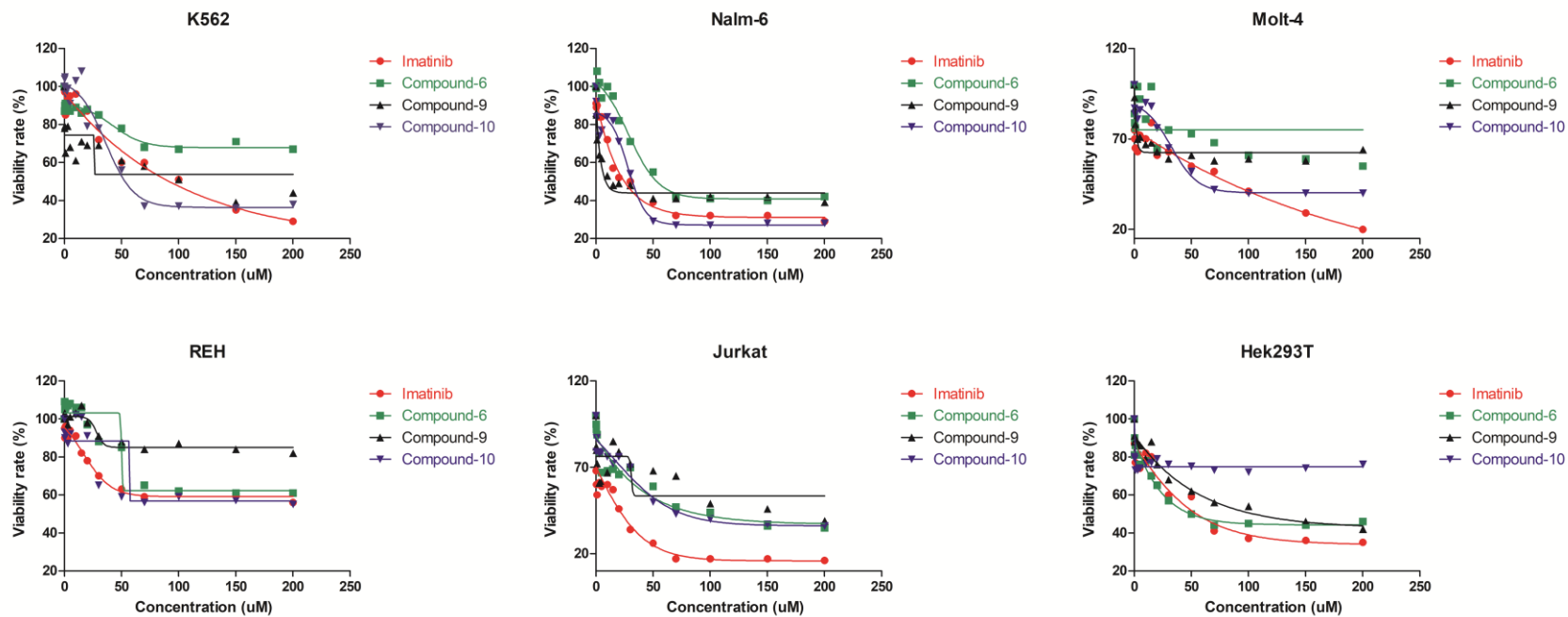


Figure S44. Comparison between imatinib and compound-6-9-10 in all cell-lines.

Table S3. Values of synthesized molecules related to target proteins.

COMPD	TARGET NAME	DESCRIPTION	P-VALUE	MAX TC
5	ACKR3	Atypical chemokine receptor 3	2.746e-153	0.38
	BRAF	Serine/threonine-protein kinase B-raf	6.849e-151	0.64
	TCF7L2	Transcription factor 7-like 2	1.228e-97	0.44
	BCR/ABL fusion	BCR/ABL p210 fusion protein	2.331e-96	0.64
	CTNNB1	Catenin beta-1	3.714e-90	0.44
6	BCR/ABL fusion	BCR/ABL p210 fusion protein	3.407e-103	0.57
	ACKR3	Atypical chemokine receptor 3	3.763e-98	0.38
	CPT1B	Carnitine O-palmitoyltransferase 1, muscle isoform	2.844e-97	0.37
	BRAF	Serine/threonine-protein kinase B-raf	1.618e-83	0.57
	CPT1A	Carnitine O-palmitoyltransferase 1, liver isoform	4.802e-70	0.37
7	BRAF	Serine/threonine-protein kinase B-raf	2.562e-159	0.58
	ACKR3	Atypical chemokine receptor 3	8.059e-152	0.39
	BCR/ABL fusion	BCR/ABL p210 fusion protein	3.446e-103	0.58
	SLC6A7	Sodium-dependent proline transporter	3.49e-81	0.36
	TCF7L2	Transcription factor 7-like 2	4.549e-59	0.42
8	BRAF	Serine/threonine-protein kinase B-raf	1.588e-158	0.63
	ACKR3	Atypical chemokine receptor 3	6.265e-147	0.38
	BCR/ABL fusion	BCR/ABL p210 fusion protein	6.853e-82	0.63
	RAF1	RAF proto-oncogene serine/threonine-protein kinase	7.135e-80	0.63
	TCF7L2	Transcription factor 7-like 2	4e-78	0.37
9	BRAF	Serine/threonine-protein kinase B-raf	2.463e-152	0.53
	ACKR3	Atypical chemokine receptor 3	5.483e-142	0.40
	BCR/ABL fusion	BCR/ABL p210 fusion protein	1.381e-90	0.53
	TCF7L2	Transcription factor 7-like 2	1.671e-89	0.39
	CTNNB1	Catenin beta-1	1.201e-82	0.39
10	BCR/ABL fusion	BCR/ABL p210 fusion protein	1.97e-102	0.49
	ACKR3	Atypical chemokine receptor 3	5.763e-97	0.40
	CPT1B	Carnitine O-palmitoyltransferase 1, muscle isoform	6.867e-81	0.38
	BRAF	Serine/threonine-protein kinase B-raf	8.972e-74	0.49
	CPT2	Carnitine O-palmitoyltransferase 2, mitochondrial	6.733e-55	0.38
imatinib	BRAF	Serine/threonine-protein kinase B-raf	1.19e-141	1.00
	BCR/ABL fusion	BCR/ABL p210 fusion protein	8.174e-117	1.00
	SYK	Tyrosine-protein kinase SYK	1.176e-88	1.00
	ABL1	Tyrosine-protein kinase ABL1	6.475e-74	1.00
	KIT	Mast/stem cell growth factor receptor Kit	9.151e-68	1.00

This values were obtained from the from <http://sea.bkslab.org/> website (Reference-40)

Table S4: Cristal structures of ABL1

PDB ID: Chain ID	Resolution	Positions	Ligand	Details
2HYY: A ^[a]	2.40	228-500	Imatinib	Inactive (DFG-out)
2E2B: A ^[b]	2.20	229-515	Bafetinib	Inactive (DFG-out)
2HZ0: A ^[c]	2.10	228-497	NVP-AEG082	Inactive (DFG-out)
3CS9: A ^[d]	2.21	229-500	Nilotinib	Inactive (DFG-out)
3UE4: A ^[e]	2.42	229-512	Bosutinib	Inactive (DFG-out)
4YC8: A ^[f]	2.90	229-512	Dasatinib Analog	Inactive (Src-like)
2HZI: A ^[g]	1.70	229-500	PD180970	Intermediate (DFG-flip)
2HZ4: B ^[h]	2.80	228-500	NVP-AFN941	Active

[a] Human Abl kinase domain in complex with imatinib (STI571, Glivec), [b] Crystal structure of the c-Abl kinase domain in complex with INNO-406, [c] Abl kinase domain in complex with NVP-AEG082, [d] Human ABL kinase in complex with nilotinib, [e] Structural and spectroscopic analysis of the kinase inhibitor bosutinib binding to the Abl tyrosine kinase domain, [f] C-Helix-Out Binding of Dasatinib Analog to c-Abl Kinase, [g] Abl kinase domain in complex with PD180970, [h] Abl kinase domain unligated and in complex with tetrahydrostaurosporine.

Table S5: Redocking the original ligands to the crystal structures of wild type ABL1

PDB ID: Chain ID	Ligand	Number of Torsions	ΔG	Size of the cluster	RMSD to reference
2HYY: A ^[a]	Imatinib	7	-14.5	38	1.1
2E2B: A ^[b]	Bafetinib	8	-14.9	32	1.3
2HZ0: A ^[c]	NVP-AEG082	8	-12.9	95	0.5
3CS9: A ^[d]	Nilotinib	7	-13.0	34	0.6
3UE4: A ^[e]	Bosutinib	9	-7.9	9	1.9
4YC8: A ^[f]	Dasatinib Analog	7	-11.0	32	1.2
2HZI: A ^[g]	PD180970	3	-11.2	100	0.6
2HZ4: B ^[h]	NVP-AFN941	4	-10.5	100	1.6

[a] Human Abl kinase domain in complex with imatinib (STI571, Glivec), [b] Crystal structure of the c-Abl kinase domain in complex with INNO-406, [c] Abl kinase domain in complex with NVP-AEG082, [d] Human ABL kinase in complex with nilotinib, [e] Structural and spectroscopic analysis of the kinase inhibitor bosutinib binding to the Abl tyrosine kinase domain, [f] C-Helix-Out Binding of Dasatinib Analog to c-Abl Kinase, [g] Abl kinase domain in complex with PD180970, [h] Abl kinase domain unligated and in complex with tetrahydrostaurosporine.

Table S6: Cristal structures of BRAF.

PDB ID: Chain ID	Resolution	Positions	Ligand	Details
1UWH: A ^[a]	2.95	448-723	BAX	Inactive (DFG-out/ α C-in)
4KSP: A ^[b]	2.93	445-723	TAK-632	Inactive (DFG-out/ α C-in)
4JVG:A ^[c]	3.09	444-723	BIRB-796	Inactive (DFG-out/ α C-in)
3C4C: A ^[d]	2.57	444-721	PLX-4720	Inactive (DFG-in/ α C-out)
5CSW: A ^[e]	2.66	442-721	Dabrafenib	Inactive (DFG-in/ α C-out)
2FB8: A ^[f]	2.90	445-723	SB-590885	Active (DFG-in/ α C-in)
3D4Q: A ^[g]	2.57	433-726	SM5	Active (DFG-in/ α C-in)

[a] The complex of wild type B-RAF and BAY439006, [b] Crystal Structure of Human B-raf bound to a DFG-out Inhibitor TAK-632, [c] B-Raf Kinase in Complex with Birb796, [d] B-Raf Kinase in Complex with PLX4720, [e] B-RAF in complex with Dabrafenib, [f] Structure of the B-Raf kinase domain bound to SB-590885, [g] Pyrazole-based inhibitors of B-Raf kinase.

Table S7: Redocking of the original ligands to the crystal structures of BRAF.

PDB ID: Chain ID	Ligand	Number of Torsions	ΔG	Size of cluster	RMSD to reference
1UWH: A ^[a]	BAX	6	-11.4	96	0.5
4KSP: A ^[b]	TAK-632	8	-13.3	20	1.3
4JVG:A ^[c]	BIRB-796	7	-14.4	62	0.7
3C4C: A ^[d]	PLX-4720	6	-9.7	23	1.3
5CSW: A ^[e]	Dabrafenib	6	-12.0	20	1.3
2FB8: A ^[f]	SB-590885	8	-8.9	62	1.9
3D4Q: A ^[g]	SM5	8	-8.7	19	1.9

[a] The complex of wild type B-RAF and BAY439006, [b] Crystal Structure of Human B-raf bound to a DFG-out Inhibitor TAK-632, [c] B-Raf Kinase in Complex with Birb796, [d] B-Raf Kinase in Complex with PLX4720, [e] B-RAF in complex with Dabrafenib, [f] Structure of the B-Raf kinase domain bound to SB-590885, [g] Pyrazole-based inhibitors of B-Raf kinase.

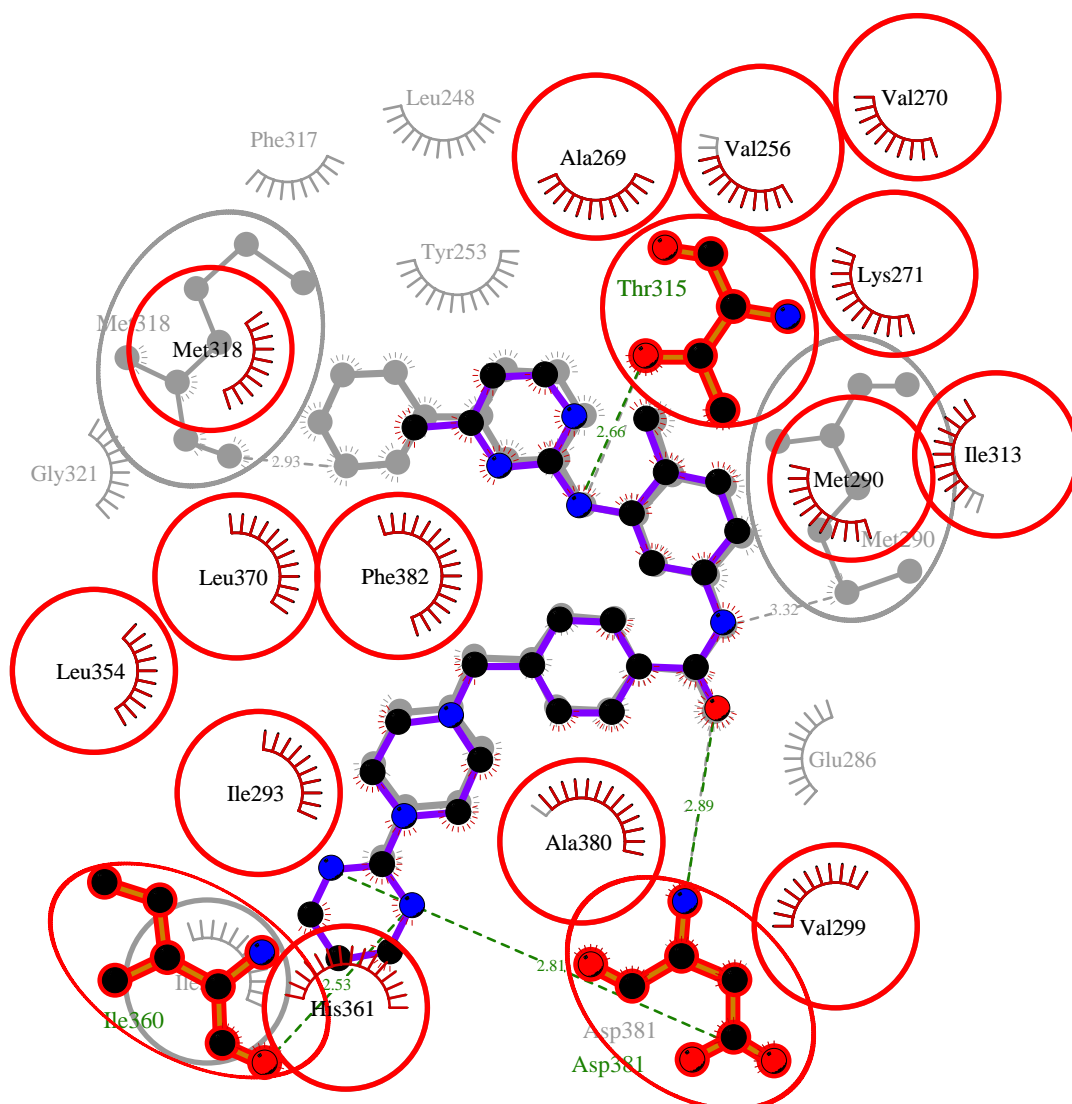


Figure S45. Comparison of ABL-imatinib (background) and ABL-Compound 5 (foreground) interactions. Imatinib and its contact residues are depicted in gray, while the common contact residues are marked with red circles.

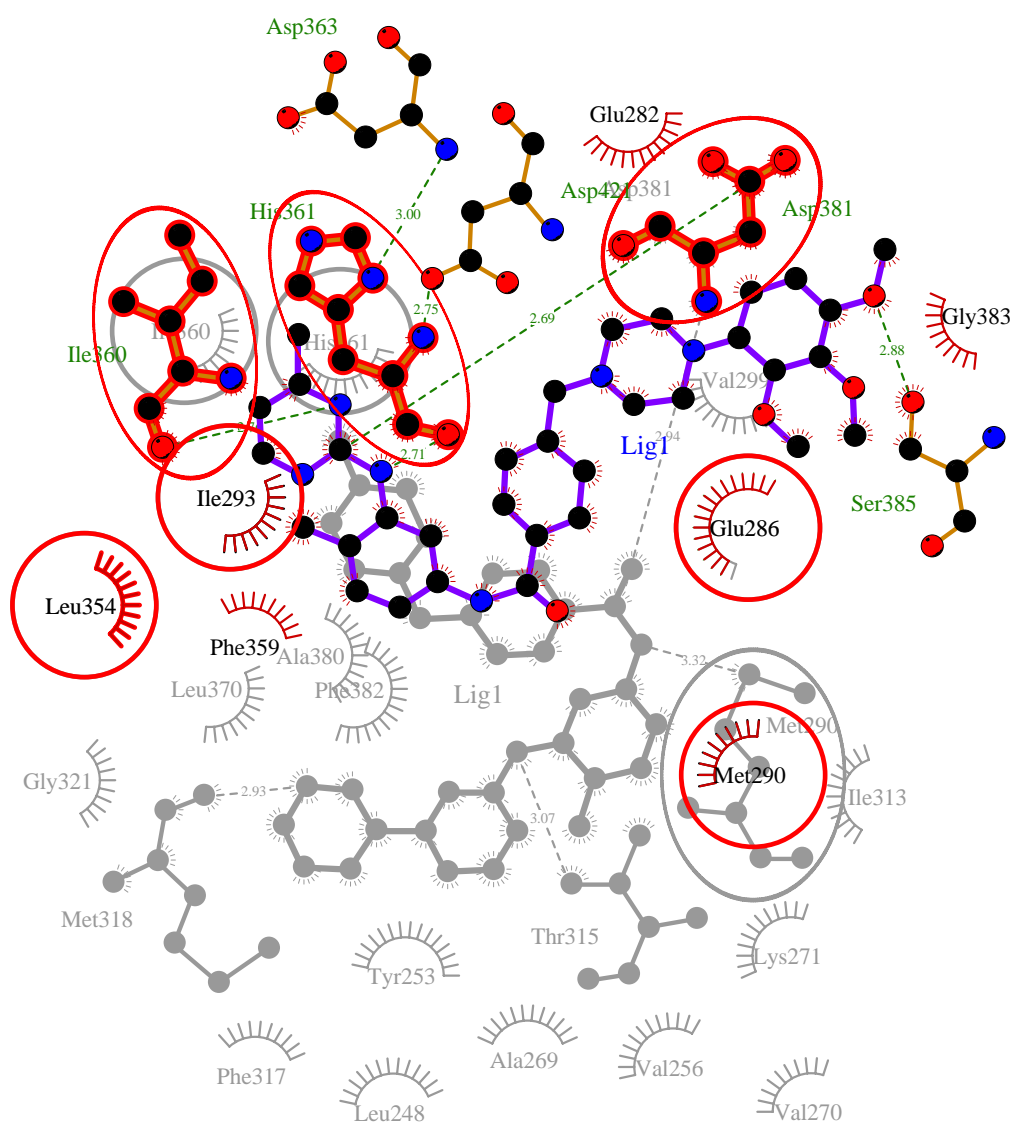


Figure S46. Comparison of ABL-imatinib (background) and ABL-Compound 6 (foreground) interactions. Imatinib and its contact residues are depicted in gray, while the common contact residues are marked with red circles.

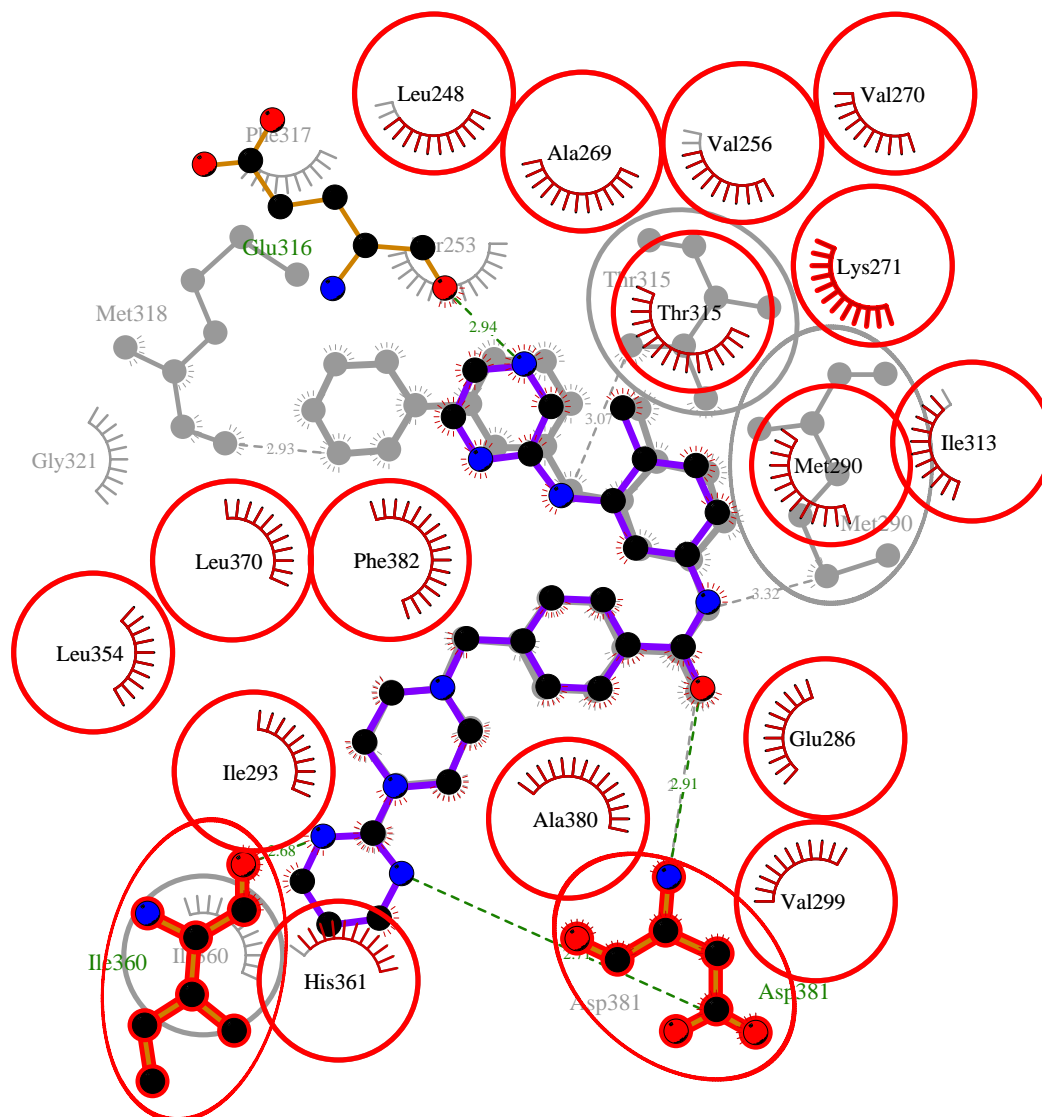


Figure S47. Comparison of ABL-imatinib (background) and ABL-Compound 7 (foreground) interactions. Imatinib and its contact residues are depicted in gray, while the common contact residues are marked with red circles.

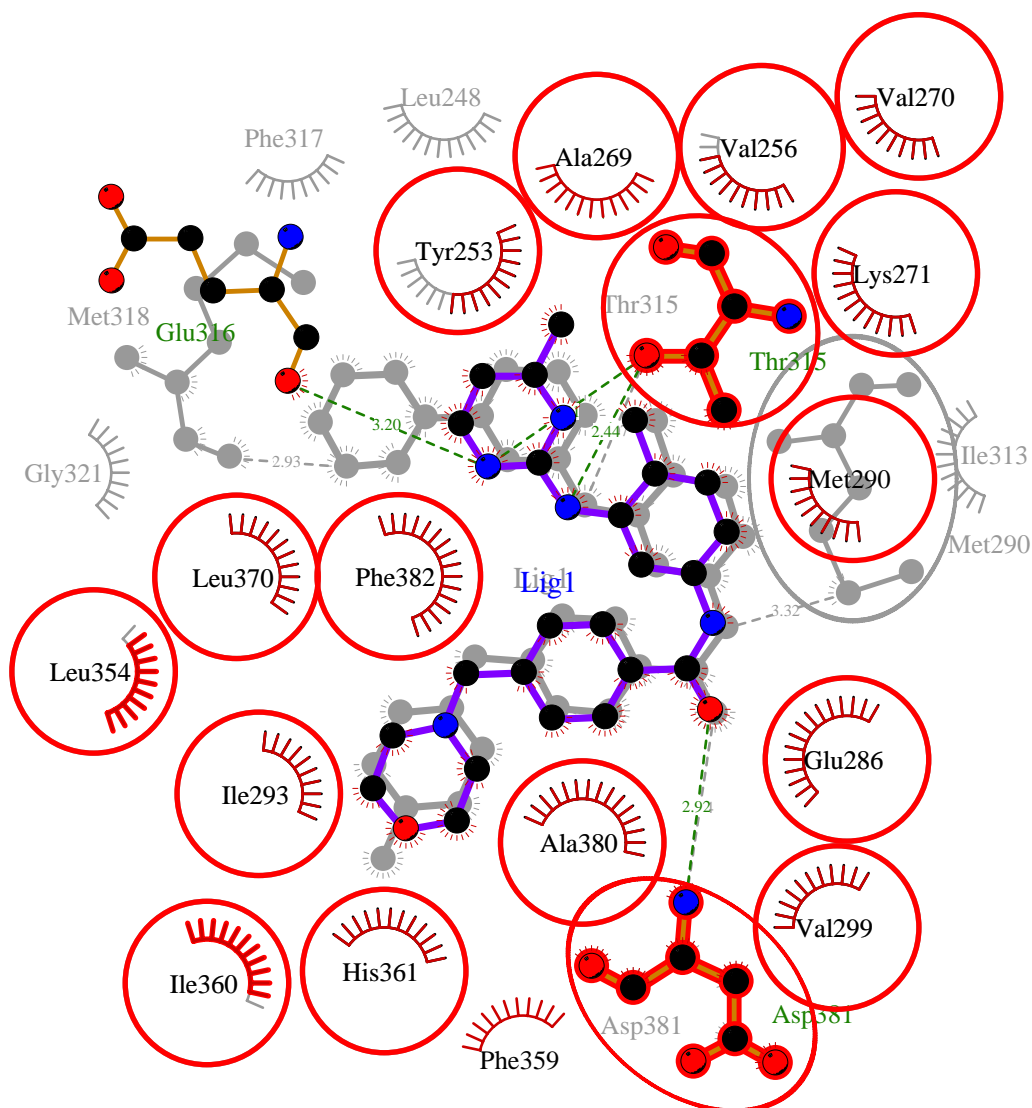


Figure S48. Comparison of ABL-imatinib (background) and ABL-Compound 8 (foreground) interactions. Imatinib and its contact residues are depicted in gray, while the common contact residues are marked with red circles.

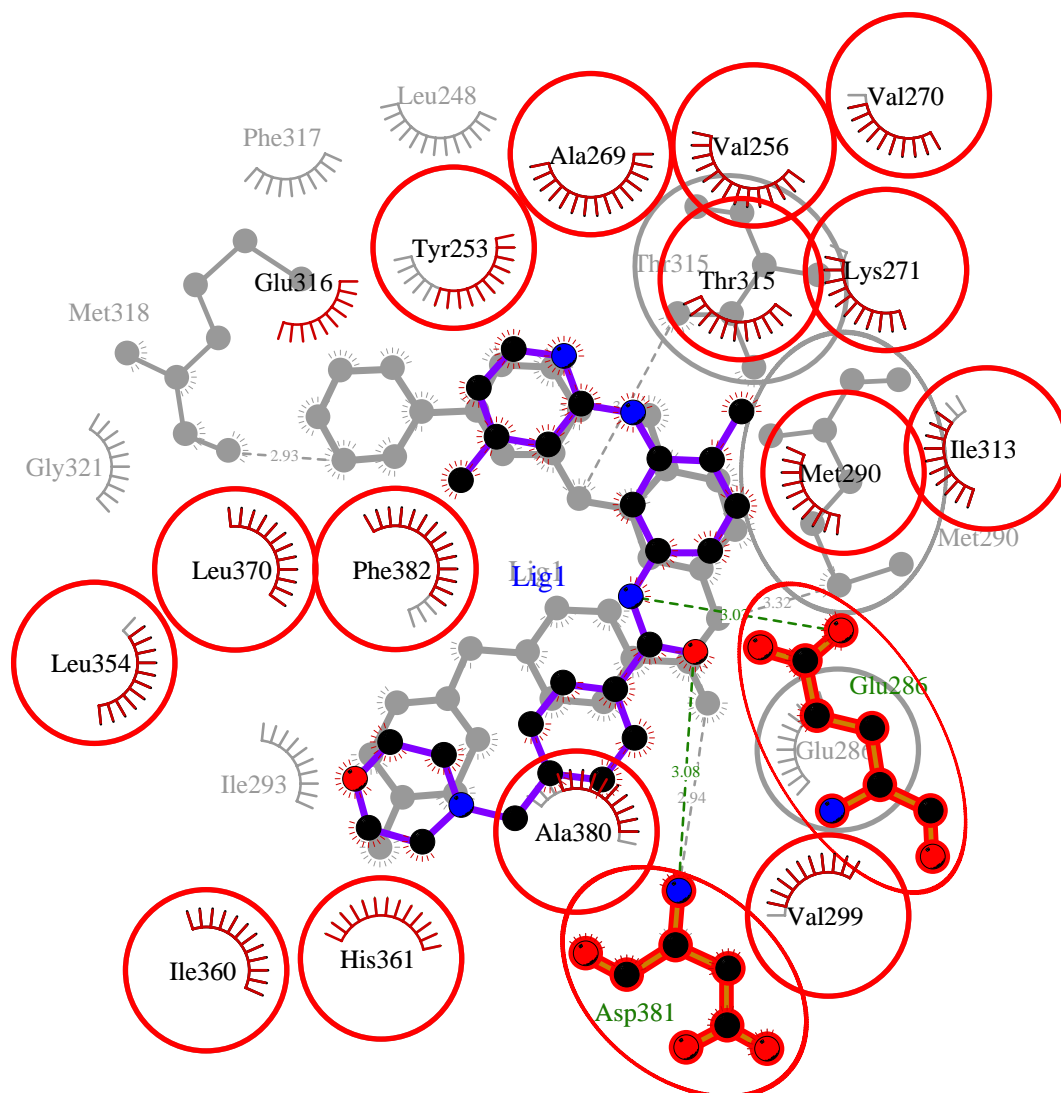


Figure S49. Comparison of ABL-imatinib (background) and ABL-Compound 9 (foreground) interactions. Imatinib and its contact residues are depicted in gray, while the common contact residues are marked with red circles.